University of Nevada, Reno

Petrography and Field Mapping of Eocene Intrusions and Adjacent Breccia Zones at the Scraper Springs Prospect, Elko County, Nevada

A thesis submitted in partial fulfillment of the requirements for the degree Master of Science in Geology

by

Bradford M Cantor

Dr. Tommy B. Thompson/Thesis Advisor

December, 2012

UNIVERSITY
OF NEVADA
RENO

THE GRADUATE SCHOOL

We recommend that the thesis prepared under our supervision by

Bradford M Cantor

entitled

Petrography and Field Mapping of Eocene Intrusions and Adjacent Breccia Zones at the Scraper Springs Prospect, Elko County, Nevada

Be accepted in partial fulfillment of the
Requirements for the degree of

Master of Science in Geology

Tommy B. Thompson, Ph.D., Advisor

Christopher Henry, Ph.D., Committee Member

Victor Vasquez, Ph.D., Committee Member

Marsha H. Read, Ph.D., Associate Dean, Graduate School

December, 2012

Abstract

The Scraper Springs project, held by Cordilleran Exploration Inc. (Cordex), is a multi-target prospect located in northwestern Elko, County, Nevada, approximately 8 miles northeast of the Midas district. Regionally, the property can be considered to be along trend with the northern-most projection of the Carlin trend, approximately 25 miles north of the Dee/Rossi area. The eastern limit of Northern Nevada Rift (NNR) is also considered to border the western margin of the Scraper Springs property. The geology at Scraper is characterized by an exposure of Paleozoic rocks from the upper-plate Vinini Formation above the Roberts Mountains thrust through a window of Eocene and Miocene volcanic cover. Additionally, there is an exposure of intrusive Eocene diorite, dated at 38.9 ± 1.0 Ma by K/Ar techniques, adjacent to the Paleozoic window. Exploration efforts at Scraper Springs date back to 1983; various exploration efforts since 1983 reveal three types of mineralized targets at Scraper Springs: Carlin-type mineralization hosted at depth below the Roberts Mountains thrust, epithermal vein-style mineralization hosted in volcanics, and polymetallic Au-bearing skarn mineralization hosted in Paleozoic sedimentary rocks in contact with the diorite intrusion. The present study employs field mapping techniques to document the geology and alteration of the diorite intrusion and adjacent silicified/advanced argillic lithocap breccias. Petrography and sodium-cobaltinitrite staining supplement field observations to aid in understanding alteration events. Geochemical data from topaz-rich samples are considered to help classify the hydrothermal system present at Scraper in addition to soil and rock chip samples. Finally, drill-hole data from 9 holes were logged and drawn in cross-section to offer one three-dimensional possibility of the hydrothermal system at Scraper. Results suggest the Eocene diorite intrusion has undergone significant potassic alteration. A separately-mapped unit of quartz syenite is also documented, revealing potassic alteration haloes around its margins. Petrography indicates this type of potassic alteration is overprinted by propylitic and ultimately sericitic events. Advanced argillic alteration in the breccia zones adjacent to the diorite intrusion is also profound and exhibits several different events. Early vuggy quartz-alunite alteration is common throughout both breccia zones and is followed by an advanced argillic assemblage containing zones of pyrophyllite, topaz, kaolinite, and alunite. Late chalcedony overprints much of the earlier alteration. In general, each pulse of advanced argillic mineralization is separated by a breccia event. Overall, the system at Scraper Springs appears to reflect that of a porphyry-epithermal transition zone. This evidence, coupled with high fluorine and molybdenum geochemistry, and alteration zoning patterns documented in the present study suggest future exploration at Scraper could credibly target a Climax-type molybdenum porphyry similar to the Mount Hope deposit in Eureka County, NV.

Contents

Introduction

Location

The Scraper Springs project in northwestern Elko County, Nevada is located at the northern-most exposure of Paleozoic rocks in north-central Nevada, projected to the northwest of the Carlin Trend (Fig. 1; Stewart, 1980). Upper plate Ordovician Vinini Formation is exposed in a window through Tertiary volcanic rocks at Scraper Springs. Exploration beginning in 1983 has identified Carlin-type mineralization in Vinini Formation and potentially at depth in the Rodeo Creek Formation, disseminated and vein mineralization in Tertiary ash-flow tuffs and other volcanic rocks, and Au-bearing base-metal skarn associated with an Eocene intrusion.

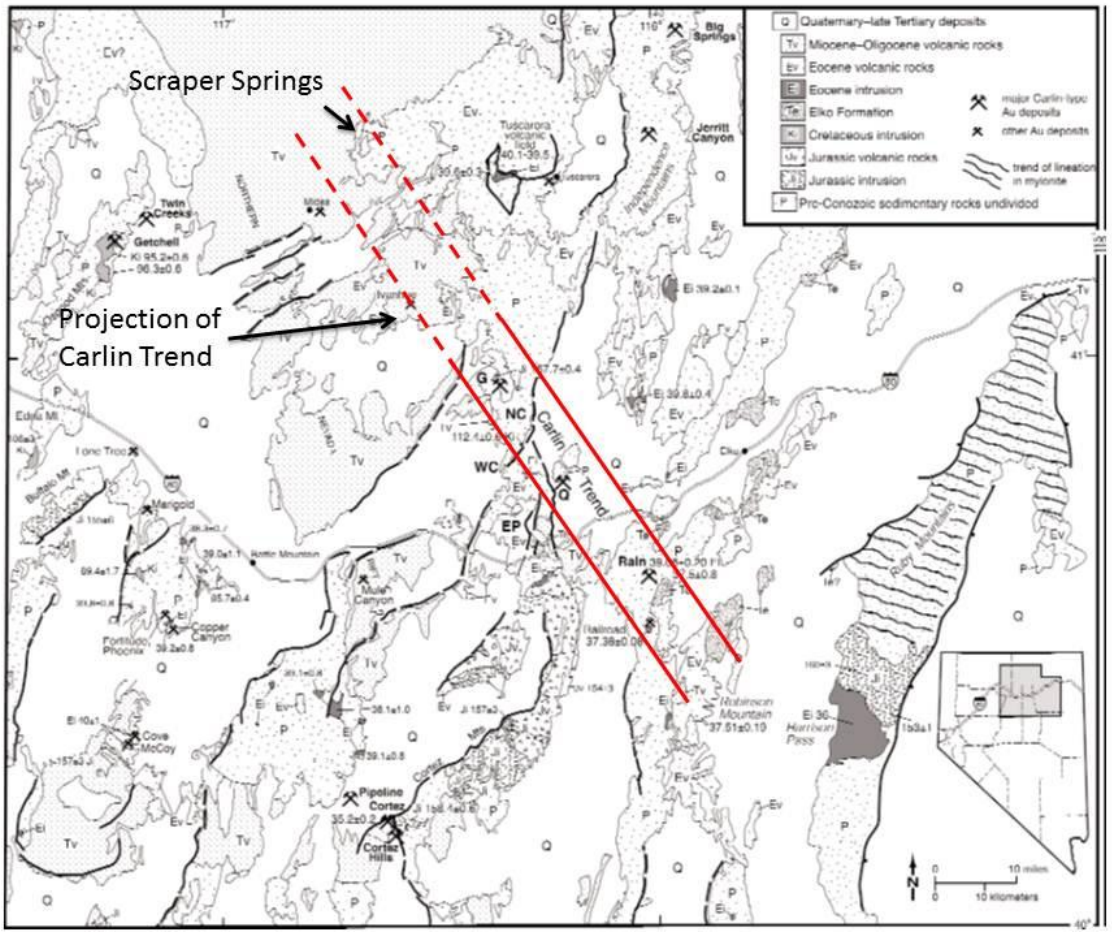

Figure 1. Location of the Scraper Springs project in relation to other large gold deposits in northern Nevada. The property occurs along the same relative lineament as the Carlin-trend and the geology at the property exposes the upper portions of favorable Paleozoic host rocks for Carlin-style mineralization. Also exposed on the property are quartz veins with anomalous concentrations of precious metals. Nearby epithermal districts include the Midas, Tuscarora, and Ivanhoe mining districts. Map modified from Ressel and Henry, 2006.

Regional Geology and Nearby Deposits

In addition to existing on the northern extension of the Carlin-trend, Scraper Springs is also situated near several Tertiary epithermal districts including the Midas district (Miocene; Leavitt et al., 2003), 8 miles to the southwest, the Ivanhoe district (Miocene; Wallace, 2003) and adjacent Hollister mine (Eocene with Miocene overprint; Wallace, 2003; Oelofse et al., 2009) 15 miles to the southeast, and the Tuscarora district (Eocene; Castor et al., 2003), approximately 20 miles to the east of the Scraper property. In addition to hosting epithermal mineralization within

the region, these districts are also relevant to the geology at Scraper Springs because they share similar stratigraphy and host rocks.

Like Scraper, the Tuscarora district also contains Eocene ash-flow tuffs and hosts an Eocene granodiorite intrusive (Henry and Boden, 1998, 1999; Henry et al., 1999). Based on the mapping of Henry and Boden (1998, 1999) and Henry et al. (1999), it was determined that there are multiple caldera complexes located at Tuscarora. These calderas are likely the source of tuffaceous units exposed at Scraper Springs. Additionally, the granodiorite exposed in the Tuscarora volcanic complex, the Mount Neva granodiorite, has been dated using $^{39}Ar/^{40}Ar$ techniques and is determined to be 39.37 ± 0.28 Ma (Henry and Boden, 1999). This age is similar to the recorded K-Ar age of 38.9 ± 1 Ma for intrusive diorite exposed at Scraper Springs (Wallace, 2005). These Eocene dates correspond with the timing of Carlin-type mineralization in Nevada and also Eocene magmatism throughout the region (e.g. Ressel and Henry, 2006; Christensen and Yeats, 1992). The Eocene magmatism present in the northeastern part of the Great Basin is part of an overall north to south trend of magmatism extending from the Colville province in eastern Washington between 54-47 Ma, the Challis volcanic field in central Idaho between 51-40 Ma, and in northern Nevada and the Great Basin starting at 43 Ma and continuing through the Eocene (Fig. 2; Christensen and Yeats, 1992; Castor et al., 2003).

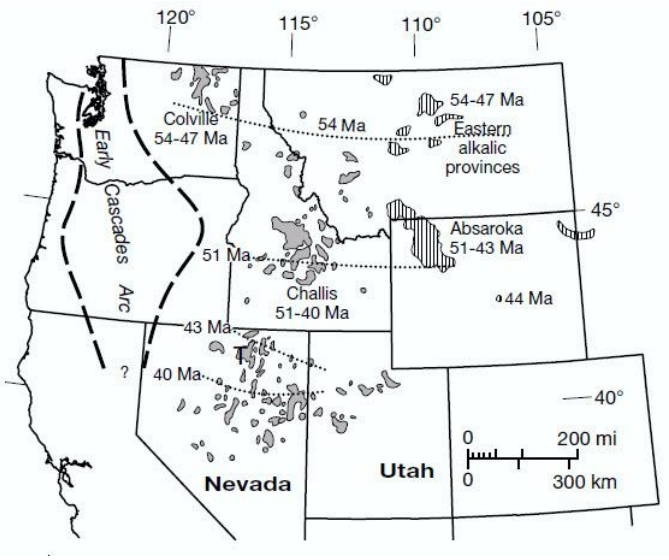

Figure 2. Tertiary magmatism in the North American cordillera. Magmatism started north in Montana and eastern Washington around 54 Ma, continued south through central Idaho between 51-40 Ma, and manifested in the Great Basin at 43 Ma, continuing through the Eocene. Figure taken from Castor et al. (2003).

The Hollister mine, located 15 miles to the southeast of Scraper Springs and adjacent to the Ivanhoe mining district, has similar host rocks as Scraper Springs. At Hollister, near-surface upper plate rocks are exposed in the mine, similar to the outcrop of upper plate rocks at Scraper. Drilling at the Hollister mine intercepted anomalous Au, As, and Sb values at 800 feet, probably in the lower-plate carbonates of the Silurian-Devonian Roberts Mountain Formation and Ordovician Hanson Creek Formation (Oelofse et al., 2009). Reverse-circulation (RC) drilling (SS-1, 1900 ft.) at Scraper Springs intercepted similar lower-plate hosted mineralization 140 ft. of 0.017 opt gold mineralization and copper-zinc calc-silicate assemblages in the bottom 100 ft. of the hole (Howell, 2007). Additionally, the Hatter stock, a biotite-quartz-plagioclase intrusion at Hollister, was dated by K-Ar methods at ~39 Ma, indistinguishable in age with the diorite intrusion exposed at Scraper (Oelofse et al., 2009). The main mineralization hosted at Hollister is Miocene and occurs in both Miocene volcanic rocks and through-going structures in the upper-plate rocks (Oelofse et al., 2009). The presence at Hollister of similar host rocks to Scraper

Springs, including Paleozoic rocks, Eocene intrusion, and Miocene volcanic rock on the western part of the Scraper Springs property, suggests that Eocene and Miocene targets at Scraper Springs could potentially be similar.

The Northern Nevada Rift (NNR) exposes Miocene volcanic rocks on the western part of the Scraper Springs property (Howell, 2004; Wise, 2008a). The NNR is characterized by a bimodal basalt-rhyolite assemblage and hosts Miocene epithermal vein systems throughout its extent (John et al., 2000). Epithermal mineralization in the NNR includes the Buckskin deposit and the nearby Midas district (Vikre, 1985; Leavitt et al., 2003). The undated Rebel fault zone and associated quartz veins and breccias, which crop out in the southwest portion of the Scraper Springs property, could also be Miocene, given its proximity to the NNR volcanic assemblage (Fig. 3) and similarity to epithermal veins hosted at Midas and elsewhere along the NNR.

Exploration History

US Steel first explored the vein system at the Hill anomaly (Rebel fault zone) in the southwestern part of the property in 1983. Freeport drilled 10 RC holes in this area, totaling 4100 ft. in 1984. Hecla followed this effort by drilling 7 holes totaling 2145 ft. in 1987. Both drill programs intercepted only anomalous gold and anomalous to significant silver hosted in quartz veins, breccias, and altered volcanic rocks (Howell, 2007).

Cordex Exploration held the property from 1989-1991 and did extensive exploration including mapping, rock and soil sampling, auger grid drilling, CSAMT and drilling 40 RC holes totaling 21,475 ft. Most of their work targeted areas to the north and northwest of Cordex's present claim block (Howell, 2007).

Western States Minerals held the property from 1994-1997. Their work consisted of mapping, rock and soil sampling, and drilling, which focused on the central Paleozoic exposure between the north and south stock, and to a lesser extent in the Rebel Fault zone. Of the 13 RC holes drilled totaling 8535 ft., two holes intercepted significant mineralization in altered Vinini sedimentary rocks along the margins of the Eocene diorite intrusive. Encouraging drill results included SS-1, which intercepted 140 feet (320-460 ft.) of 0.017 opt gold including 20 and 10 foot intercepts containing 0.031 and 0.050 opt Au, respectively. Additionally, SS-6 intercepted 25 feet (25-50 ft.) of 0.020 opt Au (Howell, 2007).

In 2003, Cordex (funded at the time by Metallic Ventures) re-mapped the property, did extensive soil sampling, contracted a ground magnetic survey, and dated the diorite intrusive before drilling 12 widely-spaced RC holes totaling 8380 ft. Encouraging drill results included SC-1, which was collared 270 feet north-northwest of the Western States SS-1 hole and drilled to a depth of 1900 feet. This drill hole encountered variably altered lower plate rocks thought to be Devonian Rodeo Creek Formation at a depth of 1650 feet. This hole contained anomalous gold both in the upper and lower plates with strongly anomalous to significant copper and zinc in lower plate sedimentary rocks. Many of the other shallow holes intercepted weakly anomalous gold, anomalous zinc, lead and silver (SC-11) (Howell, 2007).

Metallic Ventures in joint venture with Geologix Exploration conducted additional soil grid sampling in the north central part of the property, but did no drilling. Metallic gave up their interest in Scraper in late 2006 and the property reverted to Cordex.

In 2008, Newmont Mining Corp. in a joint-venture with Cordex, re-mapped geology and alteration and conducted soil sampling covering the northeastern portion of the property and the

area identified as the "Diatreme Vent Target" (referred to in this study as the "South Breccia Zone") and drilled 3 RC holes in this area (Wise, 2008b).

Project Goals and Objectives

The present study focuses on both the northern and southern exposure of the Eocene intrusion and adjacent altered breccia zones. Veins of the Rebel fault zone in the southwest part of the property, were examined briefly but are not discussed in detail in this study. Detailed mapping of the geology and alteration is combined with detailed petrography to determine the nature and extent of mineralization at Scraper Springs. To aid petrography, sodium-cobaltinitrite staining was conducted on thin section billets to determine the nature and extent of potassic alteration in the Eocene diorite intrusion (Td). Additionally, data collected at Scraper Springs over its 27-year exploration history are used to supplement field and petrographic observations.

Materials and Methods

Mapping

Field mapping for the present study was conducted during late-May to mid-August of 2009. Methods relied heavily on previous geologic maps of Scraper Springs (Howell, 2004; Wise, 2008a) for basic geologic relationships and general alteration patterns. Due to pervasive oxidation at the surface and lack of outcrop, many original textural relationships and mineral assemblages were obscured, complicating the degree of positive identification in some areas. Two target areas were identified for detailed outcrop-style mapping and include the North Stock and Breccia Zone and the South Stock and Breccia zone (Fig. 3). The Rebel Fault Zone was investigated, but not mapped in detail (Fig. 3). The purpose of mapping these areas was to identify possible relationships between the Eocene intrusive stocks and adjacent breccia zones.

Figures 4 and 5 are maps of the geology in the south stock and breccia zone and north stock and breccia zone, respectively. Appendix A is a 1:6000 scale map of the geology and alteration at Scraper Springs.

Alteration mapping in this study was conducted simultaneously with geologic mapping. While field mapping helped to identify distinct types of alteration including various forms of silicification, iron oxide staining, and acid sulfate alteration, more detailed alteration zones were separated once Na-cobaltinitrite staining and petrography were completed.

Staining

Sodium-cobaltinitrite staining was conducted on 42 thin section billets from samples representing the north and south stocks to determine degree and nature of potassic alteration. Samples were handled with tongs and etched for 60 seconds in a 50% HF solution and then briefly rinsed for approximately 5 seconds in distilled water. The samples were then handled with tongs and dipped for 60 seconds into a saturated sodium-cobaltinitrite solution at the ratio of 10 g sodium-cobaltinitrite to 20 mL distilled water and then rinsed again in distilled water for 5 seconds. Samples were left to dry under a fume hood for approximately a half hour. Stained billets were scanned using an HP ScanJet 3010 scanner at the resolution of 1200 dpi. Digital images of the billets were observed and percentages of K-feldspar flooding were estimated.

Petrography

Samples from locations in all three target areas, the North Stock and Breccia Zone, the South Stock and Breccia Zone, and the Rebel Fault Zone were collected for petrographic analysis. The hand sample locations are documented in Appendix C. Samples were chosen based on distinct rock and alteration type to acquire a representative sample of rocks in multiple alteration assemblages. In total, 116 thin sections were prepared by Spectrum Petrographics, Inc.

Thin sections were analyzed using an Olympus BX51 microscope with 5x, 10x, 20x, and 50x objectives with a 4x ocular. Photomicrographs were documented using an Olympus DP10 camera mount. Mineralogy, textures, and cross-cutting relationships were observed and documented. The base alteration maps were updated based on petrographic observations and alteration minerals documented in these observations.

Through detailed petrographic observations and documentation with photomicrographs, extensive paragenetic sequences were developed for both breccia zones and the diorite intrusive. Different alteration assemblages observed in thin section helped characterize the hydrothermal fluids that contributed to the altered zones and aided with generating a geologic model for Scraper Springs.

Drill-hole Logging

To complement mapped and petrographic observations, eleven drill holes were selected along a northwest-trending transect and re-logged. Observations included lithology and alteration, noting unique mineralogy and depth of oxidation. These logs were then synthesized and projected to develop a schematic cross-section and geologic model.

Geochemistry

Multiple geochemical datasets were utilized in the present study. Exploration data from soil samples and rock chips from Newmont's 2008 campaign are compared with geology and alteration. In addition to these data, nine hand samples with complementary petrographic samples were selected to document changes in alteration across a transect through the South Stock and Breccia zone.

Newmont's data from 2008 includes 787 soil samples and 215 rock chip samples. These samples were sent to ALS Chemex in Reno, NV. Gold values are derived from a 30g fire assay with ICP-AES analysis. Concentrations of 41 trace elements were determined using an aqua regia digestion and analyzed with ICPMS.

Nine hand samples from the present study that cover representative alteration examples across a transect in the southern stock and breccia zone were submitted to ALS Chemex in Reno, NV for analysis of 61 trace elements using four-acid total digestion and either ICPMS or ICP-AES finish based on the element. Mercury was separately analyzed using an aqua regia method, as mercury volatilizes at the higher temperatures required to perform the four-acid technique. Additionally, these samples were analyzed for fluorine due to significant topaz ($Al_2SiO_4(F,OH)_2$) and zunyite ($Al_{13}Si_5O_{20}(OH,F)_{18}Cl$) mineralization in some of the acid sulfate suites. This technique involved sample decomposition using sodium hydroxide fusion, and fluorine was determined with an ion-specific analysis. A table of these nine samples can be found in Appendix B.

Geophysics

Geophysical datasets collected during the exploration history of Scraper Springs have been considered and utilized for understanding mineralization at depth. Specifically, previously collected IP, gravity, and magnetic surveys have been particularly helpful in projecting the geology at Scraper Springs into the subsurface. Further discussion of these data follows in the results section and geophysical data are presented in Appendix C.

Field Observations and Mapping

Previous Mapping

Mapping at the Scraper Springs Property is difficult because of sparse outcrop. Where definitive outcrop does not occur, subcrop- and float-style mapping was undertaken in the present study. For clarity, outcrop outlines are included on all geologic maps in this study. Original mapping by Howell (2004) and Wise (2008a) revealed several distinct rock types. Figure 3 is a simplified version of both mapping efforts. Observations from this study and initial mapping observations demonstrate a window through Tertiary volcanic rocks into Paleozoic sedimentary rocks above the regionally-continuous Roberts Mountains thrust. This exposure consists of the Ordovician Vinini Formation (Ovi), the major unit capping the Roberts Mountain thrust. Separate lithologies within Ovi include siltstone, fine heterolithic sandstone, black chert, and argillites (Howell, 2004). Additionally, quartzite (Oviq) forms distinctive ridges throughout the property. Oviq consists of medium to coarse-grained sand and is very clean at nearly 100% quartz (Howell, 2004; present study). Lenticular quartzite pods are exposed throughout the property and the pod-like nature of these outcrops has been attributed to regional deformation stretching these resistant bodies into boudins (Henry, 2008).

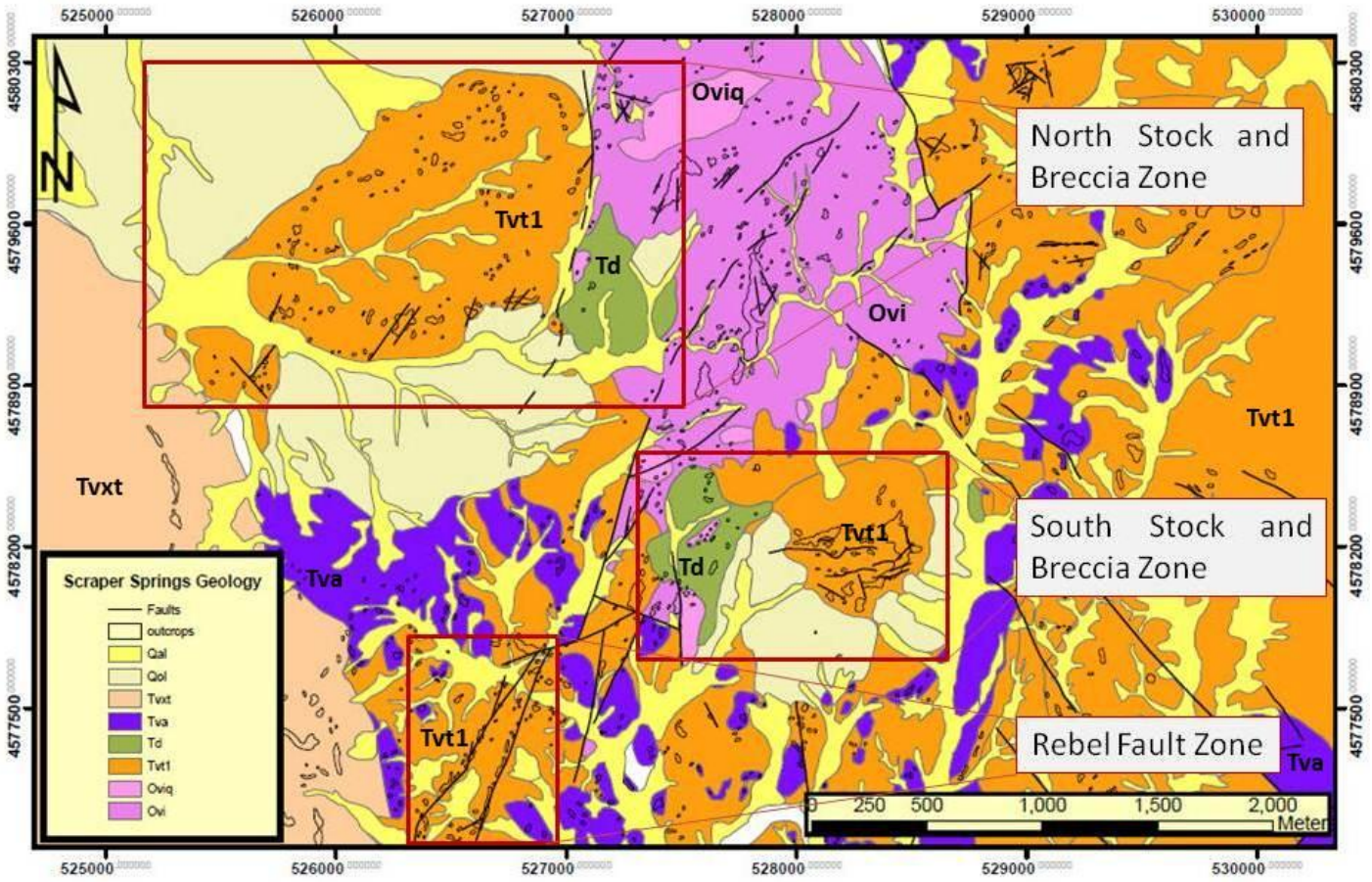

Figure 3. Simplified geologic map of the Scraper Springs Property, modified from Howell (2004) and Wise (2008). The North and South Stocks are the focus of the present study. The Rebel Fault Zone is highlighted as an area of structurally controlled mineralization, but is not discussed in this study. Detailed geologic and alteration maps accompany the North Stock and Breccia Zone and the South Stock and Breccia Zones. Coordinates are NAD27 Zone 11N.

Although not exposed in the area of Figure 3, the Pennsylvanian-Permian Edna Mountain Formation (PPem) and younger Pennsylvanian Havallah Sequence (Ph) crop out north of this area. This Edna Mountain Formation consists of fine to locally coarse-grained sandstone of heterolithic clasts and abundant black chert clasts; local phosphatic beds also occur (Howell, 2004). Outcrops form blocky and tabular masses and are exposed in the northern area of the Paleozoic window. Havallah Sequence (Ph) overlies the Edna Mountain Formation along the Golconda thrust fault. The Ph consists of various beds of black chert, sandstone, siltstone, and thin limestone (Howell, 2004).

Tertiary volcanic rocks and shallow igneous intrusions are eroded to expose the Paleozoic window. The most ubiquitous volcanic rock exposed at Scraper Springs is a felsic, ash-rich tuff, labeled throughout the study as Tvt. On most of the property, this unit is commonly bleached and locally altered with a quartz-stockwork and/or silicified breccia and is therefore difficult to ascribe to regional tuff units. Locally, fine quartz and sanidine are observed as phenocrysts (5-10%) with rare hornblende and plagioclase; cherty lithic fragments derived from the underlying Paleozoic sedimentary rocks also occur within Tvt (Howell, 2004; present study). More phenocryst-rich tuffs and moderately-welded lithic fragments are observed in the potassic alteration zone, mapped in the present study. A more detailed description of these characteristics follows. Regional tuff units from Nelson Creek (Tnc) and Big Cottonwood Canyon (Tbcc) have been dated at 40.23 ± 0.11 Ma for Tnc at Tuscarora, 20 Km to the east of Scraper Springs and at 39.98 ± 0.09 Ma for Tbcc at the Willow Creek Reservoir, 15 Km to the southeast of Scraper Springs. It is thought that Tvt at Scraper Springs is likely one or both of these regional tuffs, therefore constraining the age of Tvt to around 40 Ma (Henry, 2008). Petrographic observations from this study follow, suggesting the presence of at least the Nelson Creek tuff. Tvt is the host

in both mapped breccia zones and the Rebel fault zone, where high-level quartz veins and quartz breccias are exposed at the surface.

Two plugs of an Eocene intrusive rock are exposed in the central map area. Originally, the intrusion was classified as a granodiorite with phaneritic to locally porphyritic textures (Howell, 2004). In this original description, plagioclase, alkali feldspar, biotite, and hornblende were interpreted as phenocrysts. Later observations concluded that the intrusion was plagioclase-rich with minor (<10%) quartz and little alkali-feldspar (Wise, 2008b). The present study documents elements from both observations: alkali feldspar and biotite occur within this intrusion, but as potassic alteration products, and plagioclase with limited quartz dominate the unaltered intrusive assemblage. Therefore, the Eocene intrusion is a diorite (Td). A K-Ar date of 38.9 ± 1.0 Ma, recorded from unaltered biotite from the south stock constrains the age of Td (Wallace, 2005). Potassic alteration is documented in both the north and south stocks and an endoskarn assemblage is present in the north stock (Howell, 2004; Wise, 2008b). A propylitic alteration overprint is observed throughout the Td intrusive. Alteration assemblages within Td are discussed in the section on alteration.

Tertiary andesite flows (Tva) overlie Td and Tvt (Fig. 3). Tva occurs as mostly porphyritic volcanic rocks with plagioclase, hornblende, quartz, and local pyroxene phenocrysts (Howell, 2004). Exposures of Tva are olive-green to olive-tan and form both subcrop and prominent outcrops throughout the property. Tva is mostly unaltered to locally propylitically altered, and unweathered rock appears greenish-blue. In these propylitic assemblages, chlorite books are visible with the naked eye and disseminated pyrite (1-2%) is visible with a hand lens. Local alteration within Tva suggests mineralization is younger than these flows. A $^{39}Ar/^{40}Ar$ date of 37.23 ± 0.1 Ma has been attributed to correlative andesites to the south of the Scraper Springs

property (Howell, 2004). Therefore mineralization at Scraper Springs likely postdates both the diorite at 38.9 ± 1.0 Ma and the andesite at 37.23 ± 0.1 Ma.

In the western part of the property, Miocene volcanics related to the Northern Nevada Rift are exposed in high, prominent cliffs. In Figure 3 they are mapped as Tvxt and include crystalline and glassy pumice-rich ash-flow tuffs, thin vitrophyres, and tuffaceous volcaniclastics (Howell, 2004). These units are undifferentiated and not mapped in detail in the present study, as Eocene events are the primary focus of this study.

Quaternary deposits overly these geologic units. Quaternary units include alluvium (Qal) and colluvium (Qol).

Field Mapping – This Study

Geologic units mapped in both stock-and-breccia zones include Ovi and Oviq, Td, Tqs (north stock only), tuffisite breccia (Tt), purple breccia (Tpbx) (south breccia zone only), advanced argillic breccia (Tabx) (north breccia zone only), heterolithic breccia (Thbx), orange breccia (Tobx) (south breccia zone only), resinous breccia (Trbx) (north breccia zone only), white breccia (Twbx), and hematite breccia (Thmbx) (north breccia zone only) (Figs. 4 and 5). The breccia units are ordered in sequence based on observed cross-cutting field relationships. Tva, Qal, and Qol units are mapped in the vicinity of these areas, but since they were deposited after the hypothesized mineralizing event, were not considered in the detailed mapping.

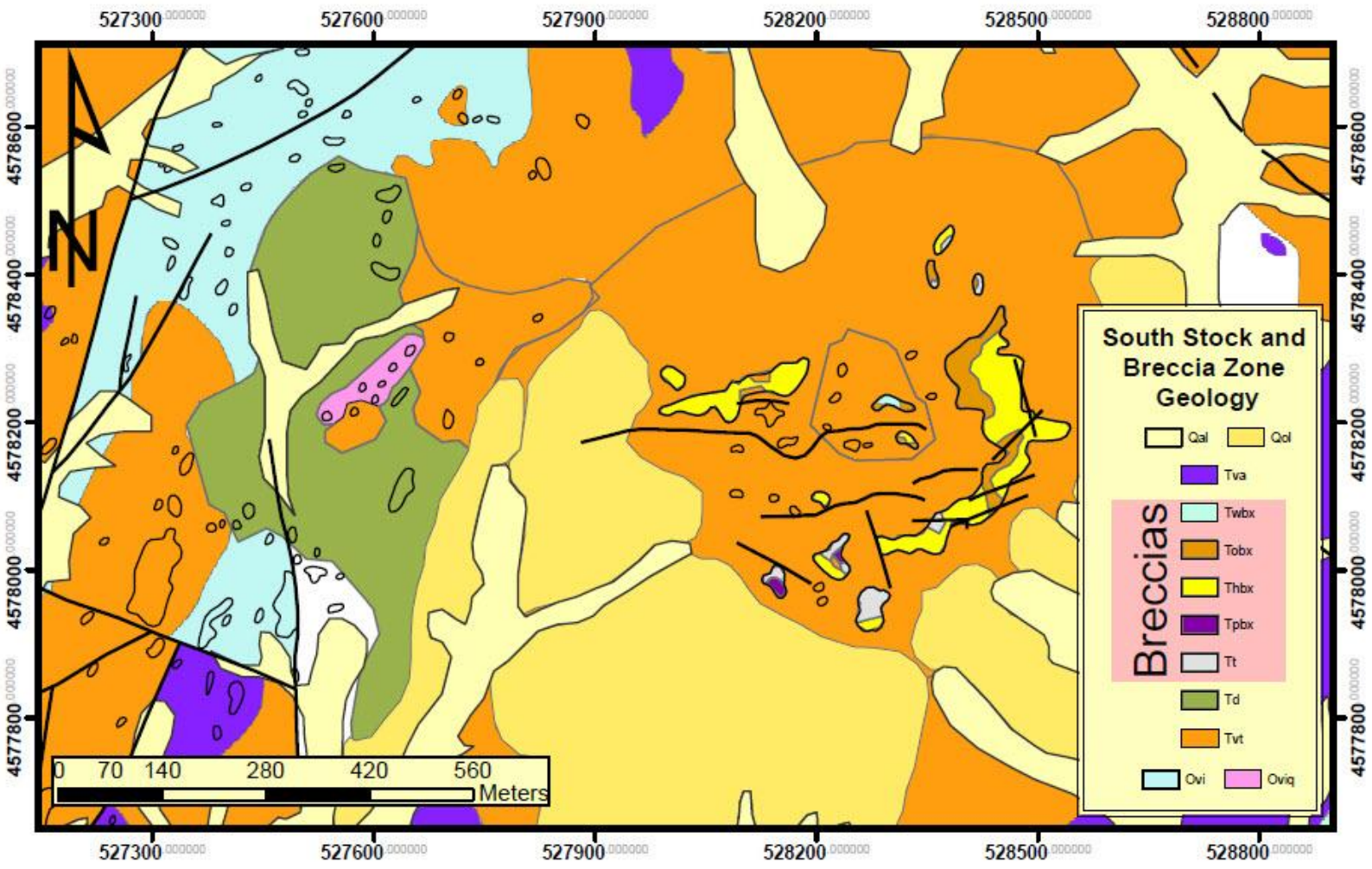

Figure 4. Geologic map of the South Stock and Breccia zone with outcrops encircled. In this area of the Scraper Springs property, the main Td intrusive unit is exposed adjacent to the south breccia zone, an area of prominent outcrop due to significant quartz-related alteration. In this breccia zone, five separate types of breccia occur and are positioned within the pink box labeled "Breccias" according to cross-cutting relations observed in the field. The text provides descriptions of each unit.

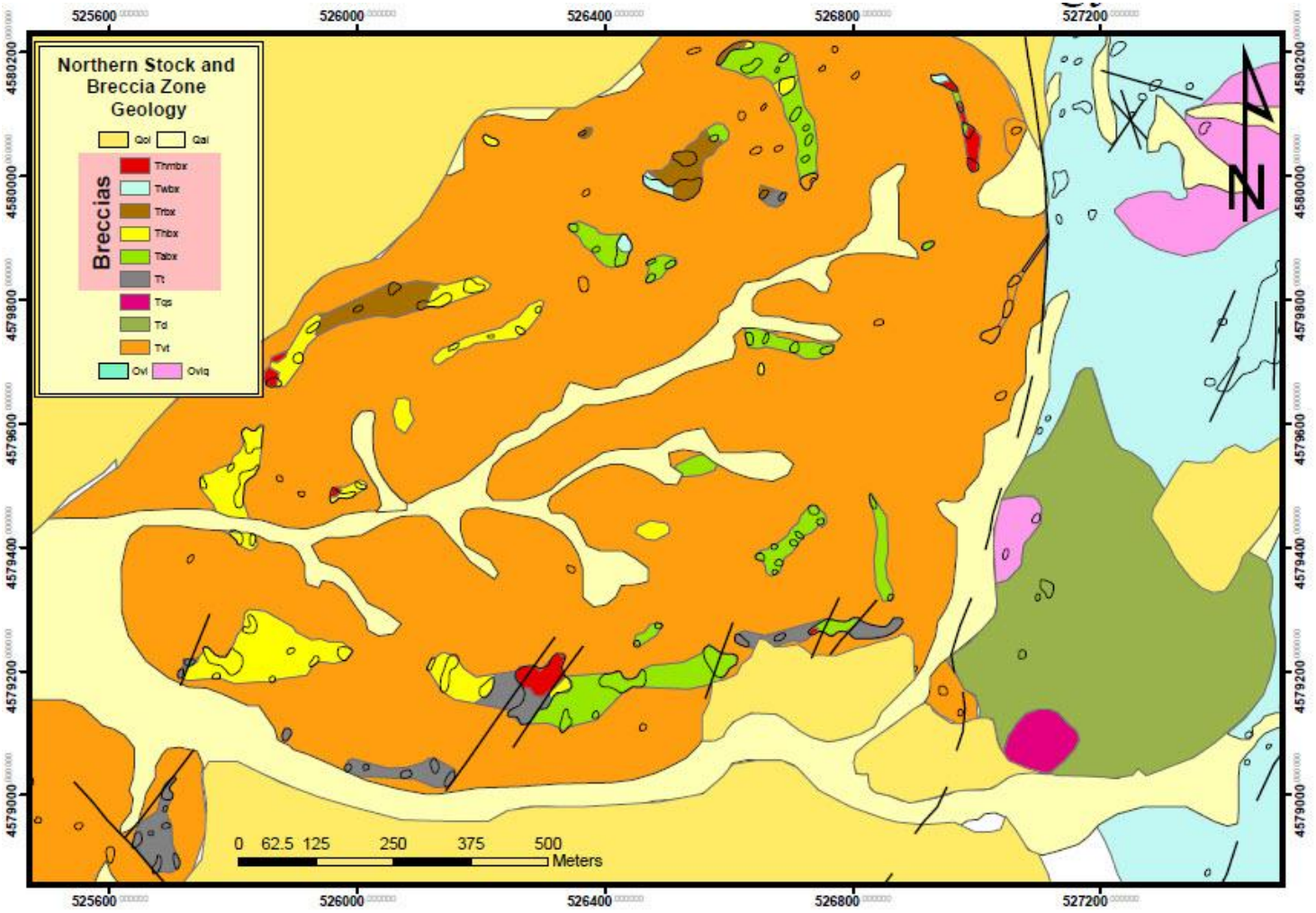

Figure 5. Geologic map of the North Stock and Breccia zone. In this area of the Scraper Springs property, the main Td intrusive unit is exposed adjacent to the north breccia zone, an area of prominent outcrop due to significant quartz-related alteration. In this breccia zone, six separate types of breccia occur and are positioned within the pink box labeled "Breccias" according to cross-cutting relations observed in the field. Lithologic descriptions of each unit are embedded within the text. In addition to the stock, mapped as Td, a later plug of quartz syenite (Tqs) is also present.

A. SC-03-55 – Brecciated Oviq demonstrates both hematite-matrix and clast-support, north stock (NS).

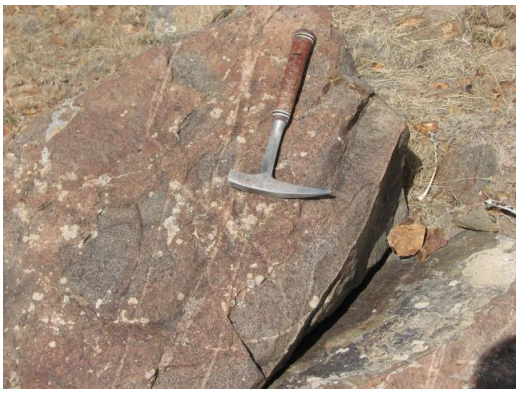

D. SC-02-52 – Td with K-feldspar stockwork veining, strong K-alteration, SS.

B. SC-02-32 – Parallel K-feldspar veinlets cross-cutting Td, strong K-alteration, south stock (SS).

E. SC-03-10 – K-feldspar veining overprinting endoskarn alteration, north stock (NS).

C. SC-02-35 – Td with stockwork K-feldspar veining, strong K-alteration, SS.

F. SC-03-13 – K-feldspar veinlet with K-feldspar flooding in Td, NS.

Figure 6. Field photos from the north (NS) and south stock (SS) zones. Photos exhibit potassic alteration within Td and alteration observed within Oviq.

Oviq

Oviq mapped in both the north and south stocks consists of fine- to coarse-grained clean quartz sandstone, as described in the previous section. In both north and south stocks, Oviq is commonly brecciated with a clast-supported matrix. Locally, the breccia is matrix-supported and hosts sub-angular to sub-rounded quartzite clasts 0.5 – 6 cm in length (Fig. 6A). It is unclear from field relationships whether this brecciation is a result of hydrothermal events or tectonic events, though a fault is mapped just to the east of this Oviq exposure, suggesting probable tectonic brecciation.

Td

Td mapped in both the north and south stocks consists mostly of plagioclase laths, 2-4 mm in length. A small amount of quartz (~ 5%) is present in the matrix, but is not obvious in hand specimen. Hornblende occurs as disseminated grains throughout the matrix between 5-10%, but is mostly altered to epidote due to the propylitic overprint in both north and south stocks. In the south stock, several prominent outcrops exhibit stockwork veining. Sodium-cobaltinitrite staining revealed that these veins are alkali feldspar veins. These K-feldspar veins occur in both parallel (Fig. 6B) and stockwork (Figs. 6C, D) fracture patterns. In the north stock, where less prominent outcrop was available, only stockwork K-feldspar veins were observed (Figs. 6E, F). Additionally, K-feldspar flooding forms cm-scale selvages adjacent to these veinlets (Fig. 6F). In the field, K-feldspar-rich zones form leucocratic rinds adjacent to veinlets in Td units. On unweathered surfaces in these zones, biotite occurs in small clots 2-8 mm in length, observable with the naked eye and with a hand lens. From these field observations, a potassic alteration signature was hypothesized. Na-cobaltinitrite staining, discussed in the

following section on alteration, confirms variable potassic signatures in both the north and south stocks.

Tqs

A small quartz syenite intrusion, Tqs, previously mapped as unaltered granodiorite (Howell, 2004; Wise, 2008a), is exposed in the southwest corner of the north stock. Tqs forms low subcroppings in a gully. The quartz syenite rock is equigranular and locally pegmatitic. Within the equigranular texture, K-feldspar phenocryts are 2 mm – 8 mm and comprise between 90-93% of the rock. The remaining groundmass is occupied by quartz grains 2 mm – 5 mm. In the pegmatitic texture, K-feldspar phenocrysts are tabular and around 1 cm in length, with local variations up to 4 cm long. Quartz in this coarser texture is observable in about 0.5 cm phenocrysts. Additionally, granophyric textures are observable in thin section (Figure 12U, V).

Tt

In both the north and south breccia areas, a unit of tuffisite, Tt, a sub-volcanic lithology, occurs along structures in association with other breccias. Tt is also locally brecciated. Based on the nature of Tt, and its subsequent alteration, it is often difficult to determine which outcrops are strictly tuffisite and which are tuffisite breccias. Commonly, Tt includes fine-grained, leucocratic and ashy material that is locally silicified (Fig. 7E). Distinct sub-rounded cherty clasts, 2-4 mm, are included within this unit and likely represent material from the underlying Paleozoic stratigraphy. Locally, accretionary lapilli are present and are 1-2 mm spheroids (Fig. 7A). The presence of accretionary lapilli suggests fluidization of the tuffisite unit and emplacement at a high level within the volcanic-hydrothermal system.

A. SC-01-25 – Accretionary lapilli in tuffisite unit, advanced argillic zone, SBZ.

B. SC-01-21 – Vuggy clast in heterolithic breccia, advanced argillic zone, south breccia zone (SBZ).

C. SC-01-43 – Heterolithic breccia at margin between silicified zone and advanced argillic alteration zone, SBZ.

D. SC-01-75 – White breccia intrudes orange breccia at contact between two zones, SBZ.

E. SC-01-89A – Vuggy silica alteration in tuffisite, SBZ.

F. SC-01-128 – Heterolithic breccia with hematite matrix supporting orange breccia clasts, SBZ.

G. SC-04-08 – Advanced argillic breccia with silicified clasts, north breccia zone (NBZ).

H. SC-04-20A – Resinous breccia with silicified clasts, alteration is siliceous with FeOx staining, NBZ.

I. SC-04-63 – Tvt altered to advanced argillic, alunite-zunyite assemblage, NBZ.

J. SC-04-76 – Hematite-cemented breccia with advanced argillic - alunite assemblage clasts, NBZ.

K. SC-04-154 – Advanced argillic breccia with advanced argillic – alunite assemblage, iron oxide staining, NBZ.

L. SC-04-183 – Advanced argillic – kaolinite assemblage in Tvt unit, NBZ

Figure 7. Field photos from the north and south breccia zones. Different lithlogies are exhibited and cross-cutting relationships are documented, where applicable

Tpbx

The south breccia zone contains a purple breccia, Tpbx, that may also be considered sub-volcanic. Locally, Tpbx supports rounded, cherty clasts on the centimeter-scale, and is commonly vesicular. Mixing of the Tpbx occurs with the Tt unit, and along the contact between these two units there are inter-fingering, cross-cutting relationships. However, Tpbx contains clasts of Tt within its matrix near these contacts and it can be determined that it was emplaced after the Tt unit. It is likely that Tpbx is also a type of tuffisite unit, as it shares similar characteristics as Tt, including a close spatial relationship. See Table 1 for comparison to other breccias.

Tabx

A distinctive advanced-argillic breccia (Tabx) occurs within the north breccia zone and is easily recognized by its intense goethite-jarosite staining (Figs. 7K, L; Table 1). It is both matrix- and clast- supported and contains clasts of vuggy silica and various advanced argillic assemblages. Clasts are sub-angular to angular and range in size from 2 mm up to about 1 cm.

Thbx

In the north and south breccia zones, a ubiquitous, heterolithic breccia (Thbx) occurs. This was described in the field as a breccia with sub-rounded to sub-angular clasts comprised of various lithologies. Commonly, these clasts are derived from other breccia types indicating multi-stage development. Acid sulfate breccia and vuggy silica clasts are common in this lithology (Figs. 7B, C, F; Table 1). Additionally, most exposures of Thbx contain some variety of iron oxide staining. In the south breccia zone, hematite-staining throughout the matrix is common (Figs. 7F) and in the north breccia zone, goethite and other iron oxide residues commonly pervade Thbx.

Trbx

A similar unit to the heterolithic breccia is the resinous breccia, Trbx. Like Thbx, Trbx contains variably-sized sub-rounded to sub-angular clasts. However, unlike Trbx, most of these clasts are silicified or altered to vuggy silica and do not exhibit obvious advanced argillic clasts. Most of the resinous breccia is clast-supported with pervasive iron-oxide staining, giving the outcrops a brownish-resinous luster (Fig. 7H; Table 1).

Tobx

Tobx, orange breccia, is observed in several locations within the south breccia zone. The orange breccia is mostly matrix-supported and contains rounded to sub-rounded breccia clasts between 2 mm and 1 cm in diameter. Most of the alteration associated with Tobx is siliceous with a distinctive area on the eastern part of the map displaying an advanced argillic-jarosite stained signature. It is associated with the white breccia, Twbx, which cross-cuts it in one prominent outcrop located in the relative center of the south breccia zone (Fig. 7D; Table 1).

Twbx

In the south zone, a white breccia, Twbx, is spatially associated with Tobx and distinctly cross-cuts it (Fig. 7D; Table 1). It has similar characteristics to Tobx including matrix-support and rounded to sub-rounded clasts of 2 mm to 1 cm in diameter. However, Twbx contains clasts of Tobx and is almost always associated with massive silicification or vuggy silica alteration. These massively silicified outcrops are more prominent in the north breccia zone.

Thmbx

A breccia with a hematite-stained matrix, Thmbx, is observed in various locations throughout the northern breccia zone (Fig. 7J; Table 1). Thmbx occurs as distinct outcrops up to 50 m in length, but more commonly occurs as small 0.5 – 6 m zones as cross-cutting breccia

pipes and offshoots in other breccias. Most Thmbx exposure contains rounded breccia clasts, with the hematite-matrix as the supporting material, including advanced argillic clasts of various advanced argillic assemblages, secondary breccia clasts, and vuggy silica clasts. In the south-central portion of the northern breccia zone, Thmbx is located between two known faults, cross-cutting several different lithologies (Fig. 4).

Breccia Name	Geometry	Clast types	Clast Sizes (cm)	Rounding	Matrix vs. Clast Supported	Matrix Type	Alteration
Thmbx	Blocky, fingers	Vuggy silica, Acid sulfate bx	Variable	Rounded	Matrix	Hematite-silica	Acid Sulfate
Twbx	Dikes, fingers	Vuggy silica, Acid sulfate bx	0.02 - 2.0	Rounded to sub-rounded	Matrix	Silica	Silicification
Tobx	Blocky	Vuggy silica, Acid sulfate bx	0.02 - 2.0	Rounded to sub-rounded	Matrix	Goethite-Jarosite	Acid Sulfate
Thbx	Massive	Vuggy silica, Acid sulfate bx	0.2 - 10.0	Rounded	Matrix	Hematite-silica	Silicification
Tabx	Dikes, fingers	Silica, earlier breccia	0.02 - 1.0	Sub-angular to angular	Both	Alunite-Cristobalite	Acid Sulfate
Trbx	Massive	Vuggy silica	Variable, some ~ 1.0 m	Sub-rounded to sub-angular	Clast	Goethite-silica	Silicification
Tpbx	Dikes, fingers	Chert, tuffisite	0.2 - 2.0	Rounded	Matrix	Silica	Vuggy Silica

Table 1. List of breccia types associated with different bodies and alteration styles observed in the North and South Breccia Zones.

Alteration Mapping

Alteration zones (Figs. 8 and 9) include endoskarn (north stock only), potassic zones of moderate potassic alteration (15-29% K-feldspar), strong potassic alteration (30-50% K-feldspar), and K-feldspar flooding (>50% K-feldspar, restricted to Tqs) (north stock only), hematite-stained breccia in Oviq, silicification, reticulate quartz (north breccia zone only), vuggy silica, undifferentiated advanced argillic alteration, advanced argillic – jarosite- and hematite-stained, advanced argillic – alunite, advanced argillic – alunite-zunyite (north breccia zone only), advanced argillic – zunyite (north breccia zone only), advanced argillic – pyrophyllite-diaspore (north breccia zone only), advanced argillic – kaolinite (north breccia zone only), advanced argillic with late chalcedony (south breccia zone only), hematite-staining, and various argillic-advanced argillic bleaching, which was undifferentiated due to lack of outcrop.

.

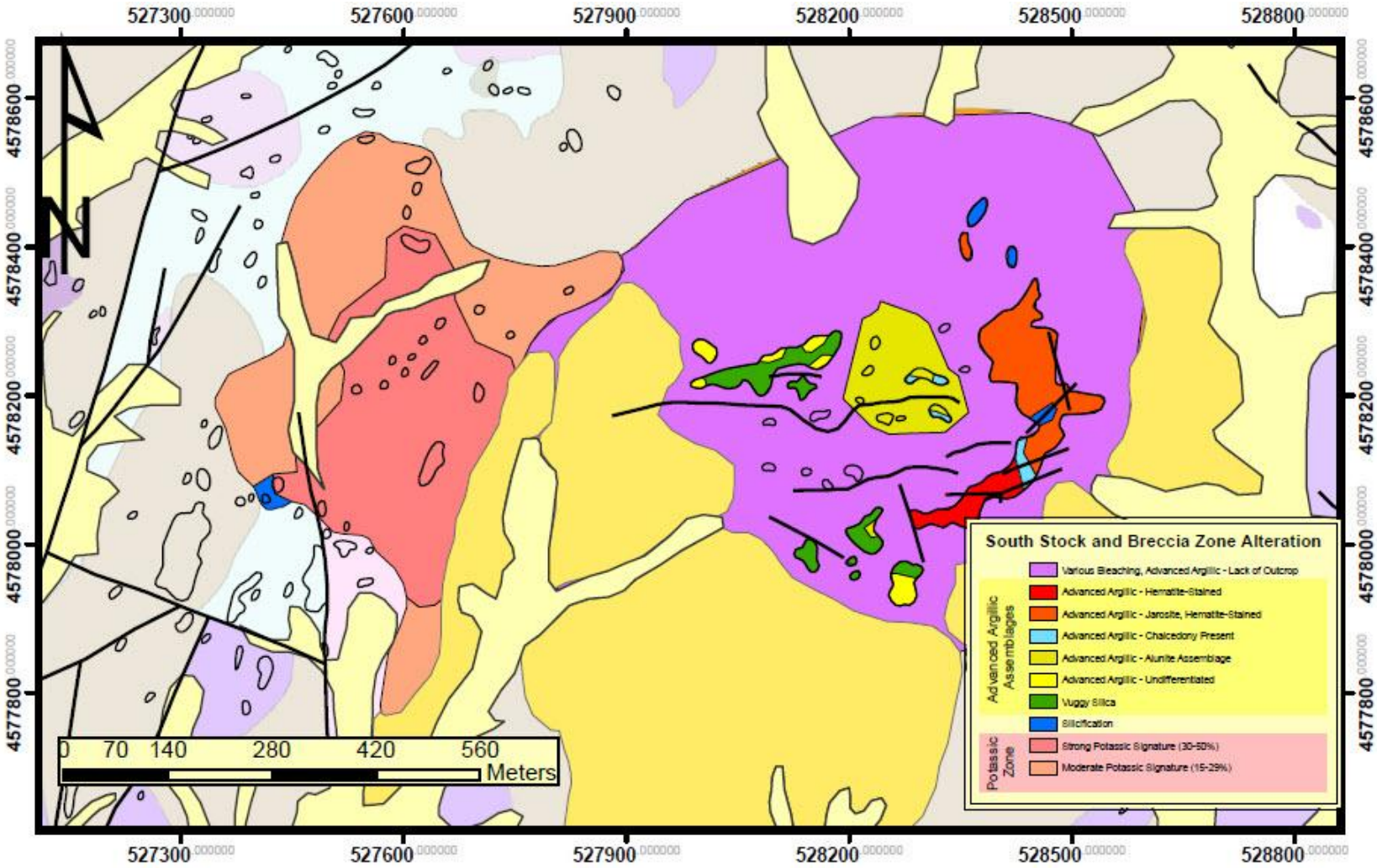

Figure 8. South Stock and Breccia Zone Alteration map. Mapping covered the south stock, Td, and the south breccia zone. A strong potassic signature covers the south stock area, which also pervades into the Tvt unit. Potassic alteration was first documented in the field and zones were separated based on degree of alteration observed from Na-cobaltinitrite staining. Similarly, advanced argillic alteration in the breccia zone was mapped as wide-spread in the field, but separated into the different alteration types based on petrography.

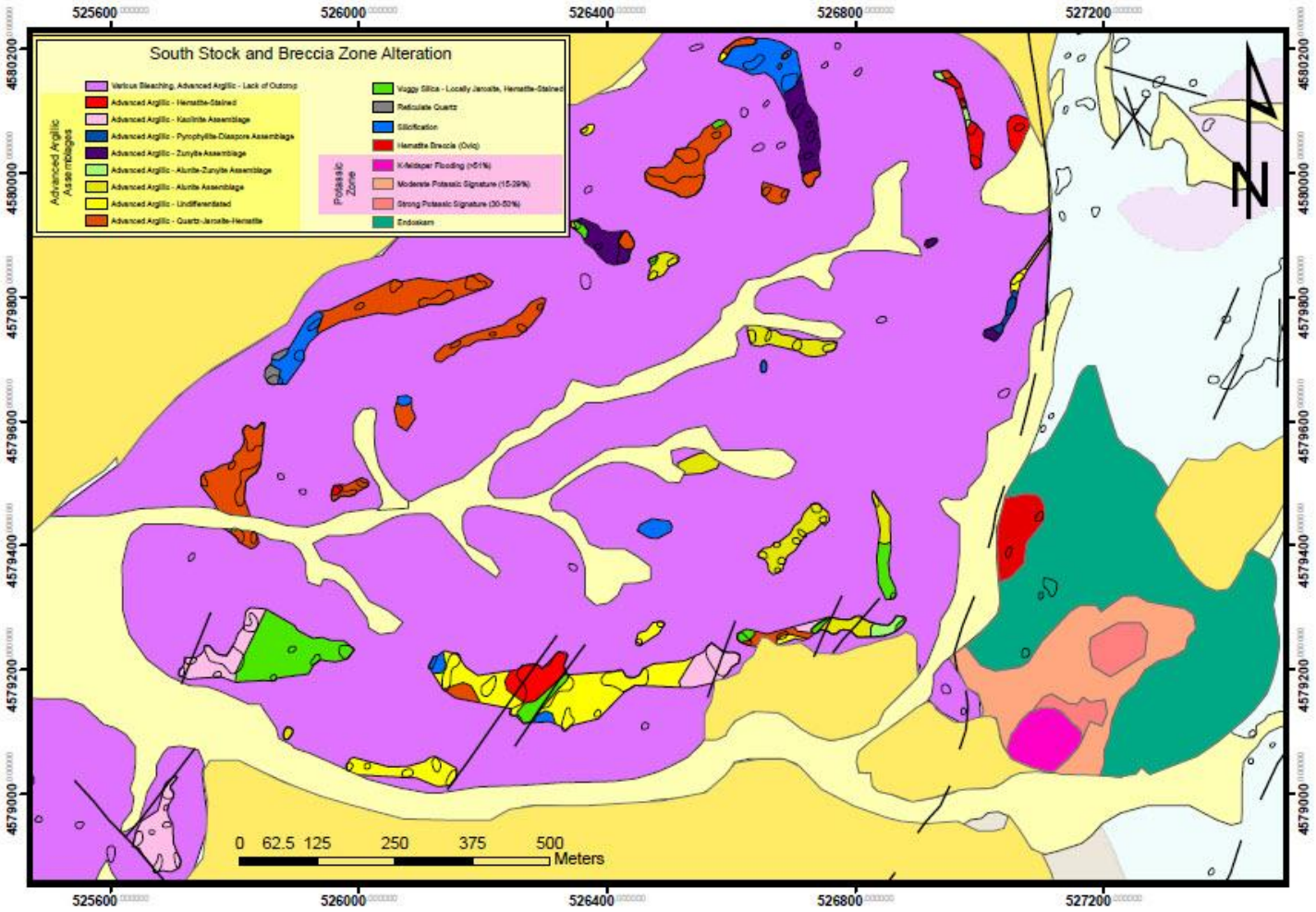

Figure 9. North Stock and Breccia Zone Alteration map. Mapping covered the north stock, Td and Tqs, and the north breccia zone. A strong potassic signature covers the north stock area. Potassic alteration was first documented in the field and zones were separated based on degree of alteration observed from Na-cobaltinitrite staining. Similarly, advanced argillic alteration in the breccia zone was mapped as wide-spread in the field, but separated based on preliminary petrography.

Endoskarn Alteration

Endoskarn alteration was first identified in maps by Howell (2004) and Wise (2008a). In the field, endoskarn assemblages were identified by greenish-bluish color and their noticeably coarsely crystalline nature. This assemblage is characterized by the presence of pyroxenes aligned in bands, visible with the naked eye and hand lens, and quartz. Additionally, Na-cobaltinitrite staining reveals a potassic overprint of endoskarn alteration as documented in Figure 10H. Endoskarn alteration is pervasive in the north stock only and exists in most of the north stock, including the potassic alteration zones. The only place it is not documented is within the Tqs unit, which is dominantly K-feldspar.

Potassic Alteration

Potassic alteration was preliminarily identified in the field based on the presence of leucocratic Td outcrop. The nature and pervasiveness of this style of alteration was confirmed through Na-cobaltinitrite staining and petrography. Weak (15-29% K-feldspar) to strong (30-50% K-feldspar) K-alteration exists in the Tvt unit (Figs. 10A, B), which is identified based on flattened pumice fragments due to welding within the ash-flow tuff. Additionally, potassic alteration is observed within the two main Td stocks, with a mostly strong K-alteration signature,

A. SC-02-14 – Tvt, weak K-alteration, SS.

B. SC-02-20 – Tvt, strong K-alteration, SS.

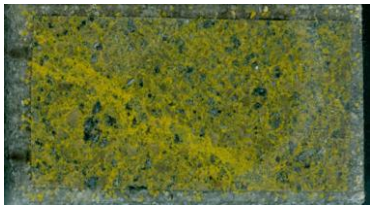

C. SC-02-36 – Td, strong K-alteration w. k-feldspar veinlet.

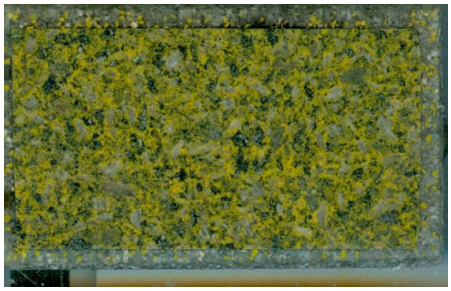

D. SC-02-44 – Td, strong K-alteration, SS.

E. SC-02-75C – Silicification in Td, SS.

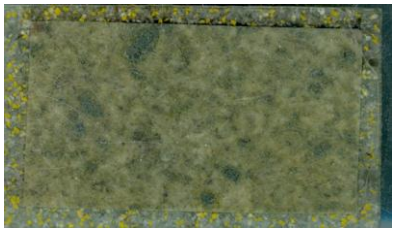

F. SC-03-01 – Td with endoskarn alteration, north stock (NS).

H. SC-03-10B – Td, endoskarn w/ K-alteration overprint, NS.

I. SC-03-21 – Tqs, K-feldspar-rich quartz syenite, NS.

J. SC-03-68B – Td, weak K-alteration, NS.

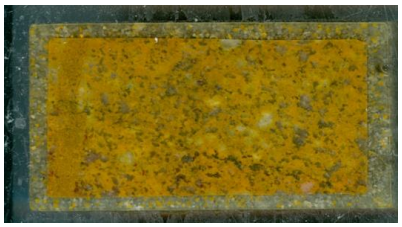

K. SC-03-69 – Td, strong K-alteration, NS.

Figure 10. Na-cobaltinitrite staining in thin-section billets.

including K-feldspar veinlets and K-feldspar flooding (Figs. 6B-D; Figs. 10C, D, K). A weaker K-alteration signatures is documented in Figure 10J. Pervasive K-feldspar flooding is observed in Tqs (Fig. 10I). In the southwest portion of the south stock, there are several outcrops that do not exhibit potassic alteration, but are rather characterized by silica-flooding, which is described in the following section (Fig. 10E).

Silicification

Silicification occurs in various forms in both north and south breccia zones and as mentioned above, in the southwest portion of the south stock. Silicification occurs in massively silicified outcrops in both breccia zones and is exhibited in various breccia clasts in other alteration areas. Vuggy silica is also another common alteration type, which is commonly associated with the advanced argillic assemblages; in most cases it occurs within the advanced argillic assemblages, overprinted by various advanced argillic minerals. An interesting silicification type is the reticulate quartz assemblage, which occurs only in a few outcrops in the north stock. Here, the reticulate quartz assemblage is intimately associated with hematite-stained rocks and appears to be a late alteration signature. This is covered in further detail in the petrography section. Additionally, one exposure of Td on the western margin of the South Stock exhibits pervasive silicification.

Advanced Argillic Assemblages

Various advanced argillic assemblages occur throughout both the north and south breccia zones. Most advanced argillic assemblages overprint vuggy silica or at least host some vuggy silica clasts, suggesting these assemblages post-date the original vuggy silica event. The more common advanced argillic assemblages that overprint vuggy silica alteration and occupy quartz

vugs include alunite, alunite-zunyite, and zunyite assemblages. These assemblages are commonly accompanied by hematite, jarosite, and other Fe-oxide and –sulfate secondary minerals. In one series of outcrops in the eastern portion of the north breccia zone, a high-temperature, high-acid pyrophyllite-diaspore assemblage is recorded. One of the later advanced argillic assemblages observed is the kaolinite assemblage, which occurs only in the north breccia zone. The kaolinite observed here occupies quartz vugs and also occurs in veinlets cross-cutting breccias and supporting breccias. It is common for the kaolinite assemblage to overprint alunite. Indistinctive advanced argillic assemblages occur in both the north and south breccia zones and are commonly characterized by Fe-oxide and Fe-sulfate staining. These typically correspond with some of the matrix-supported breccias and include the jarosite-hematite assemblage and hematite-staining assemblage. In these assemblages, clasts of earlier advanced argillic alteration are commonly observed. In the south breccia zone, there is a distinct signature of chalcedony that overprints earlier advanced argillic alteration. Here, chalcedony is observed as cross-cutting veinlets at the outcrop scale, but also in quartz vugs and along veinlet margins in thin section. A more detailed discussion of these advanced argillic assemblages follow in the petrography section.

Petrography

The following mineral paragenesis was based on petrography of 116-thin sections in all four mapped zones at Scraper Springs. The following table summarizes the minerals observed in thin section (Table 2).

Mineral	Formula	Alteration Assemblage	Mineral	Formula	Alteration Assemblage
Quartz	SiO_2	Silicification	Plagioclase (An_{45})	$Ca_2Al_2Si_2O_8$	Primary Mineral
Cristobalite	SiO_2	Acid Sulfate	Hornblende	$Ca_2(Fe_4Al)(AlSi_7O_{22})(OH)_2$	Primary Mineral
Chalcedony	SiO_2	Acid Sulfate	Anatase	TiO_2	Propylitic, Oxidation, Various
Alunite	$KAl_3(SO_4)_2(OH)_6$	Acid Sulfate, Supergene	Actinolite	$Ca_2(Mg,Fe)_5(Si_8O_{22})(OH)_2$	Propylitic
Barite	$BaSO_4$	Acid Sulfate	Epidote	$Ca_2Al_2(Fe,Al)(SiO_4)(Si_2O_7)O(OH)$	Propylitic
Fluorite	CaF_2	Acid Sulfate	Chlorite	$(Mg,Fe)_5Al(AlSi_3O_{10})(OH)_8$	Propylitic
Topaz	$Al_2SiO_4(F,OH)_2$	Acid Sulfate	Calcite	$CaCO_3$	Propylitic, Argillic
Zunyite	$Al_{13}Si_5O_{20}(OH,F)_{18}Cl$	Acid Sulfate	Pyrite	FeS_2	Propylitic, Acid Sulfate
Pyrophyllite	$Al_2Si_4O_{10}(OH)_2$	Acid Sulfate	Apatite	$Ca_5(PO_4)_3(OH,F,Cl)$	Potassic
Diaspore	$AlO(OH)$	Acid Sulfate	Sphene	$CaTiOSiO_4$	Potassic, Acid Sulfate
Kaolinite	$Al_2Si_2O_5(OH)_4$	Acid Sulfate, Supergene	Rutile	TiO_2	Potassic, Acid Sulfate
Illite	$(KH_3O)(Al,Mg,Fe)_2(Si,Al)_4O_{10}(OH)_2(H_2O)$	Argillic	Biotite	$KFe_3Al_2Si_2O_{10}(OH)_2$	Potassic
Jarosite	$KFe_3(SO_4)_2(OH)_6$	Oxidation, Supergene	Orthoclase	$KAlSi_3O_8$	Potassic
Hematite	Fe_2O_3	Oxidation, Supergene	Sericite	$KAl_3Si_3O_{10}(OH)_2$	Sericitic

Table 2. List of all minerals observed in thin section in the present study. Chemical formulas derived from Black and Mandarino (2008). Each mineral is classified and grouped into an associated alteration assemblage based on a classic porphyry-style deposit model. (*i.e.* Sillitoe, 2010).

Mineral Paragenesis

For each area studied (North and South Breccia zones, North and South stocks) a specific mineral paragenesis has been determined. The North and South Breccia zones both exhibit advanced argillic and acid sulfate alteration, but vary slightly in terms of mineral assemblages and abundance of certain minerals. Although the differences between the two breccia zones are slight, the occurrence and timing of similar minerals requires separate paragenetic diagrams to be constructed. Both the North and South Stocks have similar minerals as well, but follow a similar progression of mineralization and alteration patterns. The main difference between both exposures of diorite is that the South Stock contains significant epidote mineralization, whereas the north stock exhibits actinolite in place of epidote. This difference can be attributed to zoning within the propylitic alteration suite, with actinolite representing a more proximal and epidote a more distal alteration mineral (*i.e.* Sillitoe, 2010). A detailed analysis of this zoning pattern follows in the discussion.

The Rebel fault zone exhibits an entirely different alteration assemblage. These quartz-rich veins and breccias are sericite- and pyrite-rich, representing a low-sulfidation epithermal

alteration style. However, there is no paragenetic sequence developed for the Rebel fault zone due to the fact that it falls outside the main focus of the study.

North and South Stocks

The north and south stocks exhibit mineralization consistent with the classic porphyry model (Sillitoe, 2010). A full paragenesis is represented schematically in Figure 11 with photomicrographs documenting cross-cutting relationships in Figure 12. Primary minerals within the diorite (Td) intrusion include plagioclase (An_{45}), hornblende, biotite, and quartz. Accessory minerals are minor or obscured through alteration. Most of the diorite exposed is equigranular, but porphyritic textures are observed near the margins of the stocks, particularly evident in the South Stock (Figs. 8 and 12A). Crystallization of primary minerals within the diorite melt generally follows the sequence larger plagioclase phenocrysts and hornblende, followed by euhedral biotite, and final interstitial quartz filling remaining open spaces. These textures can be seen readily in Figure 12 and are particularly clear in Figures 12A, 12F, and 12O. Due to pervasive potassic alteration assemblages overprinting primary melt crystallization, it can be unclear which minerals are primary and which are secondary.

Potassic alteration in both stocks is exhibited through several different styles of mineralization. Most obviously orthoclase veins form stockworks in local areas (seen in Figs. 12C-F). Orthoclase veining tends to be in stockwork patterns and occurs as veinlets, approximately 50 to 100 microns in width. Veining tends to be more obvious in the porphyritic diorite. In more equigranular diorite, orthoclase veining is less obvious, but occurs in grungy selvages several millimeters wide (seen in SC-02-36, Fig. 12G). The groundmass is flooded with orthoclase in both porphyritic and equigranular diorite wherever it is potassically altered (Fig. 12A-G).

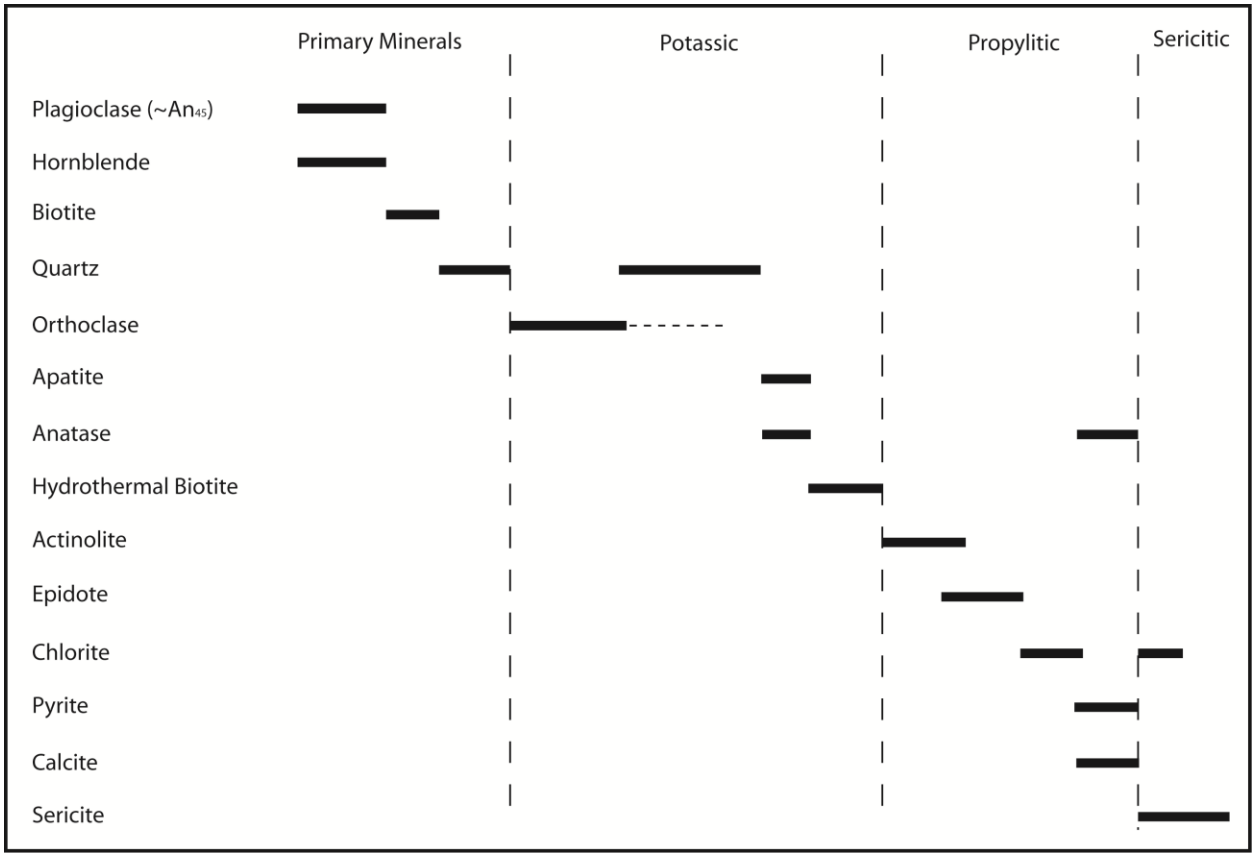

Figure 11. Paragentic diagram for the north and south stocks. See text for full discussion.

In local areas in both the north and south stock, silicification overprints orthoclase veining, flooding, and replacement of plagioclase rims. This is seen most prominently in sample SC-02-75C, where most of the groundmass is flooded with quartz. Relict phenocrysts of plagioclase are rimmed by orthoclase, but overprinted by quartz (Figs. 12H, I). Silicification occurs locally and is only seen in a few examples (Fig. 8). Also associated with potassic alteration assemblages are euhedral apatite phenocrysts, which selectively replace the cores of relict plagioclase grains altered to orthoclase (Figs. 12J, L). Additionally, fine-grained (less than 10 microns) masses of anatase tend to rim relict plagioclase and occur through the groundmass (Figs. 12K, R).

Late within the potassic alteration assemblage, hydrothermal biotite occurs as veins and clotted aggregates within the groundmass, replacing primary hornblende, biotite, and other minor Fe-Mg minerals. Most hydrothermal biotite is altered to chlorite in the later propylitic assemblage. Biotite veining is best exhibited in the porphyritic diorite and follows earlier orthoclase veins (Figs. 12C-F). Elsewhere, ratty biotite veins are observed as altered to chlorite and cross-cut silicification after orthoclase flooding (Fig. 12R). Clots of ratty biotite occur within more equigranular diorite examples and represent replacement of hornblende aggregates (Fig. 12Q). Again, most of this biotite is altered to chlorite and also pyrite as part of the later propylitic assemblage.

Propylitization is obvious in both hand sample and thin section. Hand samples tend to exhibit a greenish hue, indicative of the greenish minerals actinolite, epidote, and chlorite. Actinolite occurs as a high-relief, cross-cutting mineral in the North Stock (Figs. 12M-P). Occuring at a similar time in the paragenesis is epidote, which forms outboard of the actinolite assemblage. It is observed locally in the North Stock, but pervasive in the South Stock where it replaces primary hornblende and also the cores of relict plagioclase altered to orthoclase (Fig.12L). Chlorite is present as a major constituent in both the North and South stocks and replaces both primary biotite (Fig. 12S) and hydrothermal biotite (Figs. 12C, D, Q, R). Pyrite also occurs in significant quantities within the propylitic assemblage, where it replaces hydrothermal biotite and other Fe-rich minerals. Pyrite occurs as euhedral crystals (Fig. 12T), but also in massive aggregates with Ti-oxide minerals (Fig. 12Q, T). Calcite is observed as a late replacement of plagioclase and other Ca-rich minerals, which occur at about the same time (Fig. 11) as pyrite (Figs. 12J, K).

Sericite locally overprints late propylitic assemblages. This alteration style is characterized by a complete replacement of relict plagioclase phenocrysts (Figs. 12S, T), and also as a fine-grained replacement of orthoclase groundmass (Fig. 11T). It is likely that this sericite-rich assemblage represents a transition from centrally-located porphyry alteration to a more distal assemblage transitioning into advanced argillic assemblages (Fig. 8; Sillitoe, 2010). Consideration of a porphyry-epithermal alteration transition follows in the discussion.

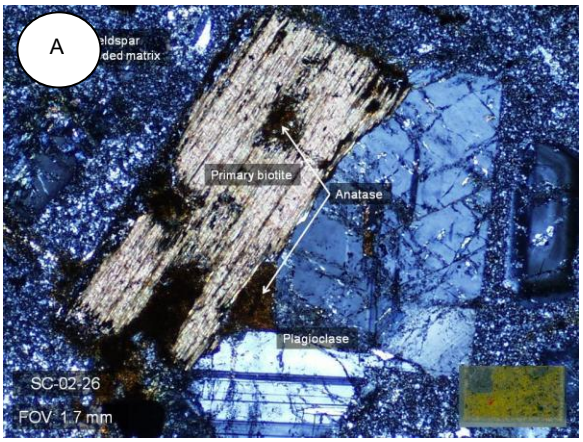
A
Primary biotite
Anatase
Plagioclase
SC-02-26
FOV: 1.7 mm

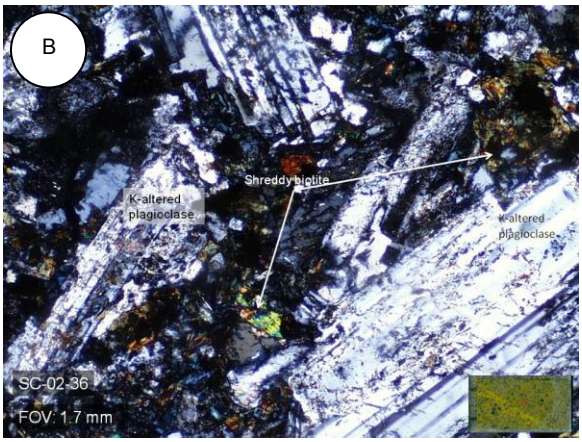
B
Shreddy biotite
K-altered plagioclase
K-altered plagioclase
SC-02-36
FOV: 1.7 mm

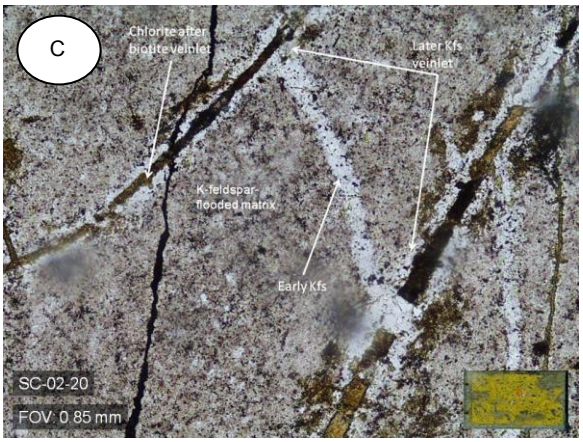
C
Chlorite after biotite veinlet
Later Kfs veinlet
K-feldspar-flooded matrix
Early Kfs
SC-02-20
FOV: 0.85 mm

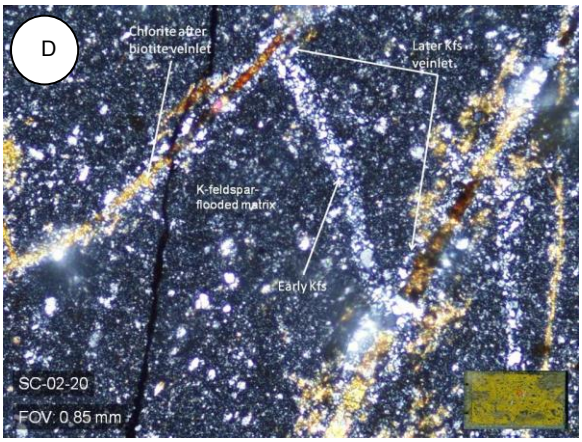
D
Chlorite after biotite veinlet
Later Kfs veinlet
K-feldspar-flooded matrix
Early Kfs
SC-02-20
FOV: 0.85 mm

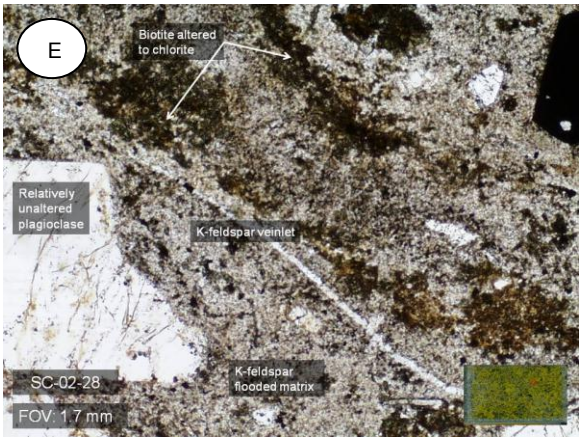
E
Biotite altered to chlorite
Relatively unaltered plagioclase
K-feldspar veinlet
K-feldspar flooded matrix
SC-02-28
FOV: 1.7 mm

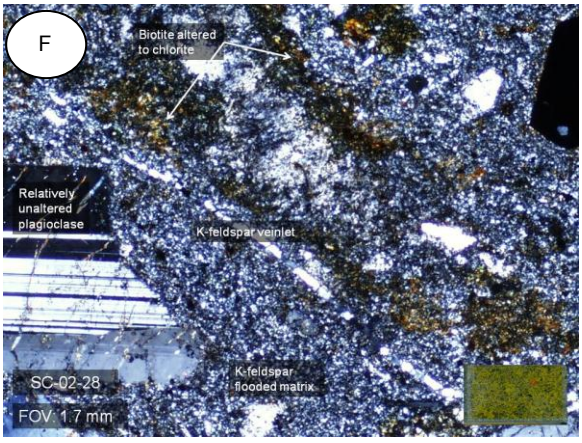
F
Biotite altered to chlorite
Relatively unaltered plagioclase
K-feldspar veinlet
K-feldspar flooded matrix
SC-02-28
FOV: 1.7 mm

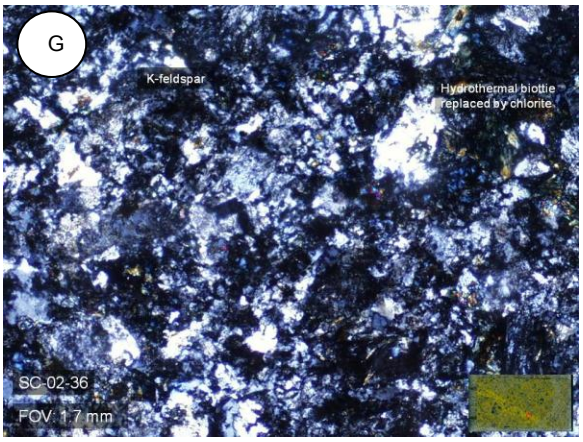
G
K-feldspar
Hydrothermal biottie replaced by chlorite
SC-02-36
FOV: 1.7 mm

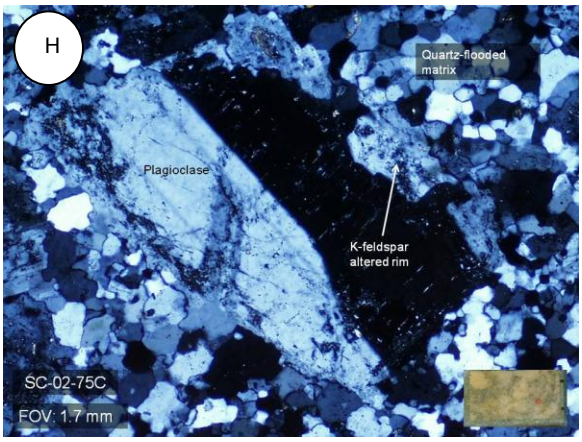
H
Quartz-flooded matrix
Plagioclase
K-feldspar altered rim
SC-02-75C
FOV: 1.7 mm

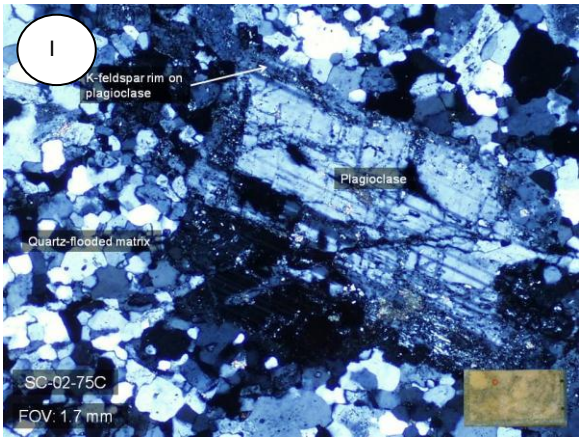
I
K-feldspar rim on plagioclase
Plagioclase
Quartz-flooded matrix
SC-02-75C
FOV: 1.7 mm

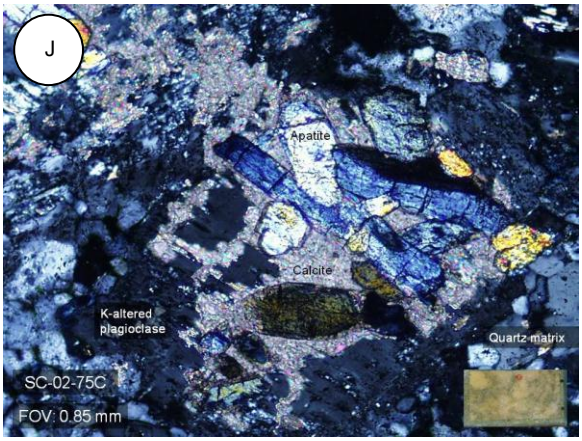
J
Apatite
Calcite
K-altered plagioclase
Quartz matrix
SC-02-75C
FOV: 0.85 mm

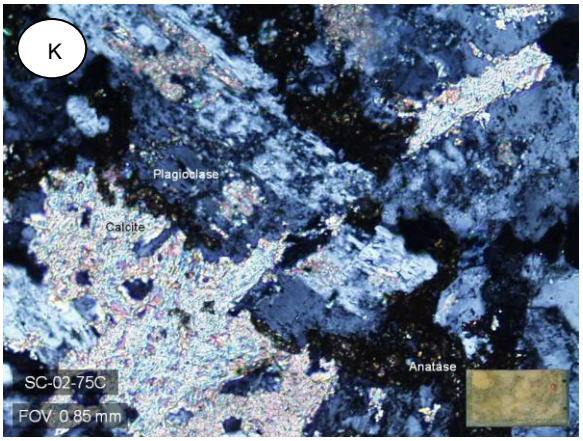
K
Plagioclase
Calcite
Anatase
SC-02-75C
FOV: 0.85 mm

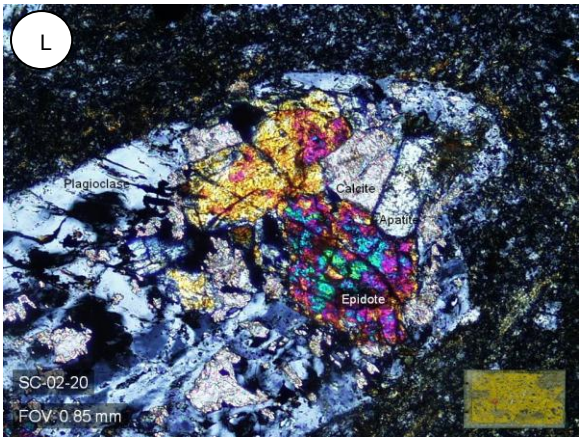
L
Plagioclase
Calcite
Apatite
Epidote
SC-02-20
FOV: 0.85 mm

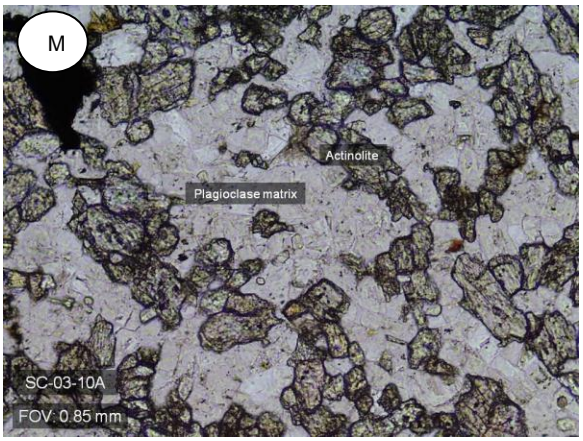
M
Actinolite
Plagioclase matrix
SC-03-10A
FOV: 0.85 mm

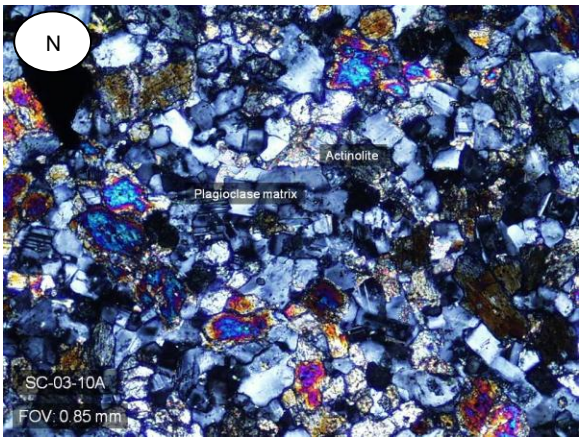
N
Actinolite
Plagioclase matrix
SC-03-10A
FOV: 0.85 mm

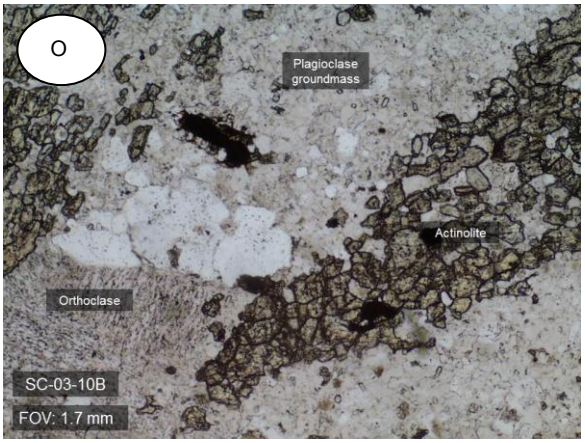
O
Plagioclase groundmass
Actinolite
Orthoclase
SC-03-10B
FOV: 1.7 mm

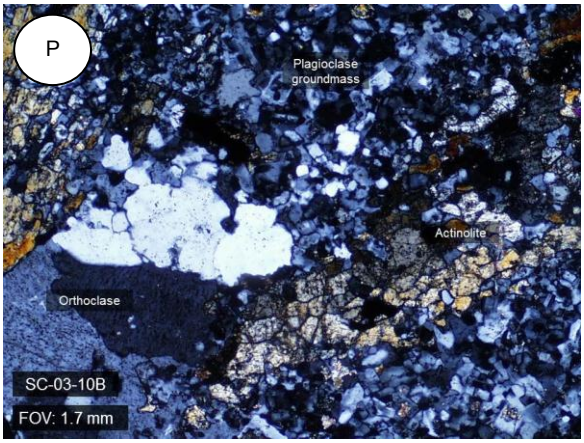
P
Plagioclase groundmass
Actinolite
Orthoclase
SC-03-10B
FOV: 1.7 mm

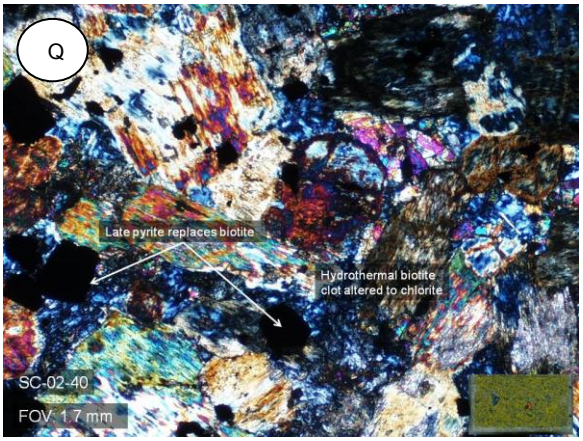
Q
Late pyrite replaces biotite
Hydrothermal biotite clot altered to chlorite
SC-02-40
FOV: 1.7 mm

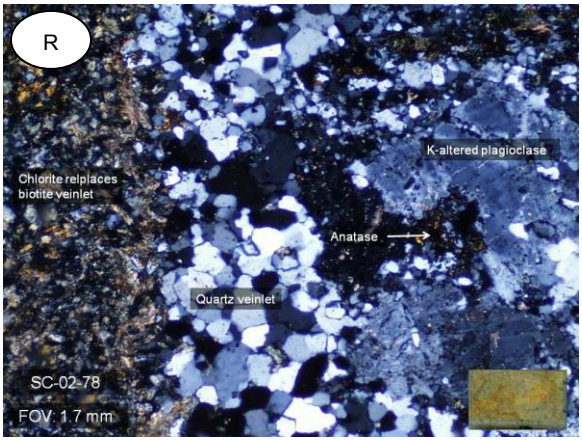
R
K-altered plagioclase
Chlorite relplaces biotite veinlet
Anatase
Quartz veinlet
SC-02-78
FOV: 1.7 mm

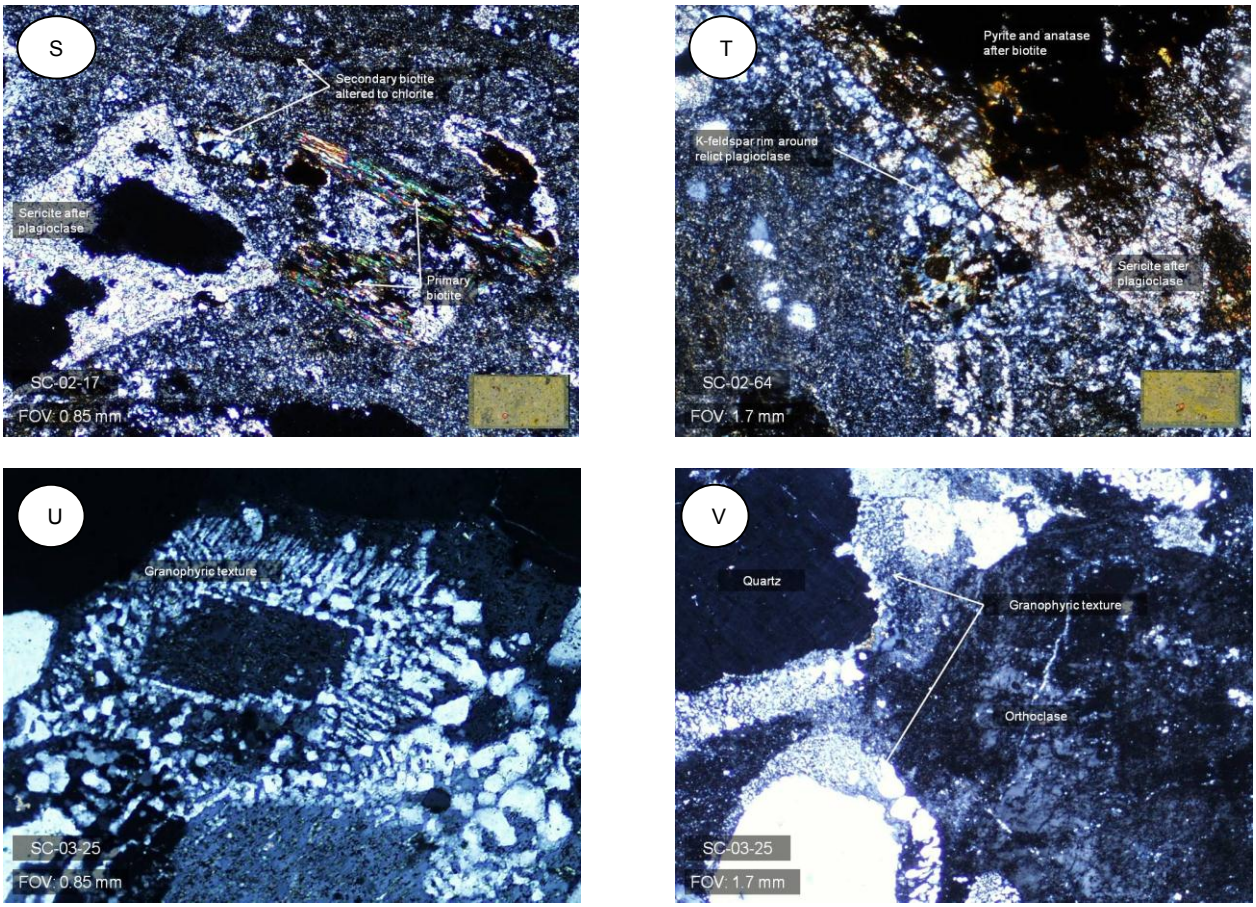

Figure 12. Photomicrographs of the north and south stocks. A, B) Examples of biotite within both the north and south stocks. Porphyritic, primary biotite (A) occurs locally, but more common hydrothermal and shreddy biotite (B) occurs as an alteration product throughout the matrix of both dioritic intrusions. C-F) Potassic alteration is a common alteration type throughout both the north and south stocks. Locally, potassic alteration consists of K-feldspar veinlets that cross cut the main matrix (C, D) and later biotite uses these same fractures as favorable pathways. This style of alteration also floods the diorite groundmass, as observed through thin section and accompanying stained billets. G-I) Ratty K-feldspar containing many fluid inclusions is commonly observed as veinlets (G) and rims on primary plagioclase (H, I). J-L) Apatite locally occurs as an alteration product of plagioclase and is commonly associated with later calcite. In some examples (L), epidote also occurs in association with apatite and calcite, helping to define an epidote alteration zone in the south stock. The presence of local silicification (H, I) probably marks the center of the main alteration system. M-P) In the north stock, actinolite occurs where epidote does in the south stock. This change in mineralogy reflects the fact that the north stock represents a more central alteration zone compared to the south stock. Q, R) Commonly hydrothermal biotite related to the main potassic alteration pulse is commonly altered to chlorite in late propylitic assemblages. S, T) Late sericitic alteration overprints all types of alteration in the south stock. Sericite selectively replaces plagioclase phenocrysts. This represents a transition between the main stocks and adjacent breccia zones. Photomicrographs U and V represent granophyric textures present within the locally pegmatitic quartz syenite.

South Breccia Zone

The South Breccia Zone is characterized by intense advanced argillic alteration consisting of significant silicification and aluminosilicate assemblages (Figure 13). Additionally, there is a significant zone of quartz-alunite acid sulfate alteration. Based on the spatial relationship of these alteration assemblages, the south breccia zone represents an advanced argillic lithocap above a porphyry system (Sillitoe, 2010). A thorough examination of the South Breccia zone's geologic context follows in the discussion.

Silicification and leaching of original porphyry textures is the most ubiquitous alteration type in the South Breccia Zone. All samples contain some form of vuggy silica alteration, whether it is the main alteration style present (Fig. 14A) or occurs as breccia clasts within a separate matrix (Fig. 14G). The samples within this area contain either quartz vugs or vugs that have been subsequently filled with later alteration minerals. Euhedral pyrite occurs coeval with massive silicification and leaching; this pyrite has been oxidized and replaced by hematite pseudomorphs (Figs. 14A, B). These grains tend to occur near and around quartz vugs and their close association with silicification suggests an early pulse of acid-sulfate fluids. Silicification tends to be pervasive and quartz ranges from fine-grained (Fig. 14C) to subhedral pseudo-jasper textures (Fig. 14D), and even prismatic needle-like crystals (Fig. 14E-H). Associated with this quartz-pyrite assemblage is also alunite, which occurs as fine-grained disseminations within the matrix. The prismatic quartz tends to occur in vugs, overprinting a quartz-alunite matrix.

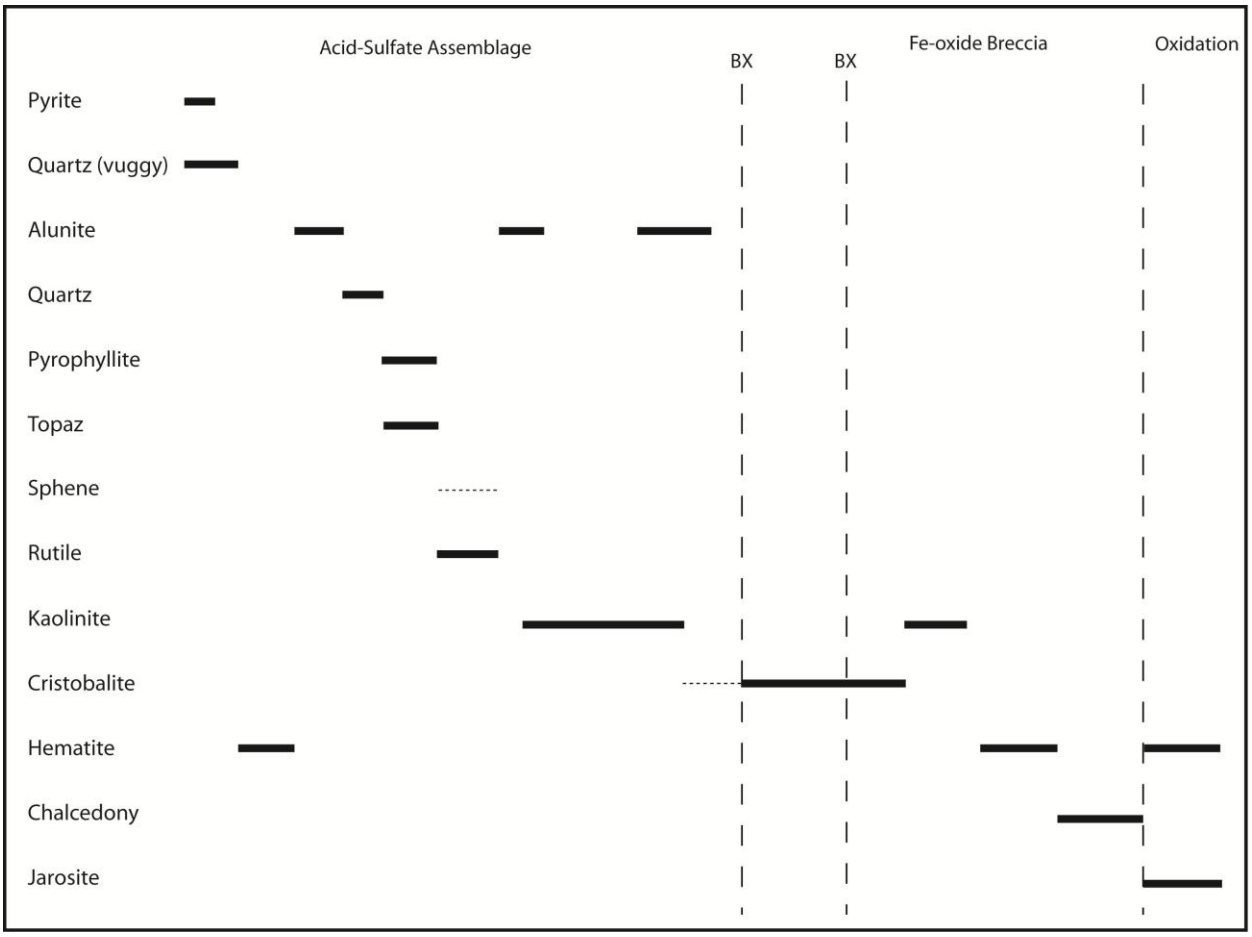

Figure 13. Paragenetic diagram of the South Breccia Zone. See text for full discussion.

Later in this assemblage, acid sulfate fluids evolved and became more acidic, leaching most cations, leaving behind an aluminosilicate assemblage. Minerals observed within this aluminosilicate groundmass consist of pyrophyllite and topaz, which do not occur together in the same sample, but are considered time-equivalent facies based on their relationships to other associated alteration minerals. Topaz occurs as euhedral replacements of original volcanic fragments (Fig. 14K), and also as a clast within a rebrecciated cristobalite matrix (Fig. 14L). Pyrophyllite occurs as veinlets cross-cutting vuggy silica (Fig. 14I) and also as fine-grained matrix material overprinting vuggy silica assemblages (14J). Rutile and/or anatase occur around this stage as well, occurring as high-relief, highly birefringent rutile overprinting quartz and topaz (Fig. 14N). The main minerals within the brecciated groundmass are kaolinite and alunite,

which occur together, and constitute the majority of the observed alteration in these samples (Fig. 14O). Alunite occurs as fine disseminations within the kaolinite matrix, but also overprints kaolinite locally. For example, in SC-01-72, late and coarse (250-400 microns) alunite veinlets cross-cut the kaolinite-alunite matrix (Figs. 14P-R). In other samples, alunite forms the majority of the breccia matrix (Fig. 14S) and the same alteration stage can be seen in alunite clasts hosted within a matrix of cristobalite (Fig. 14T). This cristobalite matrix, exhibiting multiple pulses of cristobalite mineralization, contains clasts of alunite and other earlier alteration minerals (Figs. 14T-V).

The pulse of cristobalite occurs in association with more kaolinite (Fig. 14X) and also hematite. Hematite occurs as fine red-stained disseminations within the overall cristobalite matrix, obscuring cristobalite locally (Figs. 14V, W). The presence of alunite and other advanced argillic clasts is evidence that this breccia is late.

Chalcedony also occurs as a late alteration mineral and fills any remaining vugs and pockets in various breccia matrices (Fig. 14Y) or in earlier clasts (Figs. 14Z, 14AA). Late, potentially supergene, kaolinite fills similar interstices (Fig. 14BB). Late oxidized fluids rich in iron stained most samples and oxidized any remaining pyrite into hematite and other Fe-oxides.

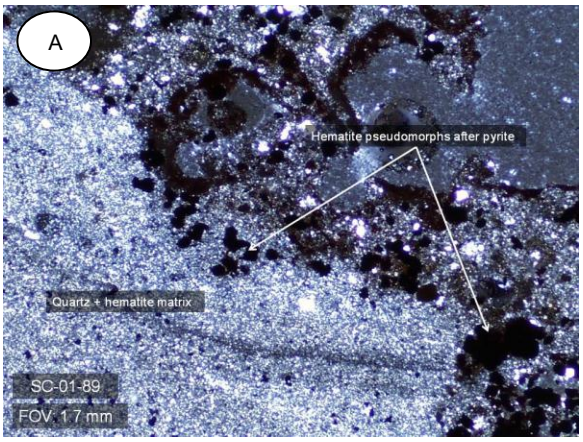
A
Hematite pseudomorphs after pyrite
Quartz + hematite matrix
SC-01-89
FOV: 1.7 mm

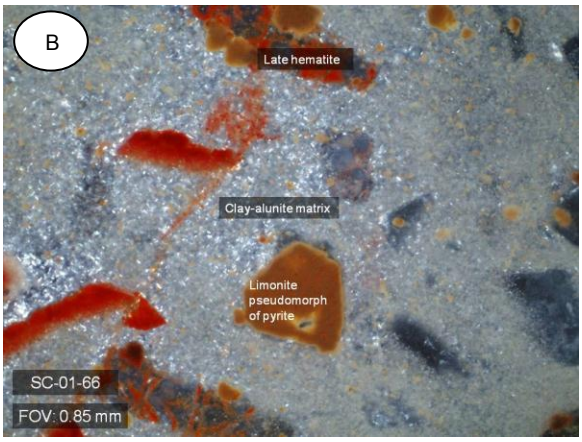
B
Late hematite
Clay-alunite matrix
Limonite pseudomorph of pyrite
SC-01-66
FOV: 0.85 mm

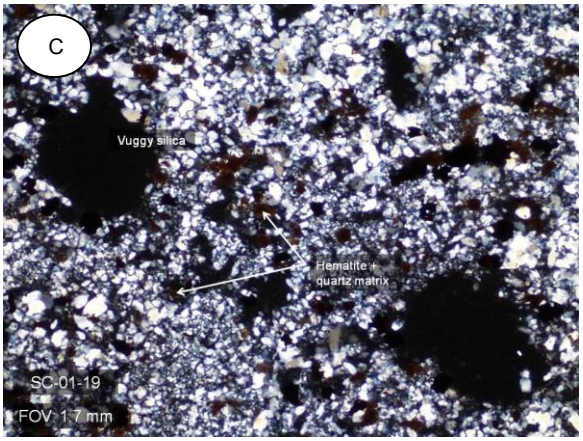
C
Vuggy silica
Hematite + quartz matrix
SC-01-19
FOV: 1.7 mm

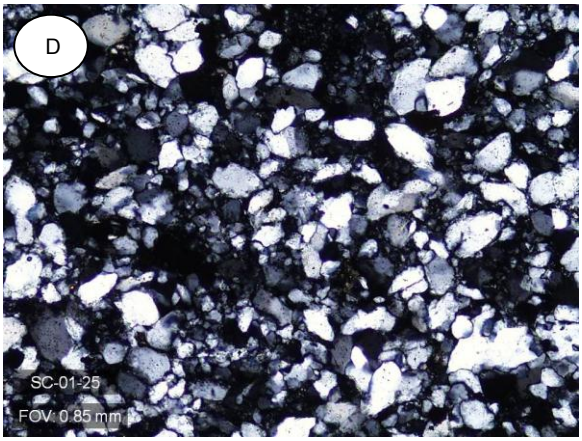
D
SC-01-25
FOV: 0.85 mm

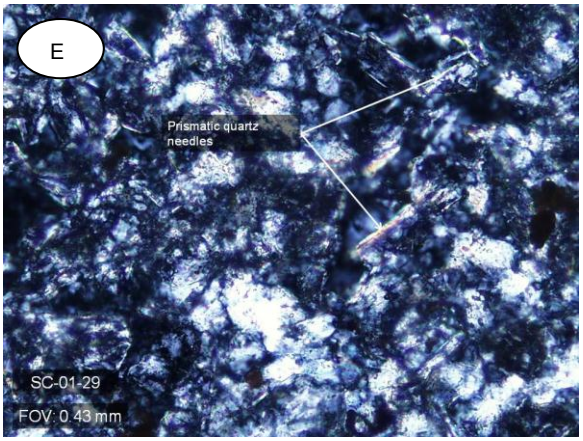
E
Prismatic quartz needles
SC-01-29
FOV: 0.43 mm

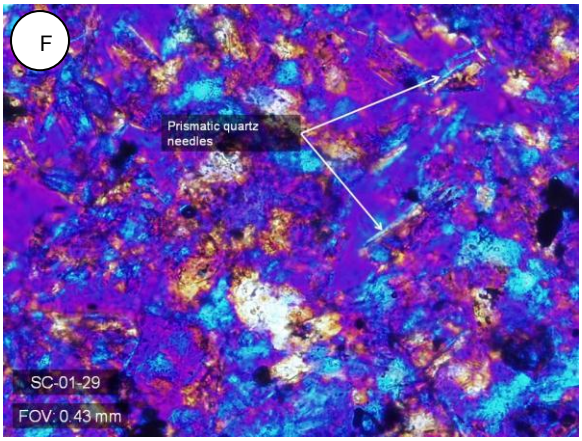
F
Prismatic quartz needles
SC-01-29
FOV: 0.43 mm

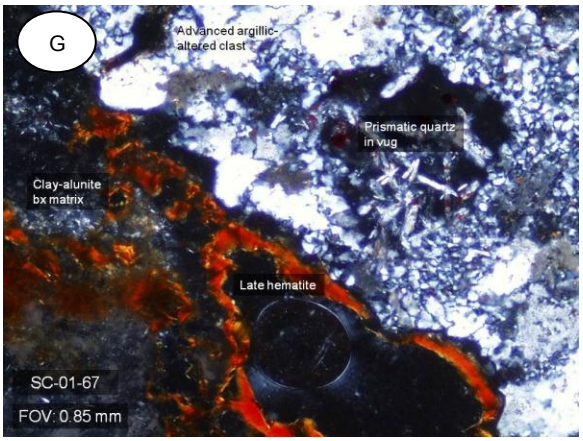
G
Advanced argillic-altered clast
Prismatic quartz in vug
Clay-alunite bx matrix
Late hematite
SC-01-67
FOV: 0.85 mm

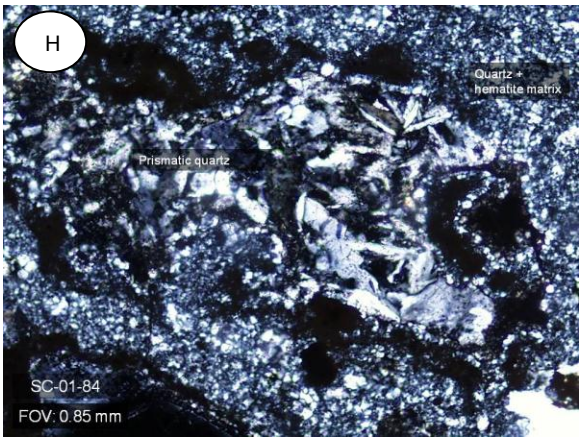
H
Quartz + hematite matrix
Prismatic quartz
SC-01-84
FOV: 0.85 mm

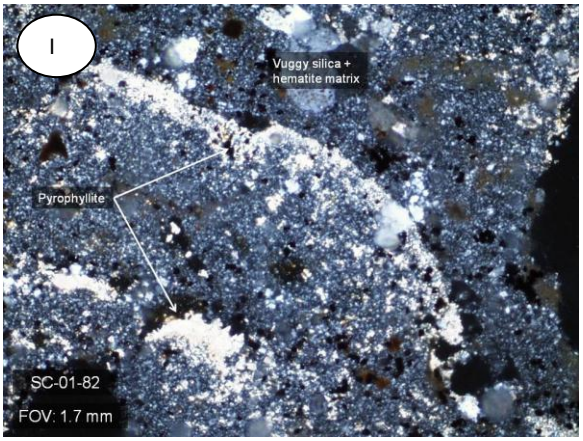
I
Vuggy silica + hematite matrix
Pyrophyllite
SC-01-82
FOV: 1.7 mm

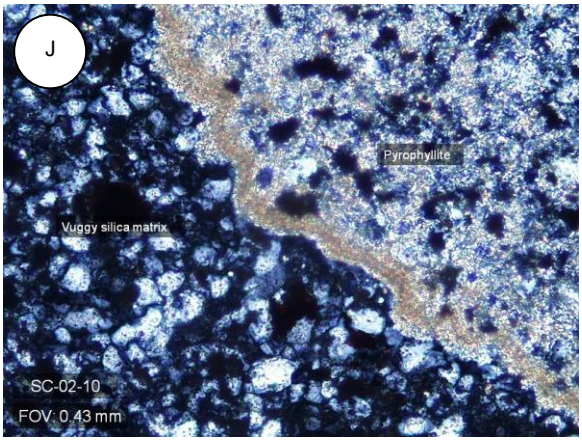
J
Pyrophyllite
Vuggy silica matrix
SC-02-10
FOV: 0.43 mm

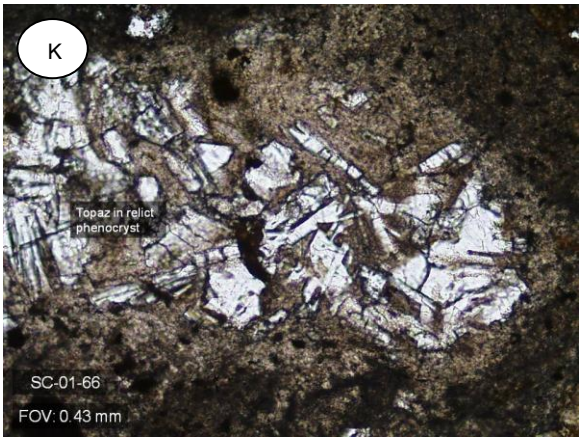
K
Topaz in relict phenocryst
SC-01-66
FOV: 0.43 mm

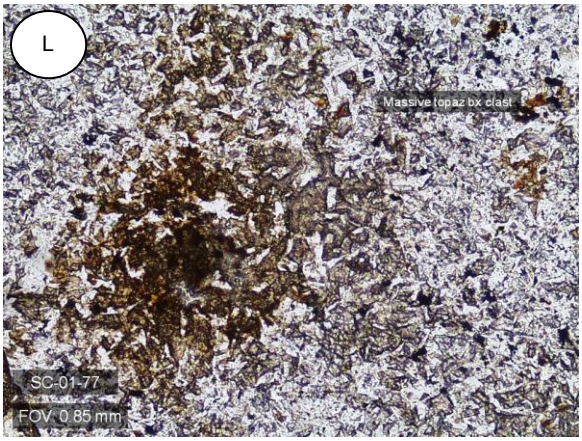
L
Massive topaz bx clast
SC-01-77
FOV: 0.85 mm

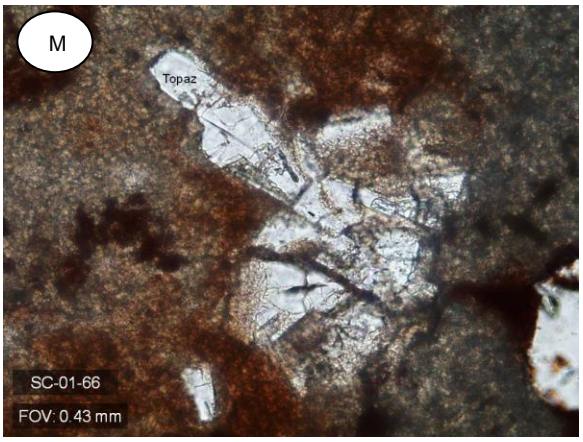
M
Topaz
SC-01-66
FOV: 0.43 mm

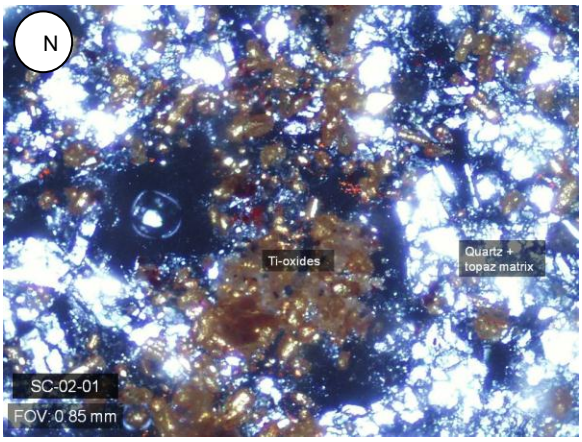
N
Ti-oxides
Quartz + topaz matrix
SC-02-01
FOV: 0.85 mm

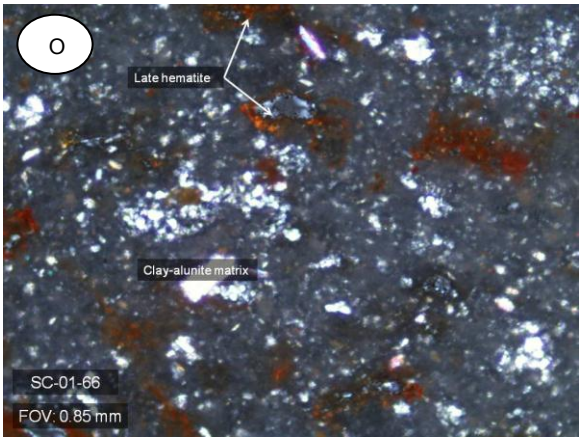
O
Late hematite
Clay-alunite matrix
SC-01-66
FOV: 0.85 mm

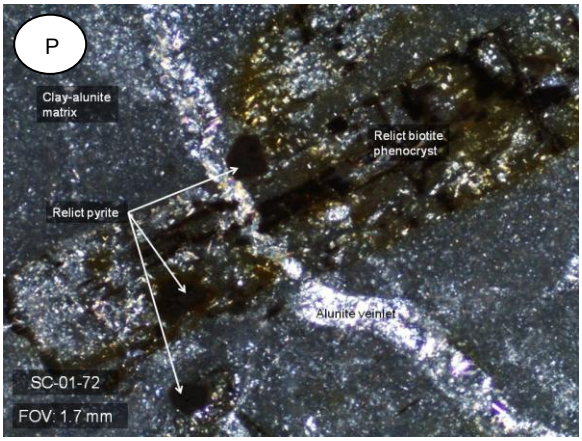
P
Clay-alunite matrix
Relict biotite phenocryst
Relict pyrite
Alunite veinlet
SC-01-72
FOV: 1.7 mm

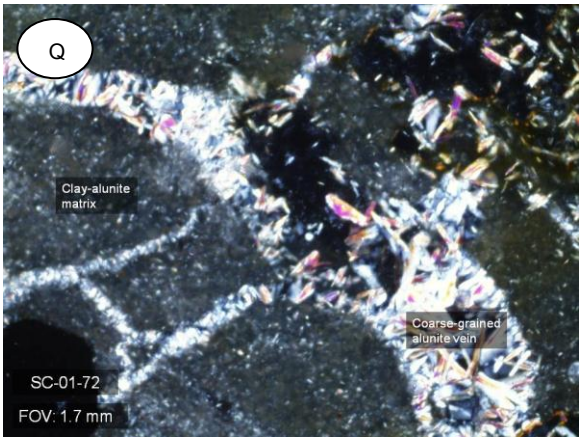
Q
Clay-alunite matrix
Coarse-grained alunite vein
SC-01-72
FOV: 1.7 mm


R
Coarse-grained alunite vein
Clay-alunite matrix
SC-01-72
FOV: 1.7 mm

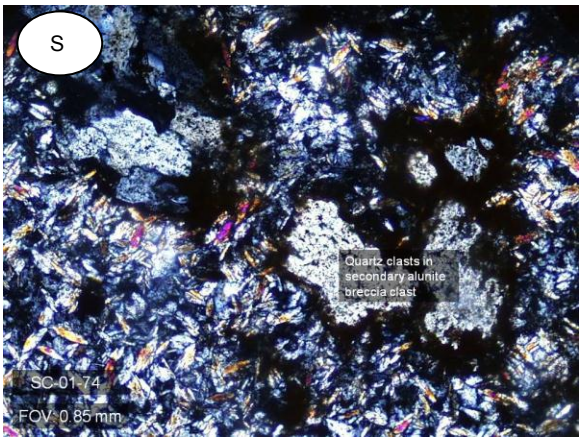
S
Quartz clasts in secondary alunite breccia clast
SC-01-74
FOV: 0.85 mm

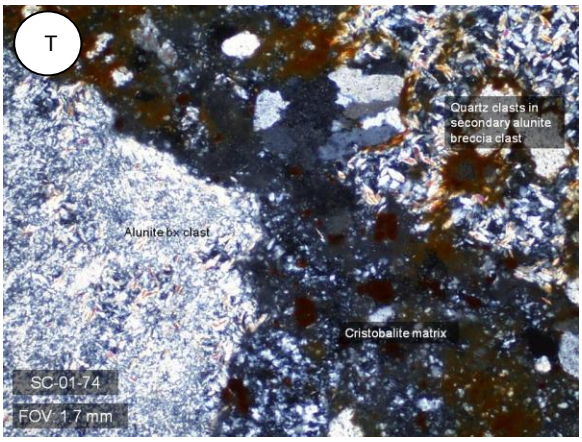
T
Quartz clasts in secondary alunite breccia clast
Alunite bx clast
Cristobalite matrix
SC-01-74
FOV: 1.7 mm

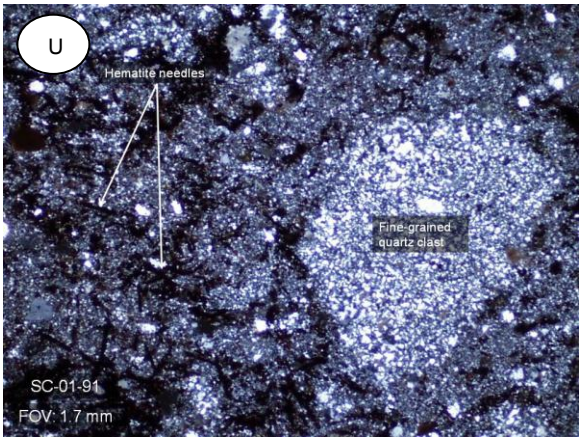
U
Hematite needles
Fine-grained quartz clast
SC-01-91
FOV: 1.7 mm

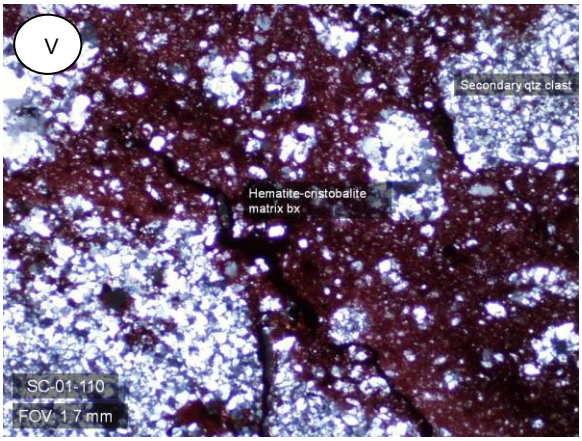
V
Secondary qtz clast
Hematite-cristobalite matrix bx
SC-01-110
FOV: 1.7 mm

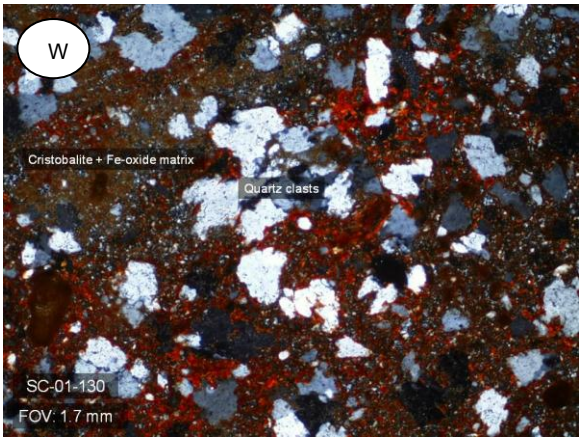
W
Cristobalite + Fe-oxide matrix
Quartz clasts
SC-01-130
FOV: 1.7 mm

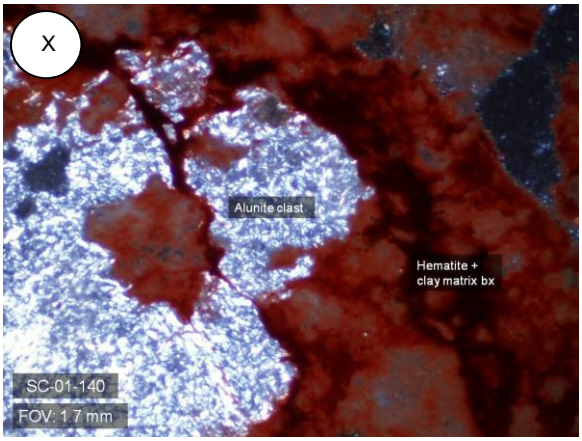
X
Alunite clast
Hematite + clay matrix bx
SC-01-140
FOV: 1.7 mm

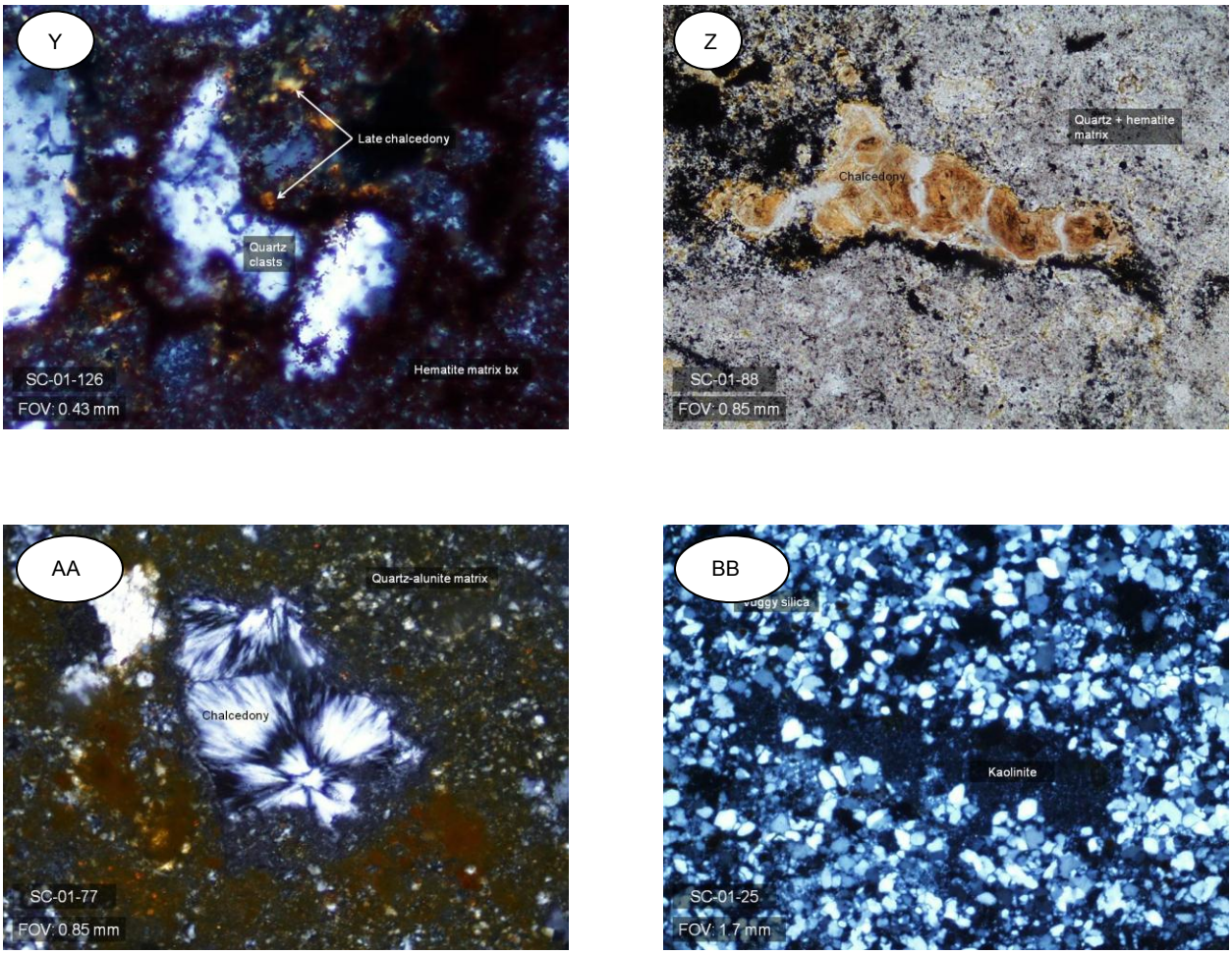

Figure 14. Photomicrographs from the South Breccia Zone. A, B: Hematite pseudomorphs of pyrite within vuggy silica assemblage. Clay and alunite also comprise the matrix of B and is overprinted by hematite. C- F: Different examples of quartz textures within the acid sulfate- vuggy silica alteration assemblages. Quartz is generally an early alteration product and ranges from fine-grained comprising the vuggy silica matrix (C) to a pseudo-jasper texture within D and local examples of prismatic quartz needles (E, F). Earlier acid sulfate alteration is brecciated as noted within G, where a clay-alunite breccia matrix cross cuts an acid sulfate clast. Late chalcedony stained with hematite fills in vugs. I, J: Seams of pyrophyllite cross-cut earlier vuggy silica alteration. Pyrophyllite occurs as fibrous intergrowths between interstices within the vuggy quartz matrix. K-N: Topaz occurs as a common alteration mineral within the South breccia zone and comes mid-way through the paragenetic sequence. Topaz occurs as a vug-filling mineral (K, M) and also as massive aggregates (L, N). Additionally, topaz is observed in close association with Ti-oxides, evidence of intense acid-leaching. O-T: Clay-alunite alteration occurs within a distinct zone in the south breccia zone and comprises several pulses. Clay and alunite occur as fibrous intergrowths within a lot of the matrix material (O) and is commonly cross-cut by coarser alunite blades (P-R). Elsewhere, coarse alunite cross cuts jaspery quartz textures (S) and alunite clasts are supported by a late cristobalite-matrix breccia (T). U-X: Hematite commonly occurs as a late mineral that stains variations of silica such as cristobalite (W) and chalcedony (Z). Y-BB: Finally, late chalcedony fills residual vugs and occurs throughout the South Breccia zone.

North Breccia Zone

The North Breccia Zone, like the South Breccia Zone, is also pervasively altered to other acid sulfate assemblages (Fig. 15). Similarly, silicification and leaching in conjunction with the precipitation of pyrite are common early alteration features (Figs. 16 A, B). Commonly, alunite precipitated with zunyite and pyrite in these quartz vugs, as seen in Figures 16A and 16B. Euhedral pyrite (observed as hematite after pyrite) is surrounded by a matrix of zunyite and alunite (Figs. 16 C, D).

The next phase of acid sulfate fluids precipitated pyrite in association with zunyite. Zunyite occurs as a main matrix constituent as both euhedral and massive varieties cross-cutting earlier vuggy silica and acid sulfate alteration (Figs. 16E-H). Zunyite comprises up to 25% of some entire samples (e.g., SC-04-60). Commonly zunyite is zoned, suggesting several pulses of precipitation with fluid composition changes during a single stage of alteration.

Elsewhere, pyrophyllite and diaspore instead of zunyite occur as pervasive aluminosilicate alteration minerals. Pyropyllite replaces original volcanic textures within the Tvt unit and related breccias. Pyrophyllite selectively replaces welding textures (Figs. 16I, J), and diaspore occurs as subhedral replacements of original volcanic fragments (Figs. 16I-L). Locally, topaz occurs in place of diaspore within these relict volcanic fragments and likely represents a flux in fluorine (Figs. 16M, N), which is explored further in the discussion. In the same manner, fluorite also occurs around this stage, but is observed with quartz, overprinting earlier silicification and alunite (Figs. 16O, P). This stage, of course, is also observed as prismatic blades (Figs. 16Q, R).

The next stage of alteration is pervasive and contains a significant amount of cristobalite as a principal matrix mineral. Fine cross-cutting veinlets with ratty edges of cristobalite occur with alunite and contain clasts of earlier alteration styles. In this cristobalite-alunite breccia, cristobalite precipitated first, but coarse-grained alunite precipitated soon after (Figs. 16S-V). Additionally, alunite continued to precipitate and formed both coarse-grained veins and a significant amount of the breccia matrix (Figs. 16W-Z). Near this stage in alteration, barite also precipitated in local vugs and interstices, but is a minor alteration mineral. Quartz is also associated with the latest-stage of cristobalite-alunite alteration and occurs as an interstitial product as well.

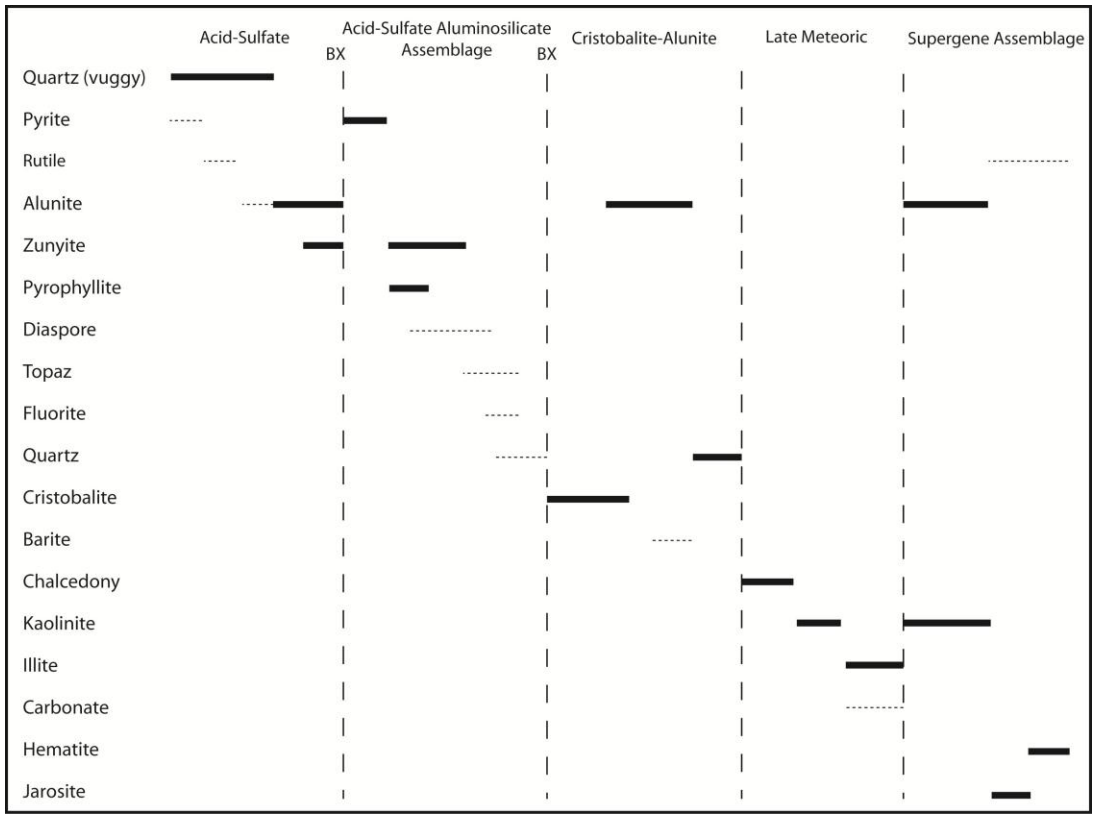

Figure 15. Paragenetic diagram of the North Breccia Zone. See text for full discussion.

Lower-temperature and more neutral pH minerals appeared late in the North Breccia Zone alteration zone paragenesis. First, late chalcedony is prominent as cross-cutting veins (Figs. 16Y, Z), but also vug and interstitial fill (Figs.16-AA, -BB). Also associated with this late chalcedony is interstitial kaolinite which occurs in cross-cutting veins, but also interstices within vugs (Figs. 16G, H). Finally, cross-cutting illite ± carbonate veins overprinted earlier alteration including chalcedony and other alteration minerals. These minerals tend to be outboard of some of the central acid-sulfate alteration zones and represent a late-meteoric signature, which is covered in the Discussion.

Finally, a late supergene overprint occurs throughout the alteration zones. Alunite and kaolinite cross-cut earlier alteration styles and contain fragments of earlier alteration minerals. For example Figures 16-EE and 16-FF show quartz fragments within alunite from earlier quartz veins in the cristobalite-alunite stage. Alunite from this stage is ratty; the euhedral, prismatic rhombs observed in other stages are not present (Figs. 16Y, Z). Since this alunite is not associated clearly with another stage, occurs solely in veinlets and not as a breccia matrix, and occurs as fine and feathery-textured crystals, this alunite has been interpreted to be supergene. Similarly, the cross-cutting kaolinite in late veins may also be supergene. Finally, a jarosite ± rutile assemblage that transitions into hematite ± rutile overprint occurs as disseminations within the groundmass, replacing Fe minerals such as pyrite, but also as overall resinous Fe-rich stains (Figs. 16Q, R).

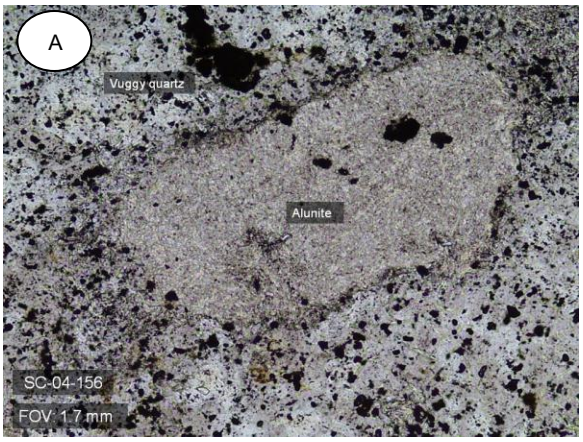
A
Vuggy quartz
Alunite
SC-04-156
FOV: 1.7 mm

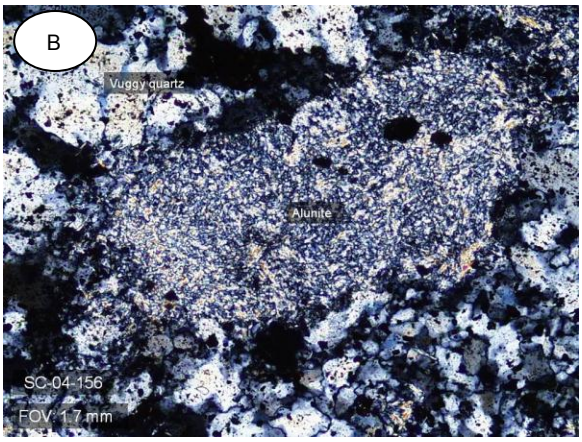
B
Vuggy quartz
Alunite
SC-04-156
FOV: 1.7 mm


C
Alunite
Hematite
after pyrite
Zunyite
SC-04-89
FOV: 0.43 mm

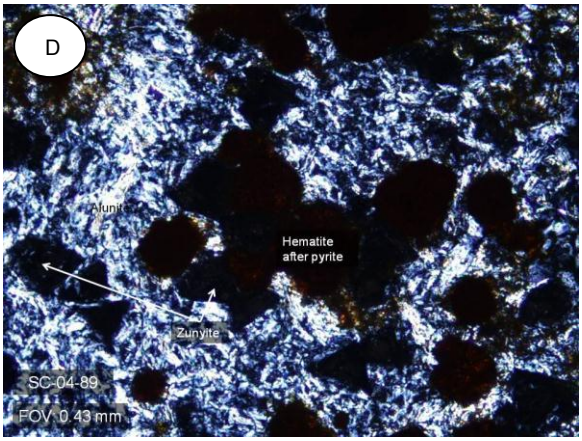
D
Alunite
Hematite
after pyrite
Zunyite
SC-04-89
FOV: 0.43 mm

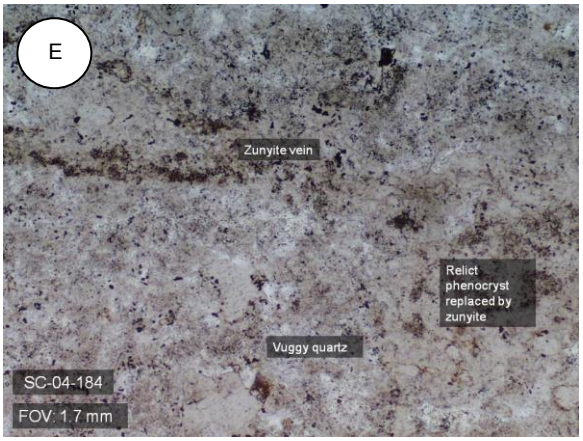
E
Zunyite vein
Relict
phenocryst
replaced by
zunyite
Vuggy quartz
SC-04-184
FOV: 1.7 mm

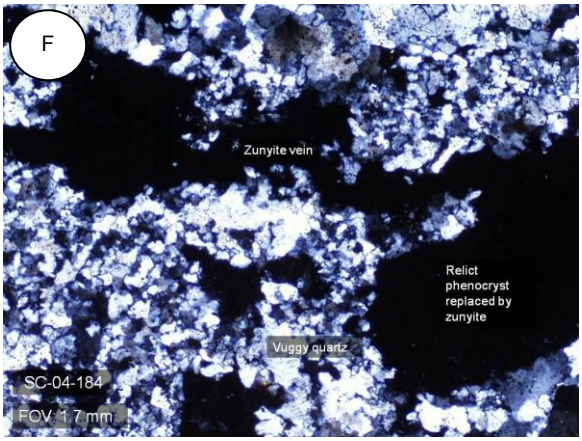
F
Zunyite vein
Relict
phenocryst
replaced by
zunyite
Vuggy quartz
SC-04-184
FOV: 1.7 mm

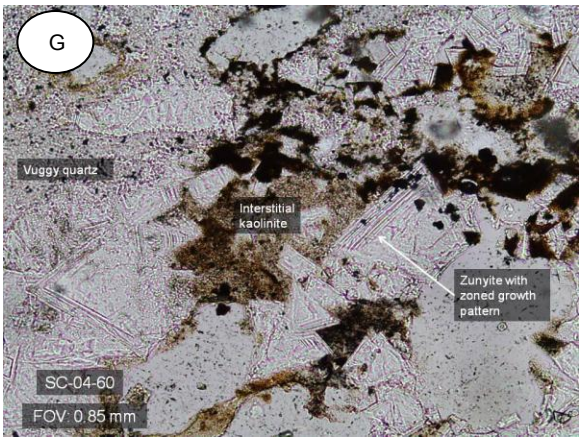
G
Vuggy quartz
Interstitial kaolinite
Zunyite with zoned growth pattern
SC-04-60
FOV: 0.85 mm

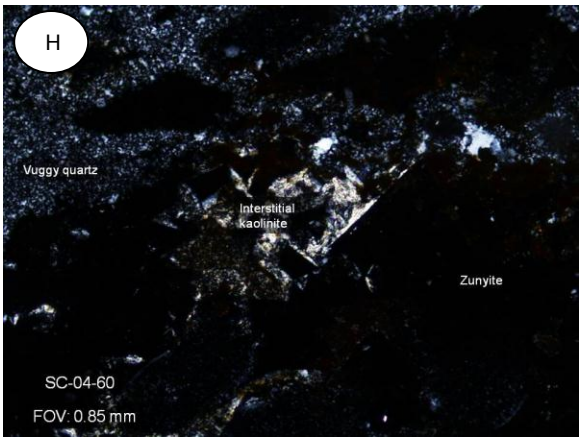
H
Vuggy quartz
Interstitial kaolinite
Zunyite
SC-04-60
FOV: 0.85 mm

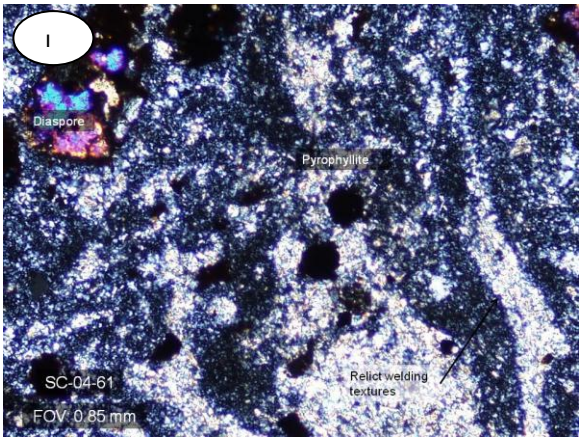
I
Diaspore
Pyrophyllite
Relict welding textures
SC-04-61
FOV: 0.85 mm

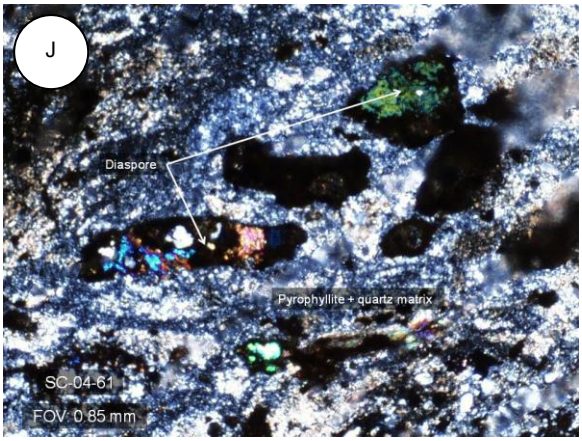
J
Diaspore
Pyrophyllite + quartz matrix
SC-04-61
FOV: 0.85 mm

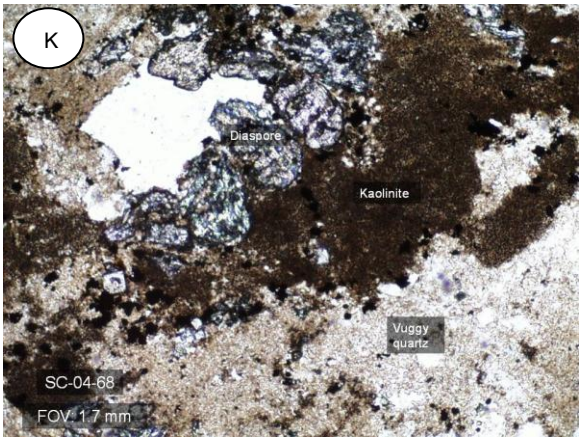
K
Diaspore
Kaolinite
Vuggy quartz
SC-04-68
FOV: 1.7 mm

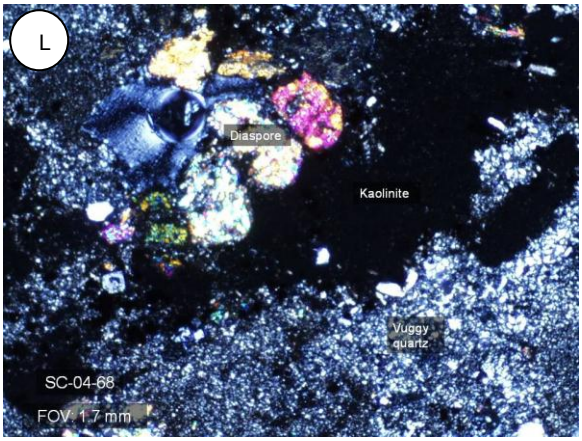
L
Diaspore
Kaolinite
Vuggy quartz
SC-04-68
FOV: 1.7 mm

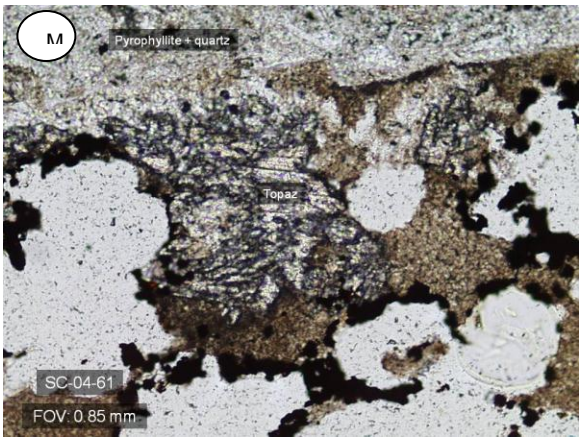
M
Pyrophyllite + quartz
Topaz
SC-04-61
FOV: 0.85 mm

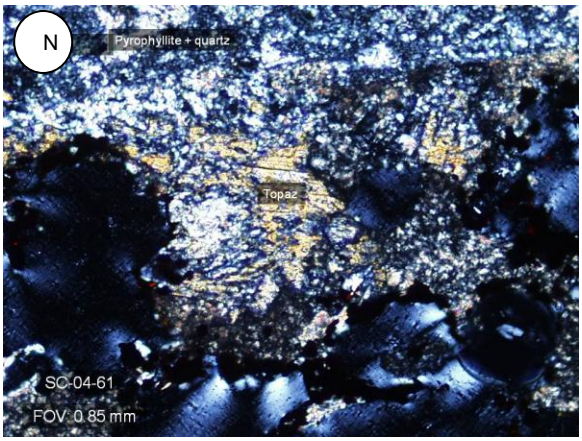
N
Pyrophyllite + quartz
Topaz
SC-04-61
FOV: 0.85 mm

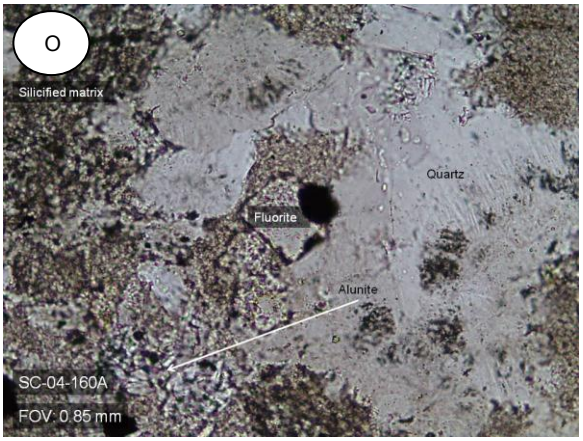
O
Silicified matrix
Quartz
Fluorite
Alunite
SC-04-160A
FOV: 0.85 mm

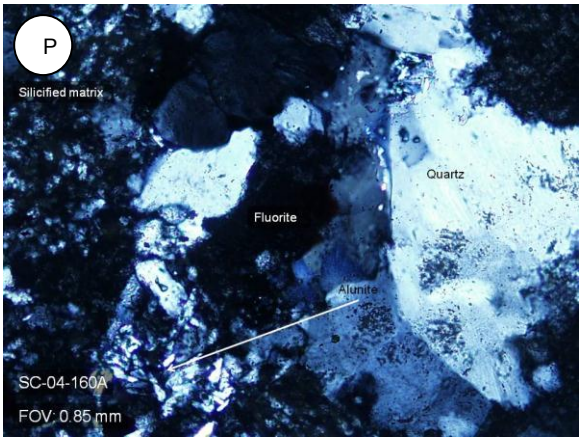
P
Silicified matrix
Quartz
Fluorite
Alunite
SC-04-160A
FOV: 0.85 mm

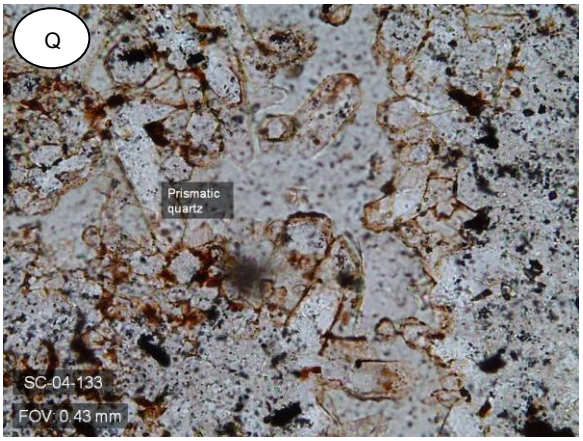
Q
Prismatic quartz
SC-04-133
FOV: 0.43 mm

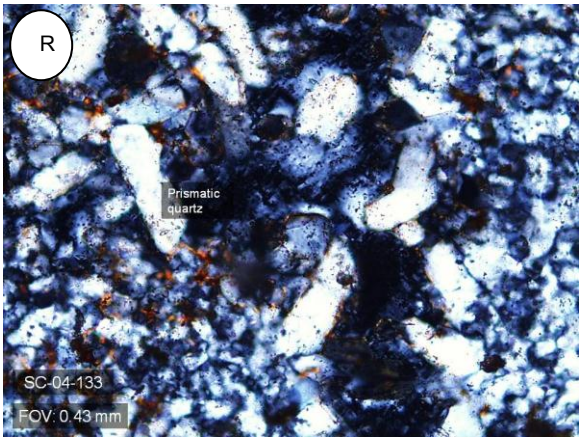
R
Prismatic quartz
SC-04-133
FOV: 0.43 mm

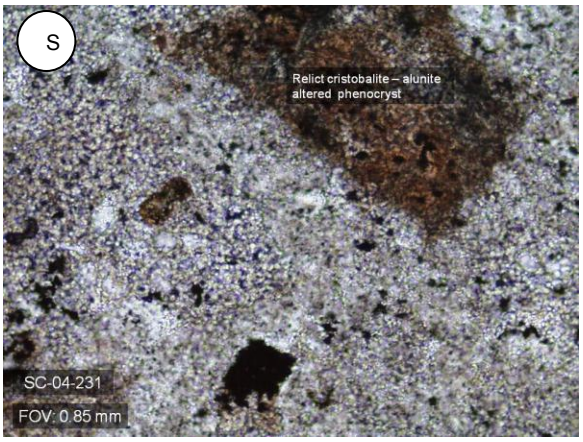
S
Relict cristobalite – alunite altered phenocryst
SC-04-231
FOV: 0.85 mm

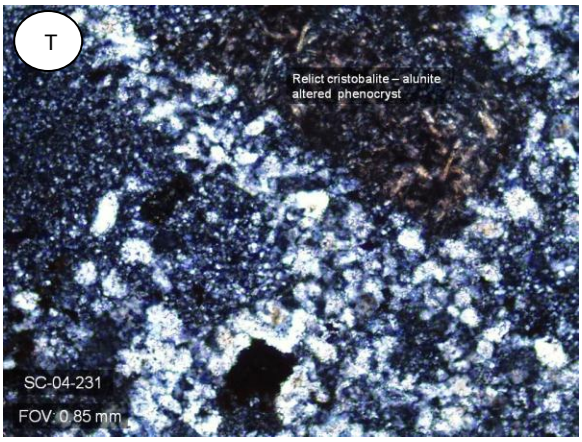
T
Relict cristobalite – alunite altered phenocryst
SC-04-231
FOV: 0.85 mm

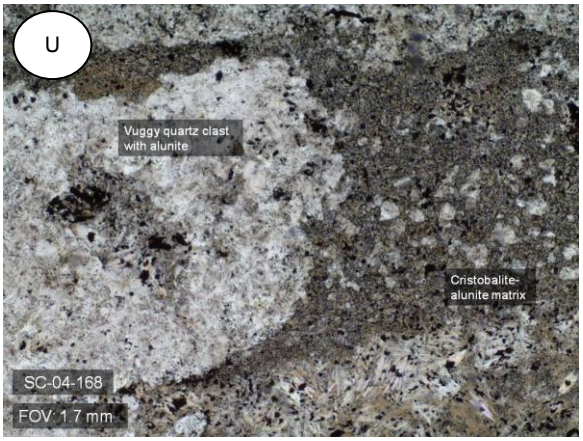
U
Vuggy quartz clast with alunite
Cristobalite-alunite matrix
SC-04-168
FOV: 1.7 mm

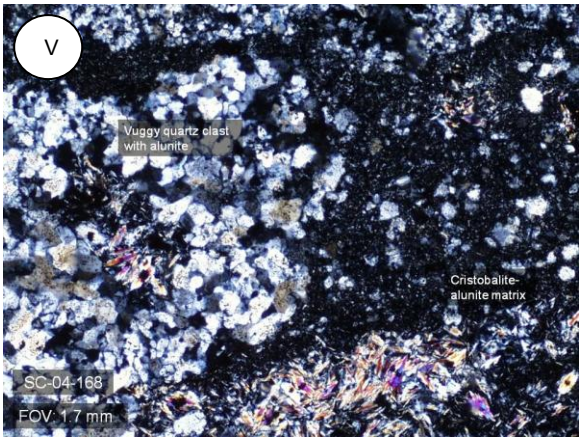
V
Vuggy quartz clast with alunite
Cristobalite-alunite matrix
SC-04-168
FOV: 1.7 mm

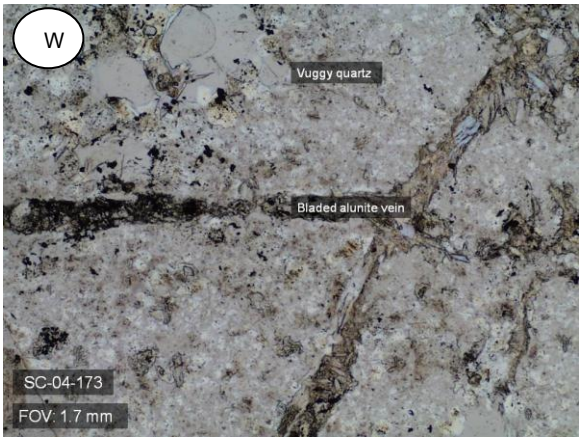
W
Vuggy quartz
Bladed alunite vein
SC-04-173
FOV: 1.7 mm

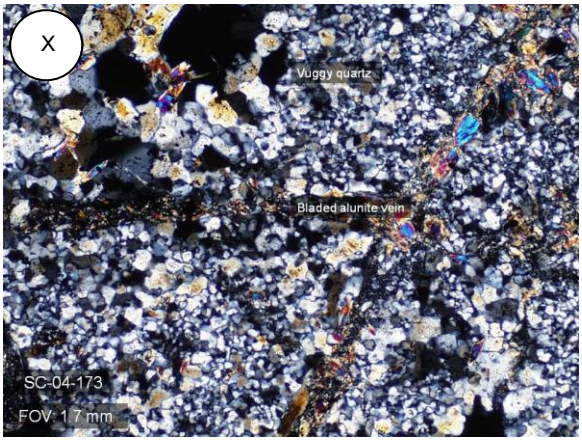
X
Vuggy quartz
Bladed alunite vein
SC-04-173
FOV: 1.7 mm

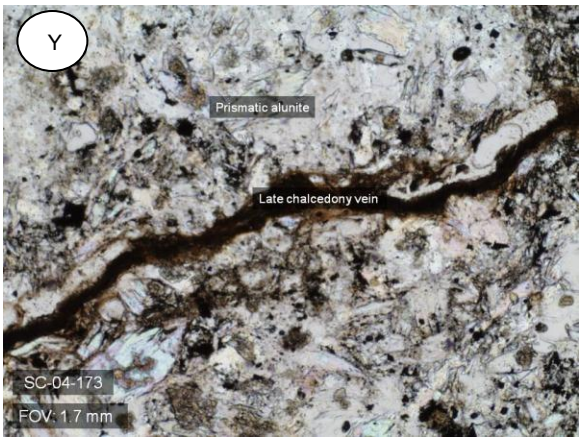
Y
Prismatic alunite
Late chalcedony vein
SC-04-173
FOV: 1.7 mm

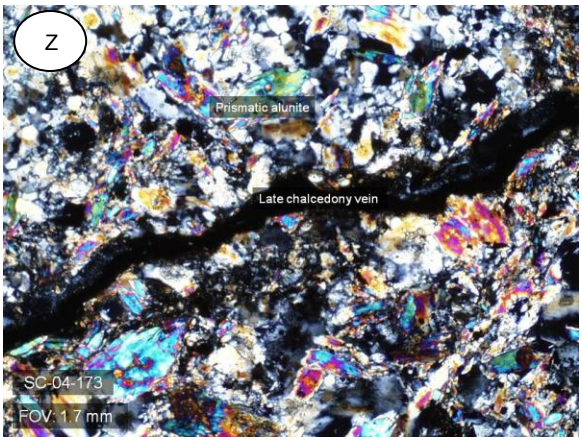
Z
Prismatic alunite
Late chalcedony vein
SC-04-173
FOV: 1.7 mm

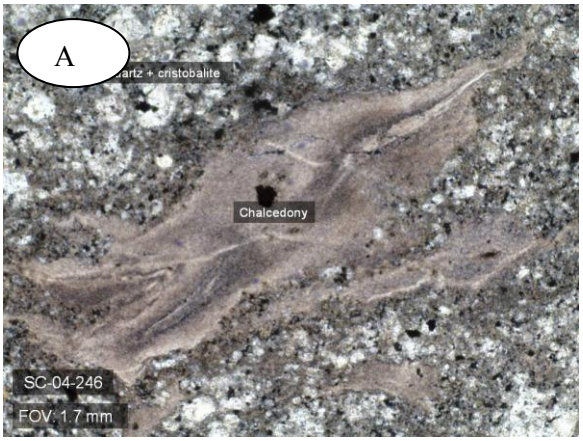
A
Chalcedony
SC-04-246
FOV: 1.7 mm

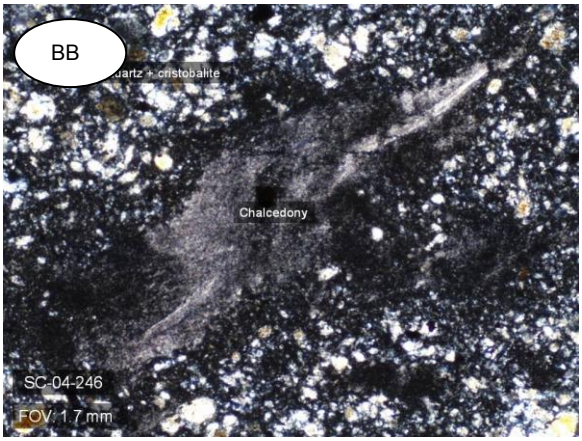
BB
Chalcedony
SC-04-246
FOV: 1.7 mm

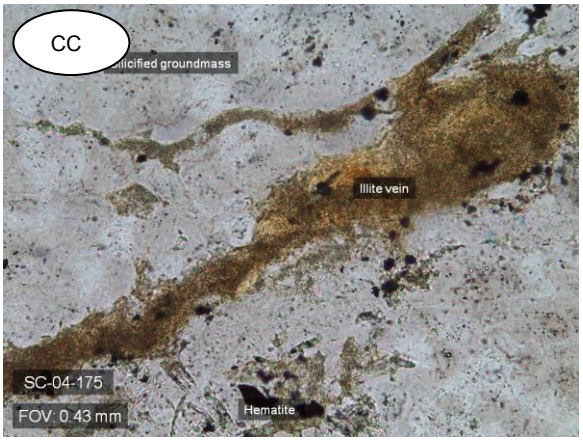
CC
Illite vein
SC-04-175
FOV: 0.43 mm
Hematite

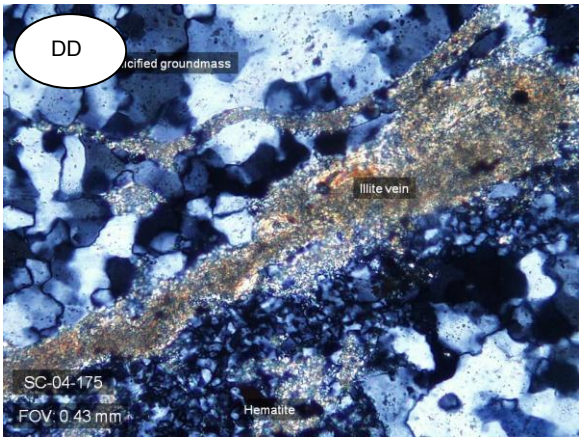
DD
Illite vein
SC-04-175
FOV: 0.43 mm
Hematite

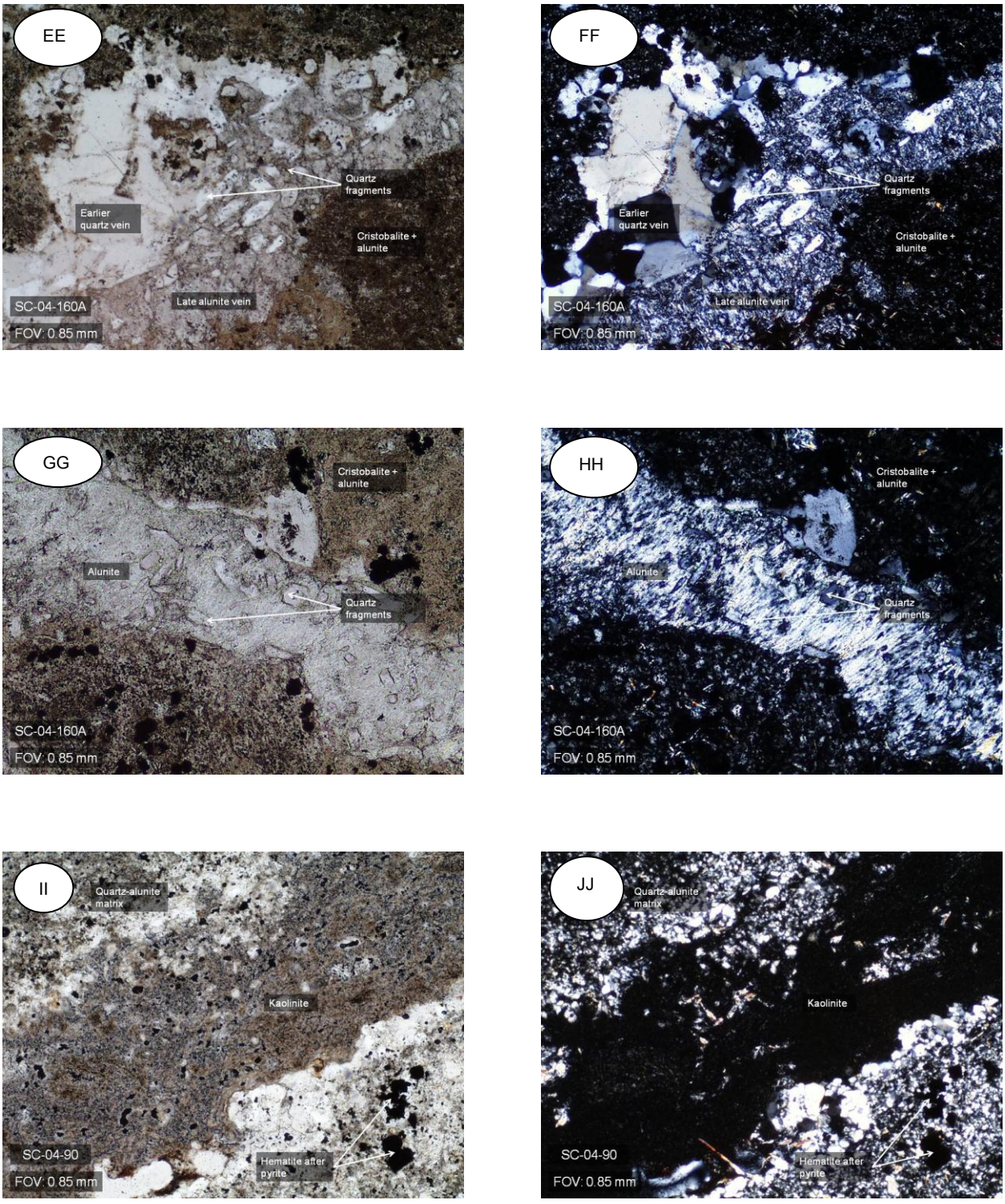

Figure 16. Photomicrographs showing alteration styles within the North Breccia Zone. A, B: Alunite occurring as vug-filling material within a vuggy silica matrix. The vuggy silica matrix is characteristic of most samples within the North Breccia Zone and represents early alteration. C, D: Early pyrite (later replaced by hematite) is seen as euhedral grains in clusters surrounded by zunyite and then alunite. These minerals formed in an earlier quartz vug.

E-H: Zunyite occurs as a relatively early mineral filling quartz vugs and also as a breccia matrix mineral. Zoned growth patterns within zunyite crystals suggest multiple pulses of fluid flow. I-N: Pyrophyllite-diaspore aluminosilicate alteration occurs within the north breccia zone. Diaspore replaces earlier volcanic fragments. Locally, topaz replaces volcanic fragments in place of diaspore. O, P: Elsewhere, fluorine-rich assemblages bearing minerals like fluorite occur cross-cutting silicified matrices and earlier alunite. Q, R: Later stages of quartz cross-cut earlier silicification and locally exhibit euhedral to subhedral prismatic aggregates of quartz. S-X: Cristobalite-alunite matrix breccias cross-cut early silicification and host breccia clasts from earlier alteration assemblages. Alunite replaces volcanic fragments locally and precipitates as coarse aggregates after cristobalite intrudes initially. The coarse nature of this alunite suggests a magmatically-derived origin rather than supergene origin. Y- -BB: Chalcedony occurs as a later cross-cutting mineral across coarse alunite and alunite-cristobalite assemblages. Chalcedony is observed within venilets but also in vugs. CC-DD: Illite +/- carbonate occurs as a late-stage alteration product outboard of the main acid-sulfate assemblage in veins and disseminations. EE-JJ: Supergene alunite and kaolinite cross-cut all forms of alteration except Fe-oxide staining. Alunite occurs as fine-grained feathery crystals, which is different from the bladed and prismatic alunite observed in earlier alteration stages and suggests a supergene origin.

Drilling

Nine RC holes from a transect covering both the north and south breccia zones and north and south stocks were relogged. These holes included four Western States (1997) holes (SS-1, SS-5, SS-9, SS-11), three Cordex (2004) holes (SC-1, SC-4, SC-6), and two Newmont (2008) holes (SCN-0013, SCN-0014) (Table 3). The lithologies and alteration types observed in these RC holes are similar to the lithology and alteration exposed at the

RC Hole	Elevation (ft)	Depth (ft)	Azimuth	Dip	UTM E	UTM N	Company	Year Drilled
SC-1	6300	1900	90	-75	527399	4578820	Cordex	2004
SC-4	6198	545	45	-60	526936	4579124	Cordex	2004
SC-6	6456	785	315	-60	526535	4579957	Cordex	2004
SS-1	6285	500	0	-90	527435	4578729	Western States	1997
SS-5	6300	500	0	-90	527366	4578854	Western States	1997
SS-9	6380	1000	140	-45	527873	4578497	Western States	1997
SS-11	6130	700	0	-90	526354	4576798	Western States	1997
SCN-00013	6565	1305	0	-90	528381	4578235	Newmont	2008
SCN-00014	6544	1200	180	-70	528146	4578296	Newmont	2008

Table 3. Reverse circulation holes relogged for the present study. A total of nine holes from three generations of drilling were relogged for lithology, alteration, and sulfide percentage.

surface. In addition to rock type and alteration type, sulfide percentage was recorded. The sulfide is almost entirely pyrite, although chalcopyrite and molybdenite were also found. See Appendix D for graphic geology, alteration, and sulfide logs.

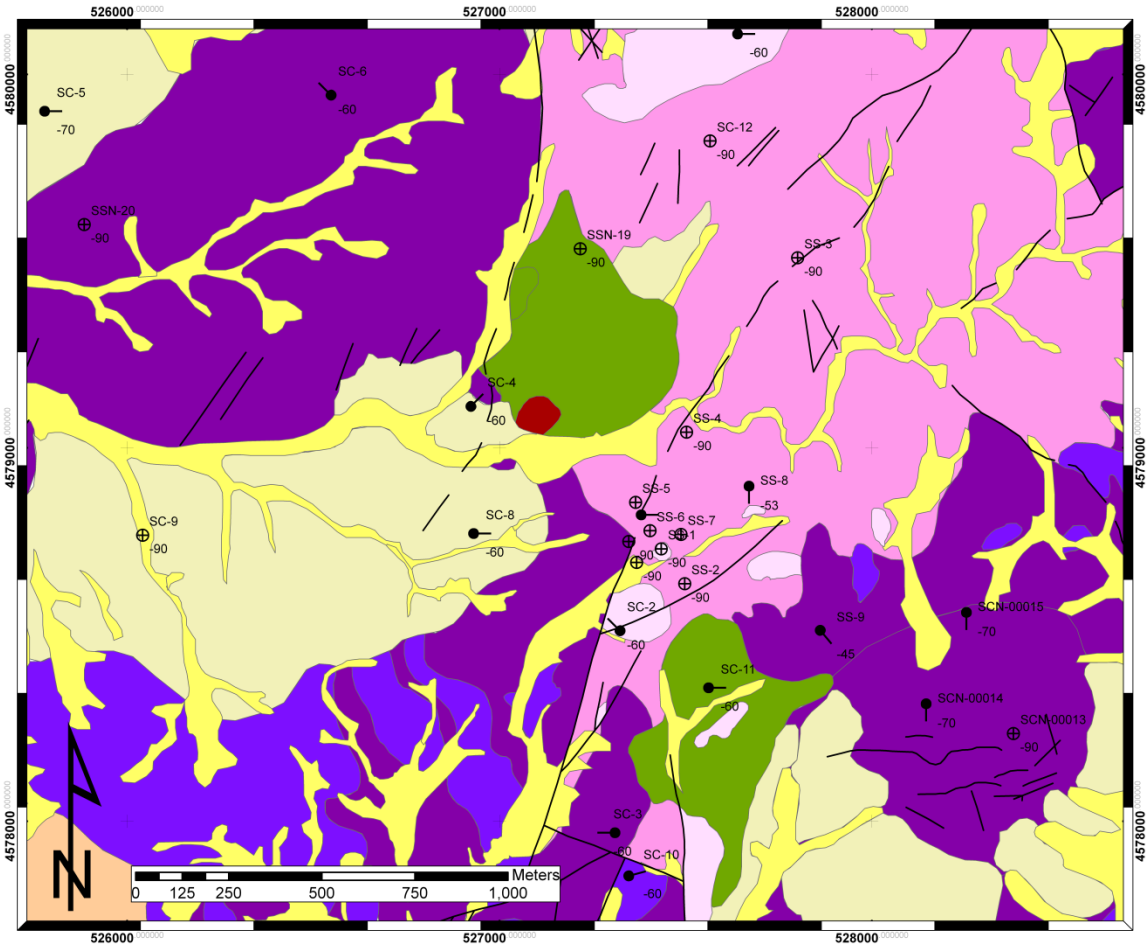

Figure 17. Placement of reverse circulation drill holes at Scraper.

SC-6

SC-6 is the northern-most drill hole relogged in this study. It is collared in advanced argillic-altered Tvt (Table 3, Figure 16). The hole encountered silicified and advanced argillic Tvt assemblages in the first 240 ft. of the hole. Here, most of the original volcanic textures present within Tvt are obscured as silicification and leaching are profound. Two intervals (0-15 ft.; 130-135 ft.) are marked by significant breccias. The interval down to 240 ft. is also significantly oxidized and likely contains supergene minerals such as alunite and kaolinite, which are observed in thin section surface samples SC-04-160A and SC-04-90 (Fig. 16EE-JJ).

At 240 feet, the alteration switches from a silicified-acid sulfate assemblage to a QSP-altered assemblage. Megascopically, the chips from this section appear bleached and are texturally clayey. Under a binocular microscope, volcanic textures are recognizeable, and aligned plagioclase laths and fragments are altered to sericite. Between 240 – 440 ft., sulfide percentage is somewhat consistent and ranges from about 3% to local intervals of approximately 8% pyrite.

A quartz syenite (Tqs) dike that cross-cuts Tvt from 440 ft. to 475 ft is characterized by intense potassic alteration as pink orthoclase. Orthoclase phenocryts are relatively equigranular, and the pyrite occurs in low to trace amounts. The remainder of the hole from 475 to 785 ft. is Tvt and alternates from sericite-dominant (QSP) intervals to more chlorite –dominant (propylitic) intervals. Locally, pyrite content reaches about 8%, but most of this interval ranges between trace to 3% pyrite.

SC-4

SC-4 is the next hole to the southeast of SC-6 (Fig. 17). SC-4 is collared in propylitic-altered diorite (Td) (Table 3). Equigranular diorite is the dominant lithology in the hole, as it occurs from 0-490 ft. Interspersed with the equigranular diorite are several quartz syenite (Tqs) dikes that contain significant orthoclase representing potassic alteration. Most of the diorite between the collar and 490 ft. is either sericite-dominant or chlorite-dominant in terms of alteration style. A significant interval (65 – 275 ft.) of sericite-dominant (QSP) alteration occurs with pyrite content approaching 25% locally. Over intervals where pyrite is less abundant, chlorite is present, which contributes an overall greenish hue to the bleached tuff. This suggests a sericitic overprint onto earlier chloritic alteration. Two other intervals (40 – 65 ft.; 275 – 425 ft.) contain a chlorite-dominant assemblage.

The end of the hole between 490 ft. and 545 ft. contains hornfelsed Ovi sedimentary rocks. Quartzite is the dominant Ovi lithology and pyrite is commonly observed in small amounts between 3%-5%.

SS-5

The next RC hole along the transect is SS-5, which is collared above the structural window exposing Ovi siliciclastic rocks (Table 3, Fig. 17). From 0-85ft., drilling encountered Ovi quartzite and chert. Hornfelsing is common here; these rocks are hard and do not exhibit any sedimentary structures. Propylitically-altered diorite occurs at 85 ft. and contains significant sericite. Calcite is a major alteration mineral along with epidote and chlorite. Most observed diorite is porphyritic, but is fine-grained with plagioclase phenocrysts approximately 0.5 cm long. This sericitic-calcite-chlorite alteration is dominant down to 180 ft., and contains trace amounts of euhedral pyrite, which can be present locally up to about 3% of the total groundmass.

Between 180 – 395 ft., diorite is altered to a chlorite-dominant propylitic assemblage without sericite. In this interval, the diorite is also porphyritic and fine-grained. QSP alteration, occurring between 395 – 470 ft., consists of a bleached, sericite-dominant assemblage with abundant cubic pyrite disseminated through the groundmass. Here, pyrite commonly constitutes between 5% - 7% of the chips.

The final 30 feet of the hole, 470 – 500 ft., is hornfelsed Ovi quartzite. Trace amounts of pyrite occur with locally up to 2% pyrite present. This quartzite is clean and unoxidized.

SC-1

The longest hole at Scraper Springs is SC-1, which is collared to the east of SC-5 in recrystallized, silicified Ovi sedimentary facies (Table 3, Fig. 17). The majority of this 1900 ft. hole is variably altered Ovi, with quartzite common near the top and more lithic facies occurring

deeper in the hole. A largely aphanitic intrusion of diorite occurs over the interval between 490 - 535 ft. This exposure of Td is propylitically-altered, consisting of probable chlorite with local disseminations of pyrite.

The section that occurs after 535 ft. to the bottom of the hole at 1900 ft. consists of different Ovi sedimentary facies. Although there is evidence of more quartzite at depth, the dominant lithology consists of more lithic and shaly units. For example, a mottled whitish-purple shaly lithology is a common rock-type encountered. The purple color of the rock suggests these are more reduced sediments and could possibly provide a favorable redox boundary for mineralization. Near the bottom of the hole, between 1815 – 1850 ft., the rock is carbonate-rich. The rock is still shaly, however this lithology displays a demonstrable reaction to hydrochloric acid. Although the final 100 ft. of this hole were not assayed, it is notable that this carbonate-rich lithology occurs here, as geochemical anomalies in copper and zinc spike just above this unit. Between 1765 and 1800 ft., Cu-values jump from low values under 100 ppm to in excess of 2100 ppm. Over this same interval, Zn-values are elevated from low-hundreds ppm to above 1000 ppm and between 1765 – 1770 ft., is measured at 10,000 ppm (Unpub. Cordex report 2004 (SP066323)).

Although the difference in lithology between 1765 – 1800 ft. and the rest of the drill hole is subtle, it is notable that an increasing amount of carbonate in shale occurs below 1800 ft. It is Hydrothermal fluids probably contributed metal to these reactive calcareous units, causing weak exoskarn mineralization with a mineral assemblage of calc-silicates.

SS-1

SS-1, collared just to the east of SC-1, is almost entirely drilled into Ovi (Table 3, Fig. 17). A 20-foot interval of diorite occurs between 90 – 110 ft., which is propylitically-altered with

epidote and chlorite replacing mafic phenocrysts. Additionally, quartz veining in this interval is evidenced through coarse quartz crystals.

The Ovi quartzite in this drill hole is variable. Although the majority of the quartzite exposed in SS-1 is clean, there are several intervals of significant clay alteration. These areas likely represent dirtier sand intervals in the sedimentary sequence or possibly through-going structures. Additionally, significant pyrite mineralization occurs in this hole starting at 210ft. Between 210 ft. and the bottom of the hole at 500 ft., pyrite is a common mineral, which is frequently observed to occur above 10% of the total groundmass. Over the interval from 265 – 280 ft., pyrite constitutes greater than 20% of the groundmass and locally accounts for 30% of the minerals within the RC chips. In these zones pyrite occurs as massive, sooty aggregates and is disseminated through the groundmass. Additionally, pyrite is also observed along fractures and other small structures.

SC-11

The next drill hole along the transect is SC-11, which is collared in chlorite-sericite altered Td (Table 3, Fig. 17). The first 240 ft. of the hole occurs within Td with a few cross-cutting quartz syenite (Tqs) dikes. The diorite exposed here is fine-grained and relatively equigranular with 2-4mm feldspar phenocrysts. Alteration along this interval is mostly chlorite-epidote-rich propylitized diorite and includes disseminated pyrite, which replaces Fe-Mg minerals in up to 3% of the groundmass. In two intervals (0 -15 ft.; 210 – 245 ft.), sericite and pyrite overprint chloritic alteration, and pyrite commonly exceeds 7% and locally comprise more than 20% vein material (210 – 220ft). In this vein material there is a mineral occurring in trace

amounts that has the observed properties of sphalerite, but was not independently verified by instrumentation.

Tqs dikes cross-cut this interval of diorite. The quartz syenite exposed in this hole contains equigranular, pink orthoclase phenocrysts that are not altered to sericite and/or clay, as are the surrounding feldspar crystals in the diorite. These dikes contain little quartz (<5% quartz) and trace amounts of biotite.

Below the igneous rocks in this hole, hornfelsed Ovi quartzite is observed to the total depth at 500 ft. Pyrite occurs in these sedimentary rocks between 3-5% as disseminations, cross-cutting veinlets, and locally coarse aggregates. No significant sedimentary features were observed within these sedimentary facies. There is another section with significant quartz vein material that occurs from 340 -355 ft. Here, pyrite and sericite accompany quartz as major vein constituents; pyrite is abundant and comprises 15%-20% of the total groundmass over this interval.

SS-9

After the kink in the transect, SS-9 occurs to the east and is collared in bleached tuff (Table 3, Fig. 17). A thin veneer of Tvt occurs at the surface, which is heavily oxidized and weathered. Tqs intrudes this unit and occurs between 10 – 50 ft. In this example of quartz syenite, both orthoclase and biotite are commonly observed. In previous holes (SS-11, SC-4), biotite was a minor phase, but here it is intergrown with orthoclase in an equigranular groundmass. Diorite intrusive follows from 50 to 210 ft. and is commonly chlorite-rich, with major intervals of sericitic alteration overprinting the original propylitic assemblage. Significant sericite and pyrite alteration occurs between 120 and 200 ft., where pyrite commonly occurs in

excess of 15% total groundmass and locally (145 – 155 ft.) accounts for as much as 25% of the groundmass. Additionally, trace amounts of a mineral identified as molybdenite are observed between 170 and 175 ft. Although these particular grains of molybdenite were not independently verified through instrumentation, similar assemblages were observed by Newmont in 2008 in the SCN-00015 at an unknown depth. Figure 18 is an SEM back-scatter image of molybdenite observed during Newmont's campaign.

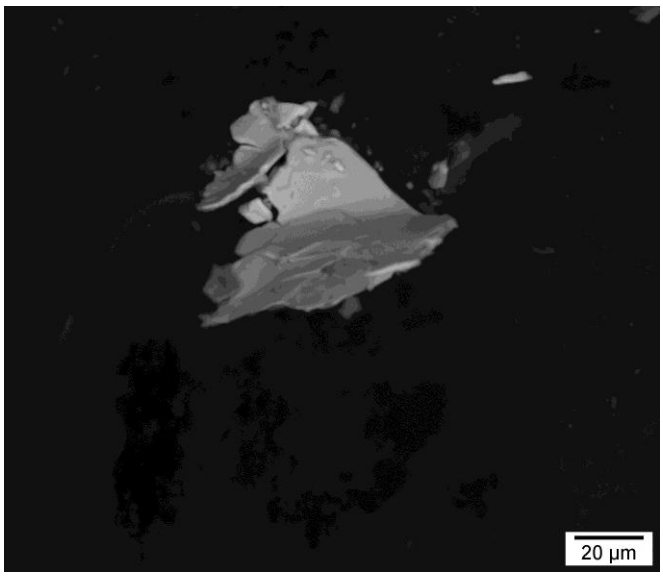

Figure 18. Molybdenite observed in QSP-altered zone in RC drilling by Newmont in 2008. Photo courtesy of Jim Wise (Wise, personal communication, 2010).

At 210 ft. drilling intercepted Ovi cherts and shortly thereafter encountered argillites and associated mudrocks at 240 ft. From 240 to 1000 ft., where the hole ends, variable Ovi sedimentary facies occur. These include cherts, quartzites, argillites, and mudrocks. No significant and/or discernable carbonate facies were observed. Additionally, most of these sedimentary rocks are hornfelsed and commonly contain pyrite in trace amounts. Local pyrite mineralization (525 – 530 ft., 825 – 830ft.) occurs in excess of 5% in massive aggregates, along bedding planes, and in veinlets.

SCN-00014

SCN-00014 is collared to the east of SS-9 in advanced argillic-altered Tvt, centered in the middle of the southern breccia zone (Table 3, Fig. 17). Between 0 ft. and 25 ft., a cover of Tvt occurs and is altered to silicified and advanced argillic assemblages. Alunite is observable in large quantities here as a pink residue. Most volcanic textures are obscured, although relict fragments and phenocrysts are locally observable. Between 25 and 1200 ft, Td intrudes with localized vein material and quartz syenite intrusions cross-cutting the diorite.

Advanced argillic alteration extends from the surface in the Tvt into the diorite where it occurs down to 100 ft. From 100 to 475 ft., an overall bleached QSP assemblage occurs. In the advanced argillic alteration assemblage, most igneous textures were obscured, whereas in the QSP assemblage, igneous textures and relict phenocrysts are observable. The amount of silicification/quartz veining over this interval is significant and accounts for more of the rock than sericite. Pyrite, with local pockets of chalcopyrite, occurs in the QSP assemblage and commonly constitutes 5-10% of the groundmass as disseminations.

From 475 – 540 ft. a large quartz syenite dike occurs. This dike, unlike dikes observed in other drill holes, is more porphyritic. It contains pink orthoclase phenocrysts and trace amounts of biotite in the groundmass. Additionally, between 575 – 615 ft. a section of quartzite occurs. Because this quartzite does not correlate with any nearby units, it is likely a xenolith in the diorite stock.

The remainder of the hole from 615 – 1200 ft. contains variably altered diorite, which alternates between chlorite-dominant and sericite-chlorite dominant alteration assemblages. Pyrite content is commonly elevated in the QSP zones with local areas consisting of up to 25%

pyrite. In the cross-cutting quartz syenite dikes, pyrite is more common in this hole than elsewhere, and still exhibits potassium-rich minerals like orthoclase with minor biotite.

SCN-00013

The last hole along the relogged transect is SCN-00013, which is collared in advanced argillic-altered Tvt in the southern breccia zone (Table 3, Fig. 17). Tvt occurs between 0 ft. and 315 ft., where it is interfingered with a diorite dike and is truncated at 345 ft. The top 75 ft. of the hole (0 – 75 ft.) contains advanced argillic assemblages that obscure most of the textures common to Tvt. Locally chalcedony fills vugs that were leached by acidic fluids and replaced by quartz. Advanced argillic and chalcedonic breccias are also observed throughout this interval. At 75 ft., original Tvt textures and phenocrysts are observable, but altered to sericite-dominant QSP assemblages. Between 90 ft. and 180 ft., pyrite occurs as disseminations and lesser veinlets, constituting between 5% to locally 25% of the groundmass.

Diorite was encountered between 345 ft and the bottom of the hole at 1300 ft. The rock is altered to sericite-dominant QSP assemblages from 345 to 1105 ft., and to a chlorite-dominant propylitic assemblage from 1105 at 1300 ft. Significant pyrite mineralization occurs between 705 and 970 ft., where pyrite commonly exceeds 15% of the groundmass (725 – 855 ft.) and locally (755 – 760 ft.) accounts for approximately 25%. Over this interval and the entire QSP assemblage, pyrite occurs as disseminations and veinlets in the groundmass. Additionally, local chalcopyrite occurs in association with pyrite throughout the same interval.

Interperative Cross-Section

Drill data combined with surficial mapping, petrography, and a magnetics survey (Appendix E) went into the creation of an interperative cross-section through the heart of the Scraper Springs hydrothermal system. The transect chosen passes through the drill holes selected (Table 3), which includes the North and South Breccia Zones and North and South Stocks.

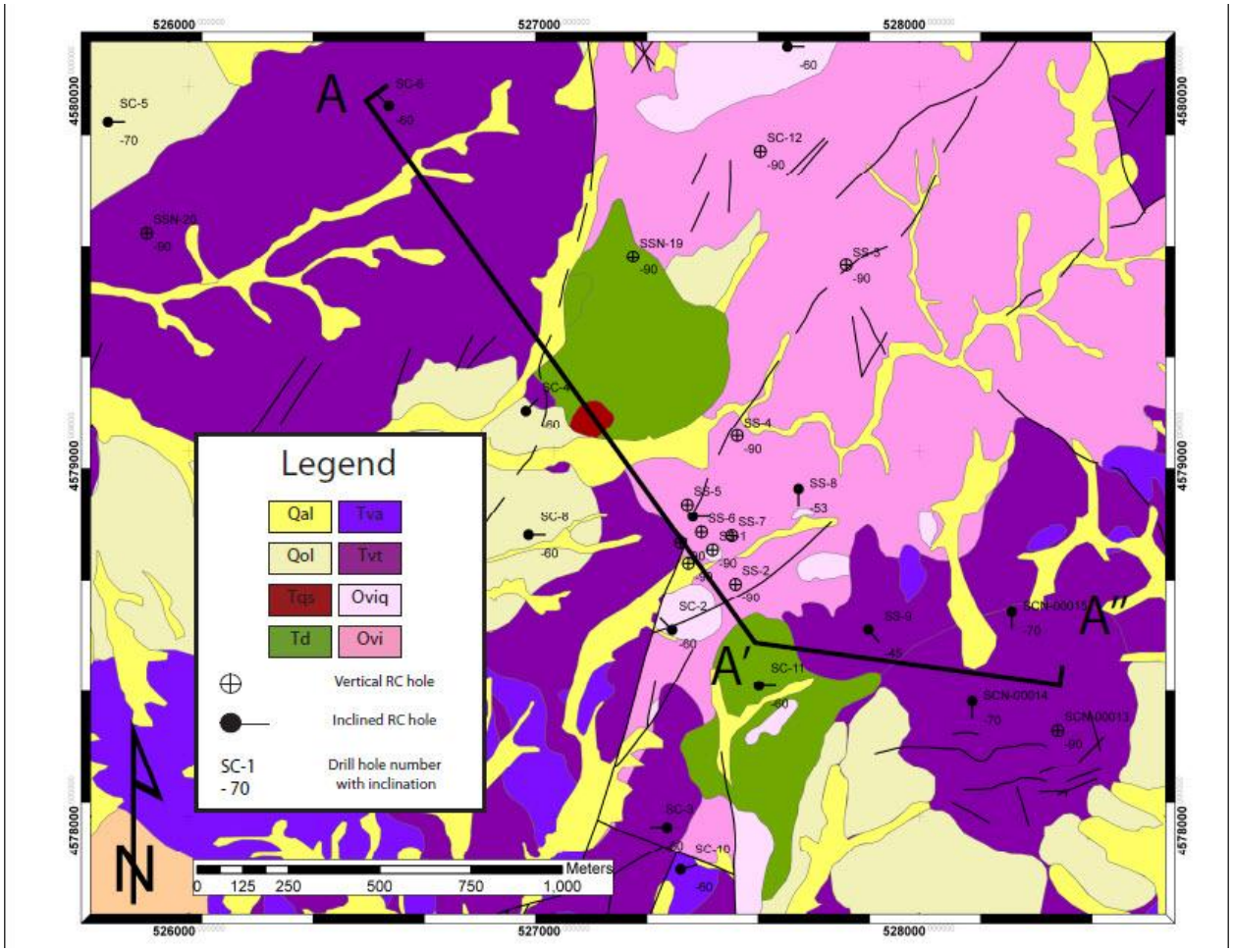

Figure 19. Transect of interperative cross-section.

The cross-section shows several different features observed at Scraper Springs (Fig. 19). First, it shows the erosional window of Ordovician Vinnini formation that occurs in the middle of the project as well as the Permian-Pennsylvanian Havallah sequence. These formations are subsequently cross-cut and intruded by Eocene diorite, which occurs as the North and South Stocks, and also occurs as dikes along major structures in the Paleozoic assemblage. The Eocene diorite is responsible for widespread QSP alteration, which is known from RC drilling. Cross-cutting the Eocene diorite is the quartz syenite intrusion of unknown age. Based on drilling results and surficial mapping, the quartz syenite unit is strongly altered to potassic assemblages and is responsible for potassic alteration.

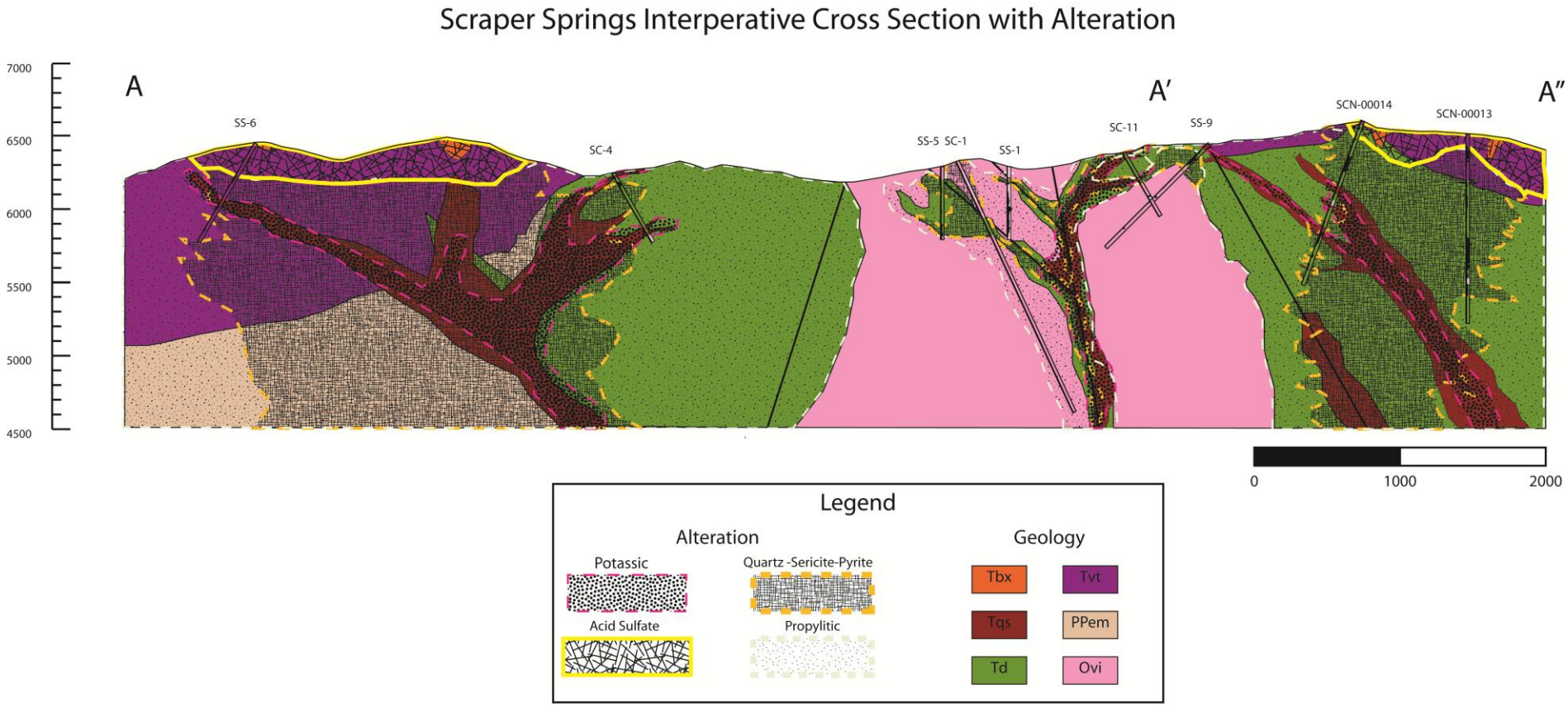

Figure 20. Interperative cross-section of Scraper Springs based on petrography, mapping, and drill hole data.

Above the main diorite intrusions are the advanced argillic lithocaps, which are related to the QSP and potassic alteration assemblages as the upper-most expression of the porphyry system. Locally, strong acid-sulfate alteration occurs along major structures and creates the advanced argillic breccias seen on the surface.

Geochemistry

The following samples (SC-02-36, SC-02-17, SC-01-88, SC-02-10, SC-02-01, SC-01-72) were submitted for geochemical analysis based on the fact that all of them share a relatively similar dioritic protolith and represent different styles of advanced argillic alteration.

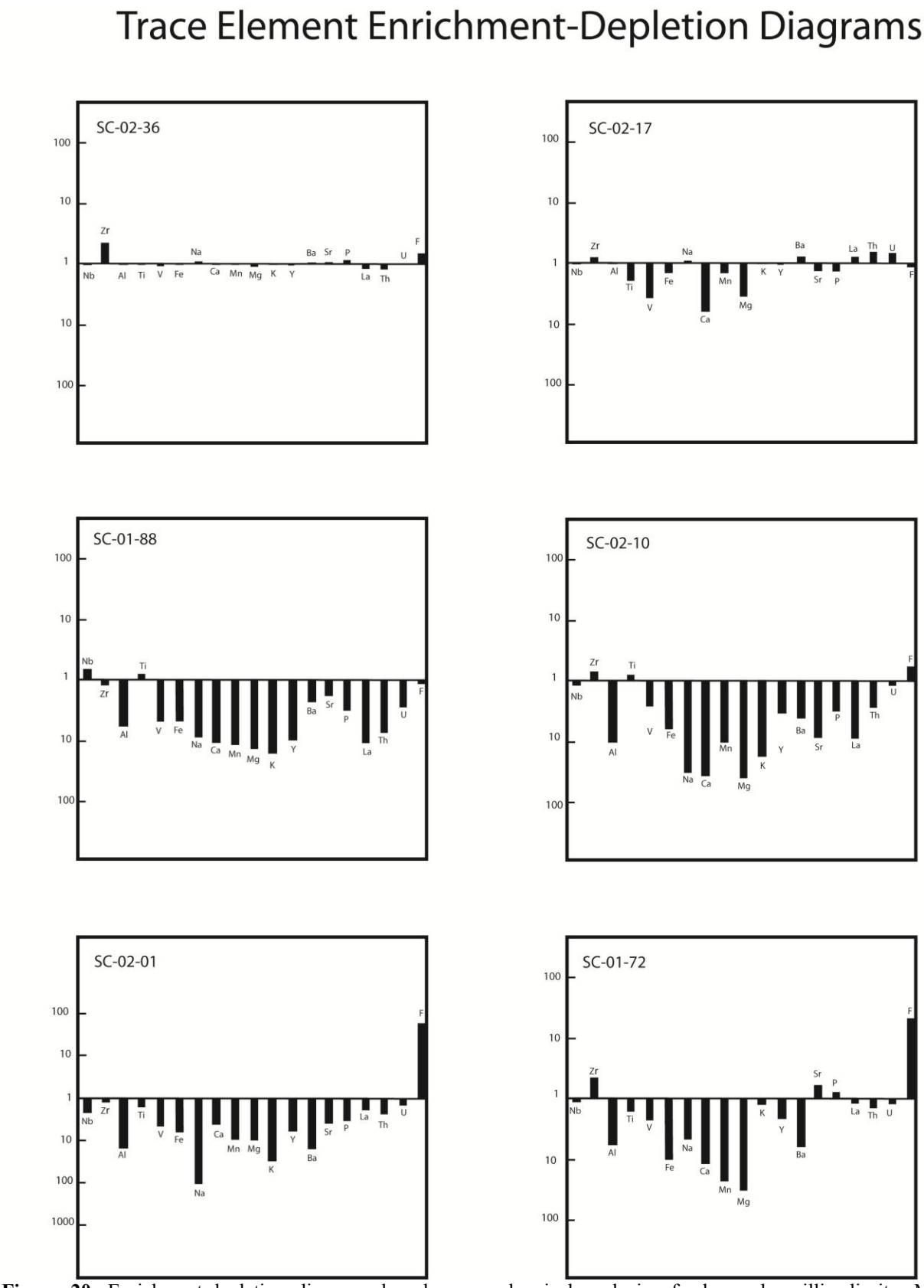

Figure 20. Enrichment-depletion diagrams based on geochemical analysis of advanced argillic diorite. Most samples are depleted in major- and trace-elements relative to least-altered diorite. Y-axis is a logarithmic scale.

Each sample was compared against a least-altered diorite sample, SC-02-75 and normalized based on those geochemical data. Nb, Zr, Al, Ti, V, Fe, Na, Ca, Mn, Mg, K, Y, Ra, Sr, P, La, Th, U, and F were all analyzed and compared. Most samples show a depletion in most major and trace-elements relative to the least-altered sample. In SC-02-01 and SC-01-72, samples which contained significant quantities of topaz, there was a significant enrichment in fluorine.

The fluorine results of this geochemical survey are also interesting when compared with the results from the 2008 soil survey. It was documented by Wise (2008b) that the soil survey, covering mostly the South Breccia Zone, is anomalous in Bi, Te, In, and Mo, which are all elements that when occurring together, suggest a source proximal to an intrusive center. This could either be represented by the Eocene diorite or a potentially deeper intrusion which contributes to those anomalous values. Based on this and the fact that the molybdenum high was particularly interesting, fluorine values are plotted on top of the hand-contoured Mo soil anomaly (Fig 22). The results are interesting in that while there are limited rock chip data containing F, the results that do occur suggest a strong correlation between the elevated Mo zones (>5 ppm) and high F values (>0.1 % F) (Fig. 22). Additionally, there are two samples taken that were assayed for fluorine that do not fall within the 2008 soil survey pattern.

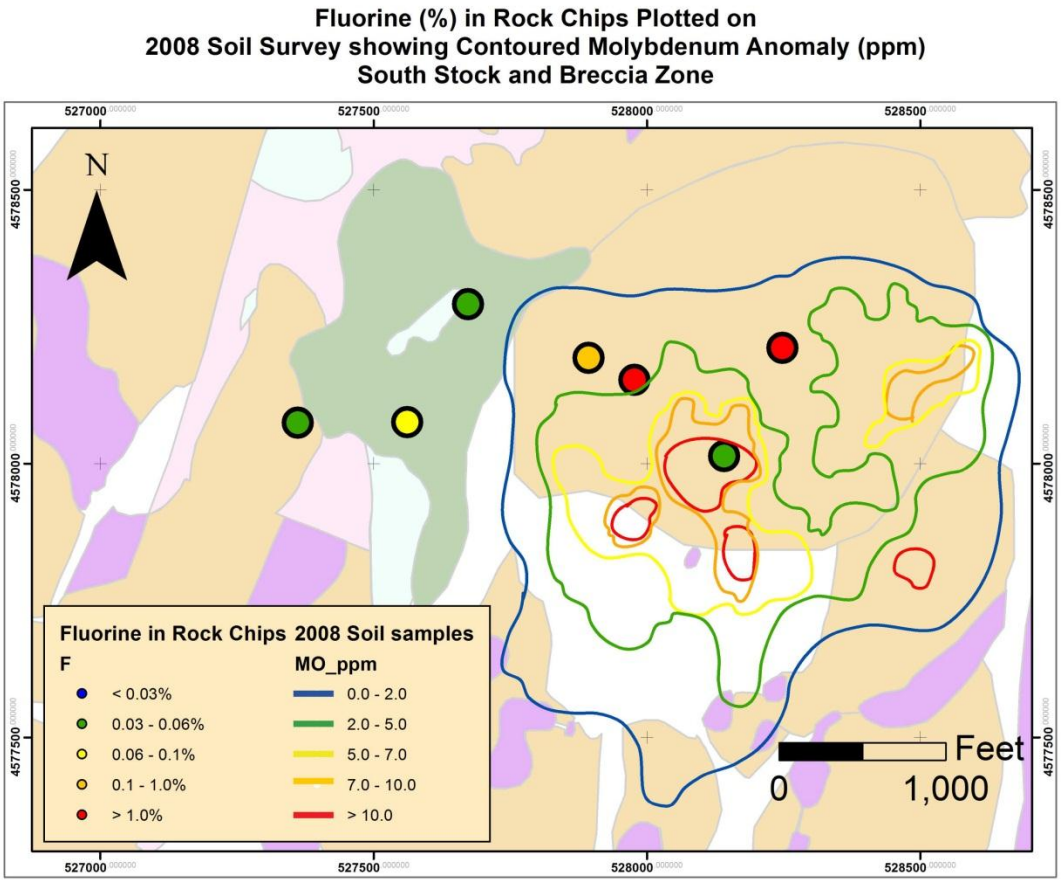

Figure 22. Map showing hand-contoured Mo values (ppm) in soils compared with F values (%) in select rock-chip samples. Although only seven samples were analyzed for F, there is a strong correlation between F in rock chips and the high Mo soil zones. The samples from the South Stock west of the contoured lines fall outside of the soil sample grid.

Discussion

The geologic, alteration, mineralization, petrographic, and geochemical observations made in the present study help characterize the geologic environment and framework for the development of the Scraper Springs mineral system. One of the most striking of these observations is the pervasive acid sulfate alteration exposed at Scraper. Mineral assemblages containing sulfates and aluminosilicates are two of the most profound types of acid sulfate

mineral assemblages observed at Scraper Springs. Large exposures of highly altered and leached volcanic rocks crop out in both the North and South Breccia Zones at Scraper Springs. As has been demonstrated through the petrographic work presented in this study, many sulfate and aluminosilicate mineral assemblages occur. These minerals were formed in an environment representative of a transition zone between a porphyry and high-sulfidation epithermal system (Sillitoe, 2010). When considering the specific mineral assemblages in this acid sulfate environment, constraints can be placed on the temperature, pressure, and chemical composition of the hydrothermal system responsible for the mineralization observed at Scraper Springs. When these constraints are put into a broader geologic framework, a better understanding of the exploration potential at Scraper can be achieved.

One acid sulfate mineral assemblage observed at Scraper Springs contains pyrophyllite and diaspore, two aluminosilicate minerals indicative of low-pH conditions and low to intermediate temperatures (Hemley et al., 1980). These minerals, in the presence of quartz, represent phases from the chemical system Al_2O_3-SiO_2-H_2O. When present together, the occurrence of diaspore and pyrophyllite suggests that temperatures were around 300°C when they formed. Additionally, this assemblage suggests the hydrothermal system was undersaturated in quartz (Hemley et al., 1980). The common process through which these minerals formed is known as hydrolytic alteration, which is a hydrolysis reaction of feldspars with H^+ ions. It can be described through the formula:

$$2KAlSi_3O_8 + 2H^+ \rightarrow Al_2Si_4O_{10}(OH)_2 + 2SiO_2 + 2K^+$$

Equation 1. Potassium feldspar reacts with acid to form pyrophyllite and quartz with excess potassium ions, likely responsible for potassic alteration observed elsewhere in the system (Hemley et al., 1980).

When halides are present within this system, topaz ($Al_2SiO_4(F,OH)_2$) or zunyite ($Al_3Si_5O_{20}(F,OH)_{18}Cl$) can form, which is the case at Scraper Springs. Additionally, when there is sulfate present within the high-acid (hydrolytic alteration) system, alunite can also form ($KAl_3(SO_4)_2(OH)_6$). Scraper Springs has a significant amount of alunite. The aluminosilicate mineral assemblage present at Scraper Springs suggests the presence of a low-pH hydrothermal fluid containing a strong concentration of halides at sustained temperatures around 300°C. (Hemley et al., 1980). This temperature lies at the higher end of the spectrum of epithermal deposits, in which most deposits occur at 300°C or less (Simmons et al., 2005).

Scraper Springs has a significant occurrence of F-bearing minerals within the advanced argillic assemblage. A widespread zunyite occurrence has long been documented (Coats et al., 1979). The largest occurrence at Scraper is hosted within what has been referred to as a "huge zunyite lode," which is a vein striking approximately 1200 ft. long and ranging between 10 and 60 feet wide (Coats et al., 1979). This vein crops out on the eastern margin of the property and consists of intergrown quartz and zunyite, comprised of up to 75% zunyite locally (Coats et al., 1979). Although this vein was not the focus of the present study, several zones containing massive zunyite (ex. Fig. 16E, F) were observed. In addition to zunyite, a significant amount of topaz was also documented in this study (Fig. 14K, L). Fluorite is the other F-bearing mineral documented at Scraper Springs (Fig. 16O, P), but has only been observed locally. Zunyite and topaz are both fluorine-bearing aluminosilicate minerals that occur within highly-leached advanced argillic alteration assemblages. The presence of the two minerals demonstrates a significant fluorine endowment at Scraper Springs. Select samples (SC-02-01, SC-01-72) contain more than one percent fluorine with SC-02-01 containing above 3% fluorine (Appendix C). The presence of these fluorine-bearing minerals suggests specific temperature and pressure

conditions occurred where they formed. Topaz can form over a range of temperatures, although higher-temperature topaz (>300°C) tends to partition more fluorine into the solid phase (Hsu, 1986). This is likely the case at Scraper Springs because samples SC-01-72 and SC-02-10 both contain significant topaz and assays returned values greater than 1% fluorine (Appendix C). Conversely, zunyite has a much more specific chemical range; the thermodynamic field for zunyite is rather limited (Hsu, 1986). Zunyite is stable in the presence of quartz rather than topaz at Scraper Springs; this assemblage requires sustained low-T (<450° C) combined with a low HF concentration (< 2M) in the presence of Cl^- within the hydrothermal fluid (Hsu, 1986). These constraints suggest the zunyite present at Scraper was formed at a temperature greater than 300°C and less than 450°C. The widespread nature of zunyite at Scraper also suggests a large hydrothermal cell with specific thermodynamic constraints over an area greater than a kilometer in strike length.

The advanced argillic minerals at Scraper Springs are largely hosted within the silicified breccia bodies of the North and South Breccia Zones. Although previously interpreted as phreatomagmatic, or diatreme, breccias (Wise, 2008b), the breccia textures and mineral assemblages described in this study suggest that the breccias are magmatic hydrothermal (Sillitoe, 2010). These breccias are common in world class ore deposits and commonly contain advanced argillic alteration assemblages (eg. Yanacocha; Turner, 1999). Diatreme breccias consist of matrix-dominated heterolithic lithologies that form irregular bodies (Sillitoe, 1985). The matrix in these breccias consists of rock flour that has been derived from magmatic sources with heterolithic fragments acquired from the explosive eruption through the country rock (Sillitoe, 1985). In many systems, intense alteration of the original lithology can obscure the composition of the original matrix material, rendering a positive determination of breccia type

difficult (Sillitoe, 2010). However, diatremes also have additional characteristics such as locally subsided basinal features with associated lacustrine sediments that are not observed at Scraper Springs (eg. Thompson et al., 1985). Therefore, due to the structurally controlled nature of the breccia outcrops, lack of discernible magmatic-derived matrix, and absence of any subsidence-related features with lacustrine sediments, Scraper Springs does not likely host a diatreme.

The breccias hosted in the North and South Breccia Zone at Scraper Springs are instead likely sourced from a magmatic-hydrothermal source deeper in a porphyry system. Sillitoe (2010) describes two types of phreatic breccias that occur in porphyry systems, both of which share features observed at Scraper Springs. The two types of phreatic breccias described by Silitoe (2010) refer to the depth within the porphyry copper system model in which they occur. One breccia is the higher, epithermal-level phreatic breccia and the other is the deeper, porphyry copper-level breccia. Both are common features of the porphyry environment; the porphyry copper level breccia occurs within and around porphyry copper deposits and the epithermal breccia occurs within the lithocaps above porphyry systems. Both types of breccias tend to form irregular bodies and contain breccia characteristics where the clasts are angular to subrounded in nature. However, the epithermal level phreatic breccia is commonly silicified, whereas the deeper porphyry Cu level breccia is more likely polymictic with a matrix of igneous material. Additionally, phreatic epithermal breccias can commonly contain cement of quartz, chalcedony and alunite among other sulfur-bearing minerals, whereas the porphyry copper level breccia more commonly contains a muddy rock flour matrix. Both breccias can host advanced argillic minerals and are commonly matrix-supported, although epithermal phreatic breccias can also have clast-supported examples. It is possible for high grade high-sulfidation type ore to occur within the phreatic epithermal breccias, but porphyry copper level phreatic breccias are typically

barren. Features of both breccias occur at Scraper Springs. At Scraper, the breccias commonly contain heterolithic clasts and are silicified, while hosting different types of advanced argillic assemblages. As described in a previous chapter, the Scraper breccias are silicified with chalcedony, quartz, and alunite occurring as major constituents within the matrix. This is more common to an epithermal breccia. However, advanced argillic and sericitic alteration commonly occur within a porphyry copper-level breccia, and contain barren grades of Au-Cu mineralization, which is the case at Scraper Springs. Based on the reported breccia types, morphologies, and mineral assemblages, the environment that led to the formation of the rocks exposed at Scraper Springs can be considered a transition from the porphyry to epithermal regime and is likely telescoped (Sillitoe, 1985; Sillitoe, 2010).

The mineral assemblages present at Scraper Springs indicate a deep level of formation within an epithermal system around 300°C. Coupled with the context of the epithermal-porphyry copper-level breccia hosts for these minerals, it can be concluded that the environment, barren in ore minerals, exposed at the surface at Scraper Springs is situated between a high-sulfidation epithermal gold environment and a larger, bulk tonnage porphyry Cu ± Au ± Mo system. Further evidence suggests there may be a porphyry system situated beneath these advanced argillic zones.

Drilling conducted by Newmont in 2008 encountered significant alteration underneath the South Breccia Zone. The Newmont holes SCN-00013 and SCN-00014 were collared in advanced-argillic altered Tvt. Drilling indicates that advanced argillic alteration underlies this area for up to 100 ft. and then transitions into a sericite-pyrite dominant alteration style. Although these rocks are mostly barren of ore minerals, this area is significant because drilling encountered widespread quartz-sericite-pyrite (QSP) alteration, commonly with pyrite

percentages around 15% and locally up to 30%. Additionally, molybdenite was also locally encountered, further supporting the notion that there is widespread untested alteration and mineral potential. This type of massive alteration can help vector toward a more productive part of the porphyry system.

The presence of zunyite and topaz in large quantities at Scraper is significant because it puts thermodynamic constraints on the formation of the system, but also because topaz and zunyite in particular are associated with world class ore deposits. It has been recognized for a long time that fluorine is associated with ore deposits (eg. Summitville, CO; Gray and Coolbaugh, 1994; Urad-Henderson; Seedorf and Einaudi, 2004a, b). One reason for this association is because fluorine plays a significant role in hydrothermal systems in controlling the composition of ore fluids. Although fluorine has been demonstrated not to be a main complex in the transport of Au or Mo, it is still found in association and in significant quantities (Tingle and Fenn, 1984). Instead of actively transporting Mo, fluorine serves a role in depressing the solidus temperature of magmatic melts several tens of degrees, aiding deposition of Mo as MoS_2 (Manning, 1981). Additionally, fluorine helps to depolymerize melts and lowers their viscocity aiding ascent and vapor evolution (Manning, 1981). This "vapor evolution," is the same process that helps to concentrate Cu, Au, and Mo in porphyry systems (Tingle and Fenn, 1984). Therefore, the presence of fluorine in hydrothermal systems is considered an important ore deposit system (Tingle and Fenn, 1984). Considering the widespread F-bearing minerals that occurs at Scraper, the potential for a prospective mineral deposit remains high.

Based on the outcropping breccias with porphyry-level and epithermal-level characteristics, widespread acid sulfate alteration and QSP alteration in the subsurface, and proximity of the potassic-altered diorite intrusive to the breccia zone, Scraper Springs can be

considered a telescoped porphyry system based on the classification of Sillitoe (2010) (Fig. 23). In telescoped porphyry systems, different zones of alteration overlap and the overall vertical extent of the system is shortened. At Scraper Springs, the two zones that are observed at the surface include the basal Quartz-Alunite assemblage adjacent to the Quartz-pyrophyllite assemblage and the Potassic assemblage juxtaposed with the Chlorite-Sericite assemblage. The Quartz-Alunite/Quartz-Pyrophyllite assemblage is manifest in the breccias at Scraper, as they are both part of the acid-sulfate alteration suite and these mineral assemblages have been documented to occur within the breccias. Similarly, the diorite at Scaper has been documented to include elements of both Potassic alteration and Chlorite-Seriecite alteration, suggesting the diorite is exposed at a relatively high, transitional level within the porphyry system. These constraints have significant implications for exploration, which will be discussed in the following section.

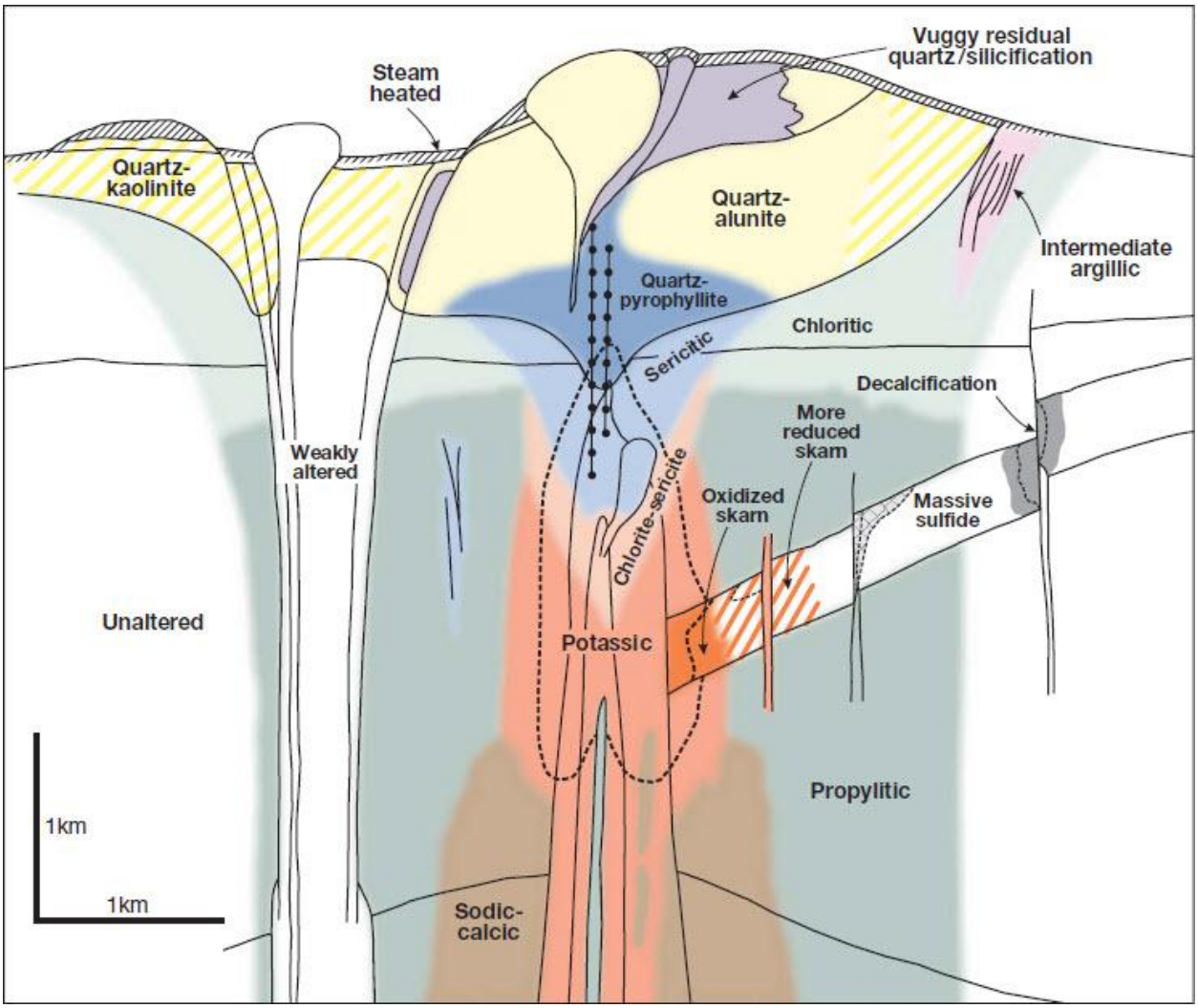

Figure 23. Telescoped porphyry system model taken from Sillitoe (2010). The hydrothermal system at Scraper Springs can be considered a telescoped porphyry that has characteristics of the Quartz-Alunite/Quartz-Pyrophyllite assemblage, which is represented in the acid-sulfate breccias. Similarly, the potassic-altered diorite has characteristics of the Potassic and Chlorite-Sericite zone, which occurs in a transitional alteration assemblage according to this model.

In eastern and northern Nevada one other Eocene system with similarities to Scraper Springs is the Mount Hope porphyry molybdenum deposit in Eureka County, NV. The Mount Hope porphyry molybdenum deposit is an Eocene Climax-type molybdenum system dated at 36.0 Ma recently by Henry (pers. Communication, 2012) through Ar^{39}/Ar^{40} methods. This deposit contains characteristics similar to several world-class molybdenum systems in Colorado and other parts of the western United States (Carten et al., 1988; Seedorf and Eianaudi, 2004a, b). These deposits are characterized by relatively high-grade molybdenum mineralization (0.1-0.5 percent Mo) with plutons enriched in fluorine (commonly >1%) and occur in association with and within felsic intrusives. High-grade molybdenum ore occurs as cupola-shaped bodies that are centered on these felsic intrusions. Alteration in Climax-type molybdenum deposits includes a strongly potassic-altered mineralized center zoning outward into greisen and phyllic assemblages (Westra and Keith, 1981). The orebody at Mount Hope does not crop out, but many of the characteristics are manifest in surficial geology including strong phyllic alteration and rocks with elevated fluorine. Additionally, the discovery at Mount Hope was made with rock chips grading between 25 to 100 ppm Mo at the surface (Riedell, 1995). Both of these traits of the Mount Hope deposit are similar to current observations at Scraper Springs.

Several factors favor the relationship between the alteration observed at Scraper Springs and its potential relationship to a Climax-type porphyry molybdenum deposit. First, the date on the diorite at Scraper Springs is consistent with the Eocene age of the Mount Hope system. More geochronology is needed at Scraper to increase the confidence of this number, but this Eocene date is encouraging considering Mount Hope has a similar date. In addition, other porphyry deposits in north-central Nevada are this age, which include the Copper Basin porphyry, the Battle Mountain porphyry, and the McCoy pluton (eg. Schmidt et al., 1988; Johnston et al.,

2008). While these deposits are enriched in Au, Cu, and base metals, it is significant that metalliferous intrusives of this age occur in northern Nevada.

The geology and alteration documented at Scraper Springs is also consistent with a Climax-type porphyry model. The South Stock has a distinct alteration zoning pattern including a small exposure of silicified intrusive, which is an early, proximal alteration type in Climax-type systems (eg. Carten et al., 1988). Outboard of this silicified exposure, potassic alteration occurs within the South Stock, and outboard of this zone, phyllic alteration has been documented in drilling. The advanced argillic and acid sulfate alteration at Scraper Springs represents a more distal (porphyry-epithermal transition) (zone) to the main system, which petrographic work has documented to occur around 300°C. The main phase mineralization in Climax-type molybdenum systems occurs between 400-600°C, suggesting that vectoring toward molybdenum mineralization at Scraper would focus on higher-temperature assemblages and earlier, centrally-located alteration phases such as the silicified zone within the South Stock (Seedorf and Einaudi, 2004a). More investigation is needed into different phases of intrusives documented at Scraper Springs. Limited petrographic work and RC chip logging from this study highlighted a quartz syenite intrusive that cross-cuts the more mafic diorite exposed at the surface. Whole rock geochemistry of this quartz syenite as well as core drilling to document cross-cutting relationships of different igneous phases would be warranted to associate felsic intrusives at Scraper Springs with their equivalents (granite, rhyolite) in Climax-type molybdenum systems. It is possible there are, in fact, multiple felsic intrusive phases at Scraper. Up to 13 intrusives have been documented, for example at Henderson, a world class Climax-type deposit (Seedorf and Einaudi, 2004a) More field investigation is needed to reconcile the geology at Scraper Springs with Climax-type deposits.

Geochemically, Scraper Springs is well-endowed with fluorine-rich alteration minerals. The endowment of fluorine-rich minerals at Scraper exists over a large area, with occurrences that are documented over several square kilometers (Hsu, 1986; Howell, 2004; Wise, 2008a; This Study). Elevated fluorine concentrations can exist outboard of large Climax-type deposits over several kilometers (Ludington and Plumlee, 2009). In proximal distances to Climax-type deposits, topaz and fluorite are documented; these minerals occur at Scraper Springs in the South Stock and South Breccia Zone. Selected rock chips of these assemblages at Scraper exceed 3% fluorine (Appendix C). Although no greisen assemblage has been recognized at the surface, it is possible that there is an existing fluorite-mica assemblage at depth, closer to a hypothesized intrusive center. In addition soil samples at Scraper Springs reveal anomalous Mo, In, Bi, and Te. These elements have been documented to occur as proximal elements to a source pluton and have been documented at Mount Hope and Spruce Mountain, NV, an Eocene porphyry-Mo ± Au prospect (Westra and Riedell, 1995; Pace, 2011). Therefore, the South Breccia Zone, where the soil survey highlighted anomalies, is likely situated relatively close to a source pluton. Rock chips at Scraper Springs also have elevated molybdenum concentrations ranging from several tens of ppm to greater than 100 ppm (highest = 164 ppm). Again, rocks chips at the surface of Mount Hope with 25-100 ppm molybdenum played a role in the discovery of that deposit (Riedell, 1995). These concentrations could be significant at Scraper Springs as well.

Future Work and Exploration at Scraper Springs

The field relationships, petrographic observations, and geochemical evidence documented in this study show that Scraper Springs is a large system with kilometer-scale alteration zoning. The widespread nature of the alteration at Scraper suggests that a large heat source was responsible for the profound alteration expressed at the surface. In closer

examination, advanced argillic-altered epithermal-level phreatic breccias as described by Sillitoe (2010) occur adjacent to an Eocene diorite intrusive which may be related to, but not necessarily responsible for these breccias. These breccias represent a zone of transition from a porphyry to epithermal environment based on the alteration assemblages gleaned from petrography. In addition, limited drilling suggests profound phyllic alteration in the subsurface. Other alteration documented from field relationships includes silicic-, potassic-, and propylitic-altered diorite. Coupled with geochemistry elevated in pluton-proximal trace elements (Bi, Te, Mo, and In) and fluorine, these observations suggest the surficial alteration at Scraper Springs is consistent with a Climax-type molybdenum porphyry model.

While the observations made within this study support a Climax-type model, much more work is needed to evaluate the mineral potential at Scraper Springs. Currently there is a dearth of geochronology at Scraper Springs. There is only one K/Ar date on biotite, which may or may not be hydrothermal in nature. Future studies should focus on $^{39}Ar/^{40}Ar$ dates of bladed, hypogene alunite from the North and South Breccia Zones (Fig. 14R, SC-01-72). These dates would help compare Scraper Springs to other similarly-aged intrusions in the Western Cordillera. Further mapping could document field relationships of the different intrusions present at Scraper Springs, specifically in the North Stock, where a small float-crop exposure of quartz syenite has been documented. Whole rock geochemistry on this unit and similar units found in RC chips would also be beneficial. Fluid inclusion data from the North and South Stock could help constrain the temperature of emplacement of these bodies and vector into a hydrothermal zone between 400-600°C, where Climax-type molybdenum mineralization occurs. A better understanding of the structure at Scraper Springs is also needed, although it would be difficult with the limited outcrop on the property. Finally, a tighter soil grid on the South Breccia Zone

and particularly the North Breccia Zone, which lacks soil sample data, would be warranted as a relatively inexpensive method to prospect for anomalous metal concentrations.

With the data presently available, there are two interesting molybdenum target areas on the Scraper Springs property. One possible target includes the silicified portion of the South Stock diorite, which would be a central alteration zone in the Climax-type model. Acid sulfate assemblages with high fluorine occur several hundred meters to the east in the South Breccia Zone area, which also corresponds with the molybdenum soil high. Any drill hole test along this transect would be a good target. The other area which is an interesting, yet a less-defined target is the North Breccia Zone (Fig. 24). This area contains rock chips with the highest concentrations of Mo observed on the property (high = 164 ppm Mo). A soil grid in this area, coupled with the present data could help highlight some structural intersection zones and a more clearly-defined target at depth. The Blind Stock highlighted by Wise (2008a) is an intriguing place to target (Fig. 23). Limited concentrations of Au and no evidence of sulfide mineralization in vuggy silica at the surface at Scraper Springs suggest future exploration at Scraper Springs should focus on Mo potential. With limited drilling (n = 28) across the property and most drilling focused on Carlin-type mineralization in the Paleozoic window, the potential for future mineral exploration is significant at Scraper Springs.

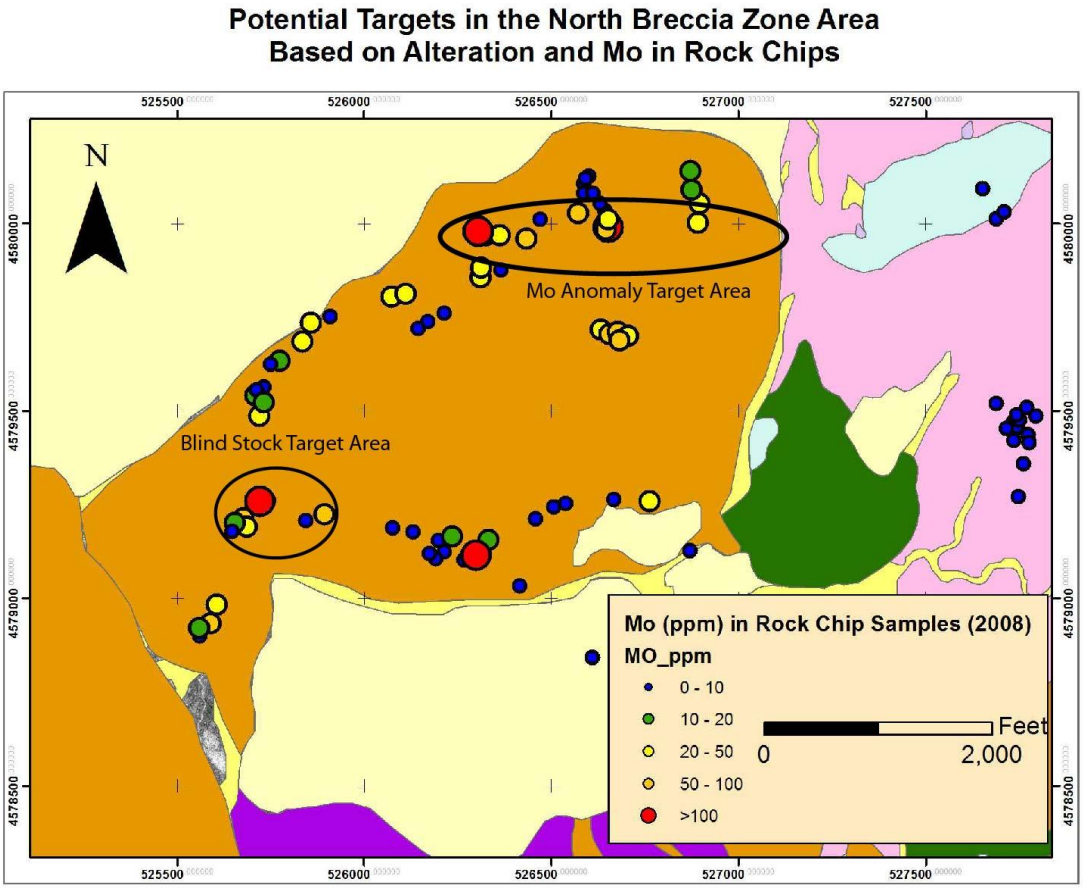

Figure 24. Target areas in the North Breccia Zone include the Blind Stock area highlighted by Wise (2008a) from a geophysical anomaly and the Mo Anomaly. Both areas contain rock chips with high Mo values including samples >100 ppm Mo. More work is needed in this area to focus these targets.

Acknowledgements

I would like to first thank the CREG program and its sponsors for project and scholastic funding and support throughout this project. I would also like to thank Cordilleran Exploration for its access to the property and the wealth of data collected at Scraper Springs. Specifically, I thank Andy Wallace for his introduction to the property and insight into certain questions about the property and Jon Vinson for originally showing me around the Scraper Springs property and orienting me to the geology there. I also thank my adviser, Tommy Thompson, for his insight and support in the CREG program and on the project and for visiting the Scraper Springs property and working through several problems incurred during initial phases of mapping. Finally, I'd like to also thank my fellow colleagues in the CREG program and in the geology department at UNR, including Heidi Drexler, Crystal Robinson, Wes Sherlock, Ben Schumer, Greg Rhodes, and Betsy Littlefield, for help and discussion over ore deposits, mineralogy, structure, and technical help with microscopy, GIS, and general insight into M.S. work.

References

Back, M.E., and Mandarino, J.H., 2008, *Fleischer's Glossary of Mineral Species*: The Mineralogic Record Inc., 346 p.

Carten, R.B., Geraghty, E.P., and Walker, B.M., 1988, *Cyclic development of igneous features and their relationship to high-temperature hydrothermal features in the Henderson porphyry molybdenum deposit, Colorado*: Economic Geology, v. 83, p. 266–296.

Castor, S.B., Boden, D.R., Henry, C.D., Cline, J.S., Hofstra, A.H., McIntosh, W.C., Tosdal, R.M., and Wooden, J.P., 2003, *The Tuscarora Au-Ag district: Eocene volcanic-hosted epithermal deposits in the Carlin gold region, Nevada*: Economic Geology, v. 98, pp. 339-366.

Coats, R.R., Consul, J.J., and Neil, S.T., 1979, *Massive zunyite rock from Western Elko County, Nevada*: USGS Open-File Report 79-764, 10p.

Christiansen, R.L., and Yeats, R.S., 1992, *Post-Laramide geology of the U.S. Cordilleran region* in Burchfiel, B.C., Lipman, P.W., and Zoback, M.L., eds., *The Cordilleran orogen: Conterminous U.S.*: Geological Society of America, The Geology of North America, v. G-3, p. 261-406.

Gray, J.E., and Coolbaugh, M.F., 1994, *Geology and geochemistry of Summitville, Colorado; an epithermal acid sulfate deposit in a volcanic dome*: Economic Geology, v. 89, pp. 1906 1923.

Henry, C.D., 2008, *Ash-flow tuffs and paleovalleys in northeastern Nevada: Implications for Eocene paleogeography and extension in the Sevier hinterland, northern Great Basin*: Geosphere, v. 4, pp. 1-35.

Henry, C.D., and Boden, D.R., 1998, *Geology of the Mount Blitzen Quadrangle*, *Elko County, Nevada*: Nevada Bureau of Mines and Geology Map 110, 20p.

Henry, C.D., and Boden, D.R., 1999, *Geology of the southern part of the Toe Jam Mountain Quadrangle*: Nevada Bureau of Mines and Geology Map 117, 12p.

Henry, C.D., Castor, S.B., and Boden, D.R., 1999, *Geology of the Tuscarora Quadrangle, Elko County, Nevada*: Nevada Bureau of Mines and Geology Map 116, 20p.

Hemley, J.J., Montoya, W., Marinenko, J.W., and Luce, R.W., 1980, *Equilibria in the system Al_2O_3-SiO_2- H_2O and some general implications for alteration/mineralization processes*: Economic Geology, v. 75, pp. 210-228.

Howell, F.S., 2004, *Geology and Alteration/Mineralization of the Scraper Springs Project*: Unpublished Report, Cordilleran Exploration Co., 1p.

Howell, F.S., 2007, *Scraper Springs project summary*, Unpublished Cordex report, 6p.

Hsu, L.C. 1986, *The stability relationships of zunyite under hydrothermal conditions:* Mining Geology, v. 36, pp. 219-230.

John, D.A., Wallace, A.R., Ponce, D.A., Fleck, R.B., and Conrad, J.E., 2000, *New perspectives on the geology and origin of the northern Nevada Rift* in Cluer, J.K., Prince, J.G., Struhsacker, E.M., Hardyman, R.F., and Morris, C.L., eds., *Geology and Ore Deposits 2000: The Great Basin and Beyond*: Geological Society of Nevada Symposium Proceedings, May 15-18, 2000, pp. 127-154.

Johnston, M.K., Thompson, T.B., Emmons, D.L., and Jones, K., 2008, *Geology of the Cove Mine, Lander County Nevada, and a Genetic Model for the McCoy-Cove Hydrothermal system*: Economic Geology, v. 103, pp. 759-782.

Leavitt, E.D., Spell, T.L., Goldstrand, P.M., and Arehart, G.B., 2004, *Geochronology of the Midas low-sulfidation epithermal gold-silver deposit, Elko County, Nevada*: Economic Geology, v. 99, pp. 1668-1686.

Ludington, S., and Plumlee, G.S., 2009, *Climax-Type Porphyry Molybdenum Deposits*: USGS Open-File Report 2009-1215. 16p.

Manning, D.A.C., 1981, The effect of fluorine on liquidus phase relationships in the system Qz Ab-Or with excess water at 1 kb: Contributions to Mineralogy and Petrology, v. 76, p. 206–215.

Pace, D.P., 2011, *Geochemistry of the Spruce Mountain Gold-Molybdenum Prospect, Eureka County, NV*: Technical Session, Northwest Mining Association Conference, Reno, Nevada.

Oelofse, J., Bentley, P., and van der Heever, D., 2009, *Revised technical report on the mineral resources and reserves at the Hollister development block gold project, Elko County, NV*: Great Basin Gold Ltd., 188p.

Ressel, M.W., and Henry, C.D., 2006, *Igneous geology of the Carlin Trend, Nevada: Development of the Eocene plutonic complex and significance for Carlin-type gold deposits*: Economic Geology, v. 101, pp. 347-383.

Riedell, B., 1995, *The Mount Hope Porphyry Molybdenum Deposit* in *Great Basin Porphyry Deposits, Trip A, 1995*: Geologic Society of Nevada, pp. 101-112.

Scraper Springs location map, 2005, Unpublished report, Geologix Explorations, Inc., 1p.

Schmidt, K. W., Wotruba, P. R., and Johnson, S. D., 1988, *Gold-copper skarn and related mineralization at Copper Basin, Nevada,* in *Buffa, R., and Schafer, R. W., eds., Gold deposits of north central Nevada--Marigold, Cove, McCoy, Rain, and Surprise*; 1988 Fall Field Trip Guidebook: Geological Society of Nevada, Special Publication 8, 6 p.

Seedorf, E., and Einaudi, M.T., 2004a: *Henderson porphyry molybdenum system, Colorado. I. Sequence and abundance of hydrothermal mineral assemblages, flow paths of evolving fluids*: Economic Geology, v. 99, p. 3–38.

Seedorf, E., and Einaudi, M.T., 2004b, *Henderson porphyry molybdenum system, Colorado. II. Decoupling of introduction and deposition of metals during geochemical evolution of hydrothermal fluids*: Economic Geology, v. 99, p. 39–72.

Sillitoe, R.H., 1985, *Ore-Related Breccias in Volcanoplutonic Arcs*: Economic Geology, v. 80, pp. 1467-1514.

Sillitoe, R.H., 2010, *Porphyry Copper Systems*: Economic Geology: v. 105, pp. 3-41.

Simmons, S.F., White, N.C., and John, D.A., 2005, *Geologic characteristics of epithermal precious and base metal deposits*: Economic Geology 100th Anniversary Volume, p. 485–522.

Stewart, J.H., 1980, *Geology of Nevada:* Nevada Bureau of Mines and Geology Special Publication 4, 136p.

Thompson, J.F.H., 1996, *Pyrophyllite* in Thompson, A.J.B. and Thompson, J.F.H., 1996, *Atlas of Alteration, a field and petrographic guide to hydrothermal alteration minerals*: Geological Association of Canada Mineral Deposits Division, 120p.

Thompson, T.B., Trippel, A., and Dwelley, P.C., 1985, *Mineralized Veins and Breccias of the Cripple Creek District, Colorado*: Economic Geology, v. 80, pp. 1669-1688.

Tingle, T.N., and Fenn, P.M., 1984, *Transport and concentration of molybdenum in granite molybdenite systems: effects of fluorine and sulfur*: Geology, v. 12, pp. 156-158.

Turner, S.J., 1997, *The Yanacocha epithermal gold deposits, northern Peru: High-sulfidation mineralization in a flow-dome setting*: Unpublished Ph.D. thesis, Golden, Colorado School of Mines, 341 p.

Vikre, P.G., 1985, *Precious metal vein systems in the National district, Humboldt County, Nevada*: Economic Geology, v. 80, pp. 360-393.

Wallace, A., *Geochronology and Isotopic Geochemistry*, 2005, Unpublished Cordex report, 2p.

Wallace, A.R., 2003, *Geology of the Ivanhoe Hg-Au district, northern Nevada: Influence on Miocene volcanism, lakes and active faulting on epithermal mineralization*: Economic Geology, vol. 98, pp. 409-424.

Westra, G. and Keith, S.B., 1981, *Classification and genesis of stockwork molybdenum deposits*: Economic Geology, v. 76, p. 844–873.

Westra, G., and Riedell, K.B., 1995, *Geology of the Mount Hope stockwork molybdenum deposit, Eureka County, Nevada:* in *Coyner, A.R. and Fahey, P. L., eds., Geology and ore deposits of the American Cordillera*: Reno, Geological Society of Nevada, p. 1639–1666.

Wise, J.M., 2008a, *Geologic Map of the Scraper Springs Project*: unpublished report, Newmont Mining Corp., 1p.

Wise, J.M., 2008b, *Annual Technical Report, Scraper Springs Joint Venture*: unpublished report, Newmont Mining Corp., 1p.

Wise, J.M., 2010, *SEM Back-scatter image of molybdenum from Scraper Springs,* personal communication, February 11, 2010.

Appendices

Appendix A

See attached map sheet for geology and alteration map.

Appendix B

Sample Number	NAD 27 Zone 11 E	NAD 27 Zone 11 N	Elevation (ft.)	Lithology	Alteration
SC-01-19	527930.9622	4578201.382	6475	Heterolithic Breccia	Silicification
SC-01-25	527978.4596	4578218.517	6521	Heterolithic Breccia	Argillic
SC-01-29	528038.8087	4578208.837	6557	Heterolithic Breccia	Argillic
SC-01-37	528018.6988	4578237.079	6518	Heterolithic Breccia	Silicification
SC-01-66	528165.4987	4578152.342	6512	Heterolithic Breccia	Acid Sulfate
SC-01-67	528170.8905	4578155.449	6523	Heterolithic Breccia	Acid Sulfate
SC-01-72	528247.8328	4578211.212	6568	Heterolithic Breccia	Acid Sulfate
SC-01-74	528230.0081	4578213.053	6620	Heterolithic Breccia	Silicification
SC-01-77	528198.9638	4578202.763	6561	Heterolithic Breccia	Acid Sulfate
SC-01-82	528154.269	4578017.558	6464	Tuffisite	Argillic
SC-01-84	528149.6272	4578015.164	6472	Tuffisite	Silicification
SC-01-88	528141.0511	4578013.465	6415	Tuffisite	Silicification
SC-01-91A	528169.4011	4578019.881	6432	Heterolithic Breccia	Argillic
SC-01-91B	528169.4011	4578019.881	6432	Heterolithic Breccia	Argillic
SC-01-110	528231.8695	4577988.44	6404	Heterolithic Breccia	Argillic
SC-01-126	528350.3232	4578101.494	6482	Heterolithic Breccia	Argillic
SC-01-130	528354.3478	4578167.565	6505	Heterolithic Breccia	Argillic
SC-01-140	528403.7371	4578109.386	6430	Heterolithic Breccia	Argillic
SC-01-156	528348.1481	4578313.406	6493	Heterolithic Breccia	Acid Sulfate
SC-01-158	528332.9951	4578295.195	6537	Heterolithic Breccia	Acid Sulfate
SC-01-159	528317.8628	4578297.379	6482	Heterolithic Breccia	Acid Sulfate
SC-02-01	527893.0274	4578192.544	6456	Tuffisite	Argillic
SC-02-10	527976.8138	4578152.911	6433	Tuffisite	Argillic
SC-02-14	527694.2428	4578279.675	6340	Diorite	Propylitic
SC-02-17	527672.9534	4578290.795	6326	Diorite	Potassic
SC-02-18	527671.2561	4578270.883	6319	Diorite	Potassic
SC-02-20	527670.1166	4578218.745	6311	Diorite	Potassic
SC-02-28A	527617.8798	4578174.14	6296	Diorite	Propylitic
SC-02-28B	527617.8798	4578174.14	6296	Diorite	Propylitic

SC-02-36	527561.4479	4578075.42	6255	Diorite	Propylitic
SC-02-37	527557.0379	4578073.638	6266	Diorite	Propylitic
SC-02-40	527529.0701	4578056.802	6217	Diorite	Propylitic
SC-02-44	527533.7962	4578089.914	6217	Diorite	Propylitic
SC-02-53	527570.065	4578226.991	6326	Diorite	Potassic
SC-02-54A	527564.1767	4578220.219	6316	Diorite	Potassic
SC-02-58	527612.3178	4578272.801	6320	Diorite	Potassic
SC-02-64	527663.2682	4578316.758	6332	Diorite	Potassic
SC-02-75A	527361.4407	4578074.43	6197	Diorite	Propylitic
SC-02-75B	527361.4407	4578074.43	6197	Diorite	Propylitic
SC-02-75C	527361.4407	4578074.43	6197	Diorite	Propylitic
SC-02-76	527364.7391	4578071.545	6225	Diorite	Propylitic
SC-02-78	527351.4046	4578078.312	6171	Diorite	Propylitic
SC-02-80	527357.3914	4578083.452	6174	Diorite	Propylitic
SC-02-84	527545.3131	4578343.697	6290	Diorite	Propylitic
SC-02-88	527519.9924	4578405.482	6341	Diorite	Propylitic
SC-03-01	527893.0274	4578192.544	6170	Diorite	Propylitic
SC-03-09	527767.8045	4578179.019	6250	Diorite	Propylitic
SC-03-10A	527976.8138	4578152.911	6202	Diorite	Propylitic
SC-03-10B	527976.8138	4578152.911	6202	Diorite	Propylitic
SC-03-10C	527976.8138	4578152.911	6202	Diorite	Propylitic
SC-03-17	527672.9534	4578290.795	6198	Quartz syenite	Potassic
SC-03-20	527670.1166	4578218.745	6210	Quartz syenite	Potassic
SC-03-21	527639.1516	4578211.589	6236	Quartz syenite	Potassic
SC-03-24	527614.5073	4578222.819	6240	Quartz syenite	Potassic
SC-03-25	527618.1516	4578210.388	6183	Quartz syenite	Potassic
SC-03-26	527619.311	4578191.508	6224	Quartz syenite	Potassic
SC-03-27	527605.024	4578184.771	6248	Quartz syenite	Potassic
SC-03-41	527510.7114	4578064.859	6225	Diorite	Propylitic
SC-03-45	527541.7773	4578100.724	6246	Diorite	Propylitic
SC-03-50	527549.8977	4578187.17	6337	Diorite	Propylitic
SC-03-54	527564.1767	4578220.219	6306	Diorite	Propylitic
SC-03-68B	527480.8221	4578223.955	6197	Quartz syenite	Potassic
SC-03-69	527468.5964	4578205.269	6214	Quartz syenite	Potassic
SC-03-77	527352.9701	4578071.346	6278	Diorite	Propylitic
SC-03-82	527510.8223	4578333.342	6317	Diorite	Propylitic
SC-03-83A	527513.3191	4578343.276	6328	Diorite	Propylitic
SC-03-83B	527513.3191	4578343.276	6328	Diorite	Propylitic
SC-03-84	527545.3131	4578343.697	6329	Diorite	Propylitic
SC-03-88	527519.9924	4578405.482	6353	Diorite	Propylitic
SC-04-01	526308.3228	4579857.461	6400	Heterolithic Breccia	Silicification
SC-04-05	526358.2917	4579853.001	6452	Heterolithic Breccia	Acid Sulfate
SC-04-15	526424.8561	4579962.418	6426	Heterolithic Breccia	Silicification

SC-04-22	526439.9177	4579978.503	6464	Heterolithic Breccia	Silicification
SC-04-37	526419.5338	4579821.118	6389	Heterolithic Breccia	Silicification
SC-04-38	526421.9202	4579831.773	6380	Heterolithic Breccia	Silicification
SC-04-58	526885.8724	4579852.151	6405	Heterolithic Breccia	Silicification
SC-04-60	526931.4803	4579718.278	6357	Heterolithic Breccia	Acid Sulfate
SC-04-61	526931.0257	4579728.091	6293	Heterolithic Breccia	Acid Sulfate
SC-04-68	526973.2087	4579798.077	6416	Heterolithic Breccia	Acid Sulfate
SC-04-76	526890.7197	4580008.558	6430	Heterolithic Breccia	Acid Sulfate
SC-04-89	526844.9219	4580142.453	6454	Heterolithic Breccia	Acid Sulfate
SC-04-90	526791.025	4580157.984	6453	Heterolithic Breccia	Acid Sulfate
SC-04-108	526497.5588	4580139.91	6418	Heterolithic Breccia	Acid Sulfate
SC-04-110	526207.3685	4580031.902	6267	Heterolithic Breccia	Acid Sulfate
SC-04-133	525727.6471	4579565.791	6177	Heterolithic Breccia	Silicification
SC-04-139B	525924.6531	4579484.673	6129	Heterolithic Breccia	Silicification
SC-04-156	526702.3521	4579700.168	6450	Heterolithic Breccia	Silicification
SC-04-160A	526626.8456	4579710.038	6469	Heterolithic Breccia	Silicification
SC-04-160B	526626.8456	4579710.038	6469	Heterolithic Breccia	Silicification
SC-04-168	526457.0353	4579481.632	6303	Heterolithic Breccia	Silicification
SC-04-173	526757.3636	4579399.36	6397	Heterolithic Breccia	Acid Sulfate
SC-04-175	526751.7493	4579372.806	6378	Heterolithic Breccia	Acid Sulfate
SC-04-184	526774.4473	4579266.625	6295	Heterolithic Breccia	Acid Sulfate
SC-04-194	526695.9686	4579280.635	6335	Heterolithic Breccia	Acid Sulfate
SC-04-195	526679.6825	4579269.773	6301	Heterolithic Breccia	Acid Sulfate
SC-04-231	525819.0567	4579068.628	6013	Heterolithic Breccia	Acid Sulfate
SC-04-246	525720.3169	4579260.425	6143	Heterolithic Breccia	Acid Sulfate
SC-04-250	525787.6927	4579244.722	6130	Heterolithic Breccia	Acid Sulfate
SC-04-254	525873.9317	4579214.244	6154	Heterolithic Breccia	Acid Sulfate

Appendix C

Sample	NAD 27 Zone 11 E	Nad 27 Zone 11 N	F (%)	Ag	Al (%)	As	Ba	Be	Bi	Ca (%)	Cd	Co	Cr	Cu	Fe (%)	Ga
SC- 01-72	528248	4578211	1.18	<0.5	6.93	15	80	<0.5	2	0.33	<0.5	2	7	12	0.52	10
SC- 01-88	528141	4578013	0.06	<0.5	1.12	<5	480	<0.5	<2	0.26	<0.5	<1	12	4	0.85	<10
SC- 02-01	527893	4578193	0.11	<0.5	0.61	15	290	<0.5	25	0.07	<0.5	<1	28	7	0.72	<10
SC- 02-10	527977	4578153	3.58	<0.5	0.47	<5	80	<0.5	<2	0.92	<0.5	<1	9	4	0.76	<10
SC- 02-17	527673	4578291	0.05	<0.5	8.16	11	1650	2	<2	0.49	<0.5	3	3	3	3.06	20
SC- 02-36	527561	4578075	0.09	<0.5	8.08	<5	1220	1.6	<2	3.68	<0.5	11	11	6	4.61	20
SC- 02-75A	527361	4578074	0.06	<0.5	8.09	8	1220	1.6	<2	3.8	<0.5	13	27	2	4.82	20
SC- 03-25	527618	4578210	0.03	<0.5	6.91	<5	1410	3.1	4	0.77	<0.5	1	4	1	0.54	20
SC- 03-26	527619	4578192	0.03	<0.5	6.75	7	2360	2.2	<2	1.08	<0.5	1	5	3	0.62	20

	Ge	Hf	In	K	La	Li	Mg	Mn	Mo	Na	Nb	Ni	P	Pb	Rb	Re	S
	ppm	ppm	ppm	%	ppm	ppm	%	ppm	ppm	%	ppm	ppm	ppm	ppm	ppm	ppm	%
SC- 01-72	0.12	3.2	0.024	2	23.7	2.3	0.05	40	1.96	0.48	10.6	2.3	1690	29.2	11.2	<0.002	5.2
SC- 01-88	0.05	1.4	<0.005	0.1	2	12.3	0.09	57	3	0.2	19.1	1.4	360	15.9	3.1	<0.002	0.6
SC- 02-01	0.07	2.2	0.017	0.1	2.7	8.5	0.03	69	3.07	0.05	10.2	2	370	81.4	6.6	<0.002	0.1
SC- 02-10	0.09	1.1	0.009	0.07	14.1	2.2	0.16	87	1.51	0.02	5.2	2.1	370	3.7	2.4	<0.002	0.04
SC- 02-17	0.24	2.1	0.02	2.29	37.1	10.7	0.39	584	2.24	2.36	12.7	1.4	900	8.2	68.5	<0.002	0.03
SC- 02-36	0.25	3.2	0.057	2.19	23.6	13.9	1.47	856	1.23	2.4	11.8	5.1	1530	17.5	60.4	<0.002	0.03
SC- 02-75A	0.27	1.6	0.057	2.23	28.2	9.2	1.63	872	1.63	2.19	12.1	9	1320	7.8	63.3	<0.002	0.01
SC- 03-25	0.1	0.5	0.054	4.56	10.7	1.1	0.19	77	0.95	1.46	12.7	1.2	270	9.4	115.5	<0.002	<0.01
SC- 03-26	0.12	0.8	0.048	4.33	28.2	1.4	0.24	88	2.49	1.52	9	1.2	200	13.2	100		

	Sb	Sc	Se	Sn	Sr	Ta	Te	Th	Ti	Tl	U	V	W	Y	Zn	Zr
	ppm	ppm	ppm	ppm	ppm	ppm	ppm	ppm	%	ppm	ppm	ppm	ppm	ppm	ppm	ppm
SC- 01-72	0.81	5.5	1	5.4	928	0.73	0.39	5.8	0.341	1.38	1.9	60	1.1	8.4	33	109.5
SC- 01-88	1.12	1.3	3	2	318	0.7	0.5	0.9	0.71	0.5	0.7	26	1.5	1.4	26	39.7
SC- 02-01	5.83	7	3	14.1	61.1	0.49	1.09	2.8	0.559	0.56	1.9	47	1.8	4.8	48	75.8
SC- 02-10	0.31	1.7	2	9.4	152.5	0.1	0.13	3.4	0.338	0.17	1.5	29	0.3	2.8	8	39
SC- 02-17	0.81	5	7	0.9	419	0.87	0.06	13.6	0.261	0.82	3.3	29	0.8	17.4	37	65
SC- 02-36	0.72	13.2	1	1.8	661	0.78	<0.05	6.7	0.553	0.72	2.2	123	0.9	17.2	96	113.5
SC- 02-75A	0.44	13.9	1	1.4	619	0.8	<0.05	8.3	0.556	0.39	2.2	132	0.7	18.1	177	50.4
SC- 03-25	0.12	0.9	1	4.8	256	2.09	<0.05	2.9	0.018	1.39	1.9	5	0.1	5.2	17	7.1
SC- 03-26	0.18	1.4	1	1.7	369	0.88	<0.05	13	0.055	1.24	1.7	12	0.2	5.8	26	23.7

Appendix D

See attached sheet for graphic drill hole geology, alteration, and sulfide logs.

Appendix E

Reduced to pole magnetics survey conducted by Zonge, 2005.

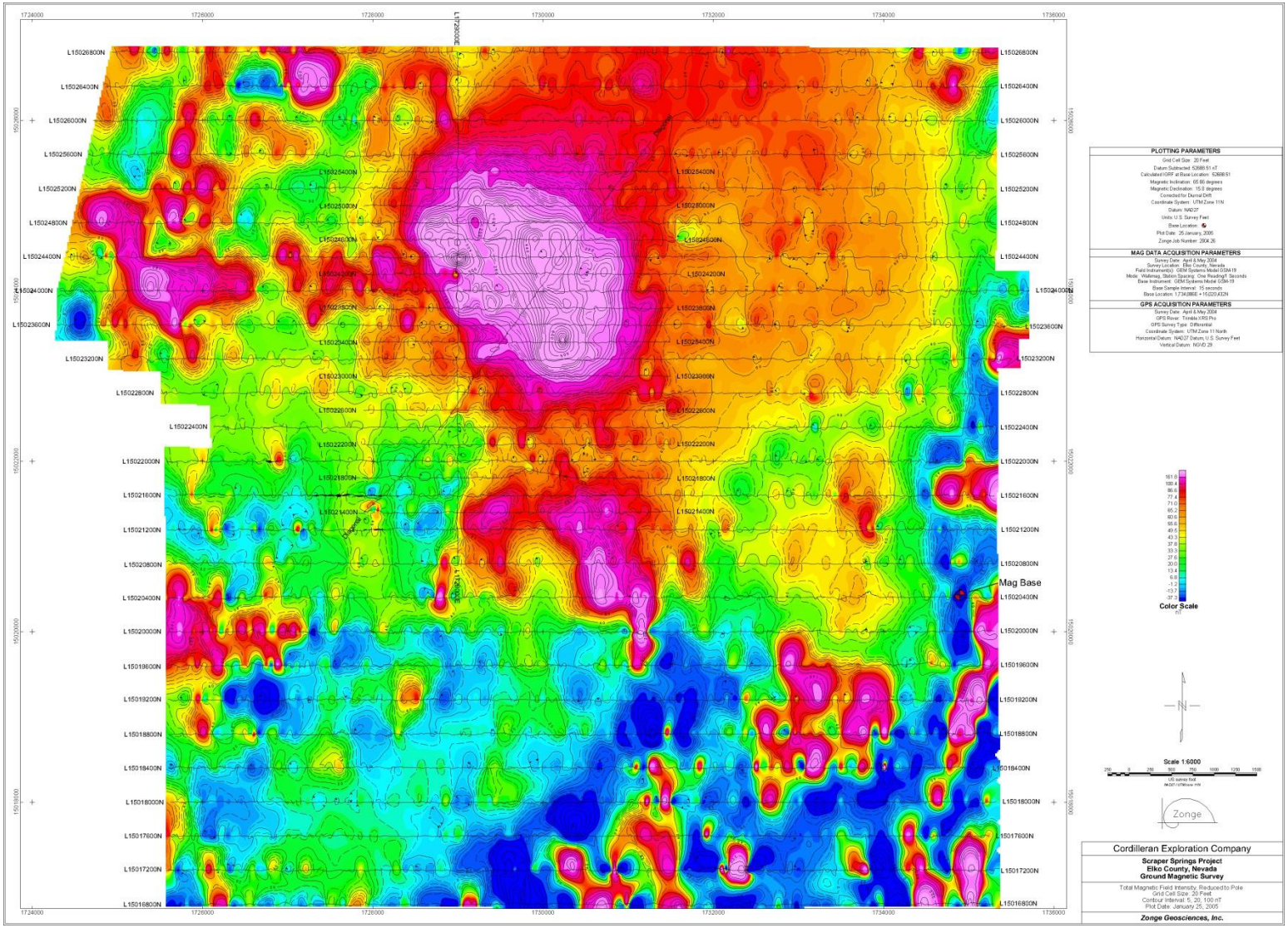

Same magnetics survey with diorite stocks outlined for geologic reference, produced by Geologix (2005).